Understanding estuarine processes in uMfolozi/uMsunduzi/St Lucia estuary from Earth Observation data of vegetation composition, distribution and health

Report to the
WATER RESEARCH COMMISSION

by

Moses A. Cho, Heidi van Deventer
Earth Observation, Natural Resources and Environment, The Council for Scientific and Industrial Research (CSIR), Pretoria, South Africa

Melanie Lück-Vogel, Lara van Niekerk
Coastal Systems, Natural Resources and Environment, The Council for Scientific and Industrial Research (CSIR), Pretoria, South Africa

Janine Adams
Nelson Mandela Metropolitan University, Port Elizabeth, South Africa

Onisimo Mutanga
School of Agriculture, Earth and Environmental Sciences, University of KwaZulu-Natal

WRC Report No. 2268/1/15
ISBN 978-1-4312-0754-1

March 2016

Obtainable from
Water Research Commission
Private Bag X03
GEZINA, 0031

orders@wrc.org.za or download from www.wrc.org.za

EXECUTIVE SUMMARY

UNDERSTANDING ESTUARINE PROCESSES IN UMFOLOZI/UMSUNDUZI/ST LUCIA ESTUARY FROM EARTH OBSERVATION DATA OF VEGETATION COMPOSITION, DISTRIBUTION AND HEALTH

BACKGROUND

The uMfolozi/uMsunduzi/St Lucia estuary is situated in the largest fluvial coastal plain in South Africa and the largest estuarine system in Africa (155 000 ha). This estuarine system hosts the highest diversity of wetland habitat types for its size in the whole of southern Africa (Cowan, 1999). The estuary faces a number of threats as a result of human interference over several decades including habitat fragmentation and loss of species diversity. Understanding the uMfolozi/uMsunduzi/St Lucia estuary system is crucial, yet difficult, considering the regional extent and difficulty in accessing the area. The physicochemical processes (hydrodynamic, chemical and sedimentological) largely determine the biological components (e.g. vegetation composition/distribution, health and the habitat types) in the estuary. For example, (i) wetland plant communities vary across estuarine salinity or water quality gradients, and (ii) mangroves have been adversely affected by sediment burial of roots. Furthermore, changes in composition and condition of estuarine habitats could influence the spatial distribution of faunal populations including amphibians, fish, birds, reptiles and mammals. Therefore, the spatio-temporal monitoring of the uMfolozi/uMsunduzi/St Lucia estuarine vegetation should be considered as an integral part of understanding the estuarine biological processes and detecting changes in particular and by proxy, the underlying physicochemical processes.

RATIONALE

The paucity of exhaustive spatial-temporal information on estuarine vegetation composition, distribution and health in South Africa undermines a holistic understanding of estuarine processes and potential threats to their functioning. The development of new Earth Observation (EO) methods is essential to providing time-cost effective ways of assessing estuarine processes. Conventional field-based surveys are laborious, time-consuming, expensive and risky in the estuarine environment. Remote sensing, using current or anticipated space-borne sensors is widely viewed as a time- and cost-efficient way to proceed with inventorying of estuarine vegetation, water quality and processes such as

channel development. Conventional EO techniques are however inadequate because of the low spectral/spatial resolutions of commonly available sensors.

AIMS

This study has explored the utility of earth observation data consisting of remote sensing and other ancillary data to provide information on the spatial distribution on the uMfolozi/uMsunduzi/St Lucia estuary vegetation types and condition. The general approach consisted of understanding leaf-to-spaceborne remote sensing of wetland tree species, vegetation community or habitat types and vegetation nutrient status. The aims were:

Aims	**Description of work and key findings**
1. To spectrally discriminate and map estuarine tree and grass/reed species 2. To accurately map estuarine habitat types, habitat heterogeneity and land use/land cover (LULC) types	Models for species (or vegetation type) separation using remote sensing are based on the assumption that within-species (or vegetation type) spectral differences resulting from differences in their chemical and structural properties are much lower that between species (or vegetation type) spectral differences. In this study, we assessed the above assumption at the leaf spectral and spaceborne sensing levels. At the leaf spectral level, twenty-two spectral bands out of 2100 bands of the field spectrometer (a hyperspectral sensor) were identified as the most important spectral variables for classification of six dominant evergreen tree species in the St Lucia estuary. A higher accuracy for classifying vegetation types was obtained from WorldView-2 when compared to RapidEye. However, the accuracy of classifying vegetation types involving RapidEye images was comparable to that obtained from the WorldView-2 image when RapidEye images for several seasons were used.
3. To assess the estuarine vegetation condition/health using new multispectral imagery such as RapidEye and WorldView-2	Vegetation condition is considered in this study to be the relative health of vegetation compared to undisturbed vegetation of the same type. The main indicator of vegetation condition considered in this study is the leaf nitrogen (N) or phosphorus (P) content. In this study, both leaf and spaceborne remote sensing was used to assess leaf N or P content. Very strong correlations were found between laboratory measured leaf N (%N) and leaf spectral reflectance, particularly in the shortwave infrared region for evergreen tree species. The results for leaf P were not so promising. Leaf N in the region varies according to the season, showing maximum variability among species during spring and the lowest variability in winter. However, winter leaves contain the highest amounts of leaf N. Spaceborne remote sensing also showed a good potential for assessing leaf N at the broad landscape using RapidEye imagery. This is possible

	thanks to the red-edge band of RapidEye which has been shown to vary with subtle changes in leaf chlorophyll content. The map of leaf N for the estuary showed that conversion of indigenous forest into subsistence grazing land or farming landscape leads to loss of N from the system.
4. To explain the physiochemical processes underlying the composition and distribution of vegetation	Macrophyte habitats in the estuary, including submerged macrophytes, reeds and sedges, mangroves, grass and shrubs, salt marsh and swamp forest, were mapped for 2008 and 2013. The distribution of macrophytes was related to sediment characteristics. The results indicated that changes in salinity and water level caused die-back or expansion of particular habitats. Submerged macrophytes increased while salt marsh decreased due to inundation.
5. To ensure that the knowledge generated serves to inform sustainable management of the uMfolozi/uMsunduzi/St Lucia estuary.	A geoportal data viewer for the project map deliverables has been created and is hosted by the Department of Environmental Affairs (DEA), Branch: Oceans and Coasts, Chief Directorate Integrated Coastal Management at http://mapservice.environment.gov.za/Coastal%20Viewer/.

CONCLUSIONS

In conclusion, the study has highlighted the potential contribution of remote sensing technology and science to understanding the vegetation status of uMfolozi/uMsunduzi/St Lucia estuary. Estuarine systems are complex and difficult to access. Therefore, developing a monitoring system based on remote sensing data and other in-situ ancillary information will enhance the ability to rapidly assess changes in the vegetation composition and condition of the estuary. The availability of new multispectral sensors such as RapidEye and WorldView-2 moves remote sensing closer to widespread monitoring of estuarine vegetation condition including species and nutrient status.

Please note:

Throughout the project publications, the names 'uMfolozi' and 'uMsunduzi' have been interchangeably used with 'Mfolozi' and 'Msunduzi' for these two Rivers.

ACKNOWLEDGEMENTS

Satellite images were funded by the South African Department of Science and Technology (DST). The National Research Foundation (NRF) funded a number of studies and HR was funded between the Council for Scientific and Industrial Research (CSIR) and the Water Research Commission (WRC). We thank the iSimangaliso Wetland Park Authority and Ezemvelo KwaZulu-Natal (KZN) Wildlife for granting access and logistical support. Dr Ricky Taylor, former ecologist at Ezemvelo KZN Wildlife for guidance and advice. We are grateful to the many fieldwork assistants: Mr S. Gumede, Dr F Durand, Ms R van Deventer, Mr A van Deventer, Mr S Mfeka, Dr E Adam, Mr T Colins, Mr K Barker, Mr O Malahlela and the iSimangaliso bursary students Ms N Nkosi, Ms T Sibiya, Ms N Gumede, Mr B Mdamba and Mr B Gumbi.

The authors would like to thank the Reference Group of the WRC Project for the assistance and the constructive discussions during the duration of the project: Dr B Petja, Dr MS Liphadzi, Dr C Moseki, Prof GC Bate, Dr P Gama, Dr RH Taylor, Prof A Whitfield, Prof C Everson, Ms N Govender, Ms T Ndukwana, Mr K Reinecke, Ms S van Rensburg and Dr A Grundling.

TABLE OF CONTENTS

LIST OF FIGURES

LIST OF TABLES

LIST OF ABBREVIATIONS

a.m.s.l	Above mean sea level
ANOVA	Analysis Of Variance
ASD	Analytical Spectral Device
CSIR	Council for Scientific and Industrial Research
DAFF	Department of Agriculture, Forestry and Fisheries
DSM	Digital Surface Model
DST	South African Department of Science and Technology
DWA	Department of Water Affairs
ED	Euclidean Distance
EKZNW	Ezemvelo KZN Wildlife
ENVI	Environment for Visualizing Images
EO	Earth Observation
GEF	Global Environmental Facility
GIS	Geographic Information System
GPS	Global Positioning Systems
HCD	Honest Significant Difference
ICP-OES	Inductively Coupled Plasma Optical Emission Spectrometry
ILWIS	Integrated Land and Water Information System
LC	Land Cover
LiDAR	Light Detection And Ranging
LULC	Land Use and Land Cover
MAP	Mean Annual Precipitation
MS	Multispectral
MTCI	MERIS Terrestrial Chlorophyll Index
N	Nitrogen
NDVI	Normalised Difference Vegetation Index
NIR	Near Infrared
NMMU	Nelson Mandela Metropolitan University
OA	Overall Accuracy
P	Phosphorus
PCA-RF	Principle Component Analysis – Random Forest algorithm
PLS-RF	Partial Least Square – Random Forest algorithm
PRI	photochemical reflectance index
RE	RapidEye
RMSE	Root Mean Square Error
ROI	Region of Interest
SAM	Spectral Angle Mapper
SEP	Standard Error of Prediction

SU	Stellenbosch University
SWIR	Shortwave Infrared
UKZN	University of KwaZulu-Natal
VHR	Very High Resolution
VI	Vegetation Index
WRC	Water Research Commission
WV2/3	WorldView-2/3 sensor

GLOSSARY

Earth Observation. Is the gathering of information about the Earth's surface's physical, chemical and biological systems via remote sensing technologies supplemented by earth surveying techniques, encompassing the collection, analysis and presentation of data (International Journal of Applied Earth Observation and Geoinformation).

Field Spectroscopy. The quantitative measurement of radiance, irradiance, reflectance or transmission in the field / on the ground.

Hyperspectral (imaging). Data collected in a high number (> 100) of continuous narrow (1-2nm) spectral bands across the electromagnetic spectrum.

Multispectral (imaging). Data collected of the Earth's surface in few (typically 3-8) relatively broad (>50 nm) spectral bands.

LiDAR. A kind of imaging technology. Usually mounted on an aircraft, the LiDAR sensor sends light pulses to the earth surface and measures the time until the reflected signal returns to the sensor. From the time past, i.e. the distance between the airborne sensor and the earth surface, information on ground elevation and vegetation canopy structure is derived. A common product is a fine scale Digital Elevation (or Surface) Model which can be used for further geospatial analysis.

1 INTRODUCTION AND OBJECTIVES

1.1 Introduction

Estuarine systems face a number of threats as a result of global change, including nutrient enrichment, sea-level rise, habitat fragmentation and loss of species diversity. Understanding these systems is crucial, yet difficult, considering the regional extent and difficulty in accessing these systems.

An estuary is defined as “a partially or fully enclosed water body that is open to the sea permanently or periodically, and within which the seawater can be diluted, to an extent that is measurable, with freshwater drained from land” (RSA, 1998a). Thus, estuaries form a transition zone between river and ocean environments and are subject to both marine influences such as waves, tides and the influx of saline seawater and riverine influences, such as flows of fresh water and sediment. It is therefore the unique combination of both freshwater and saltwater that dictates many of the hydrodynamic, chemical, sedimentological and biological processes within the estuary. The decline of intact estuarine environments around the world could be attributed to many factors, including increased sedimentation from upstream soil erosion due to overgrazing and poor farming practices; overfishing; drainage and filling of wetlands; eutrophication due to excessive nutrients from sewage and animal wastes; pollutants including heavy metals, hydrocarbons from sewage inputs; damming for flood control or water diversion and habitat fragmentation. For example, changes in nutrient concentrations in rivers and estuaries have been be related to land use (Ball 1994). Upstream land use or cover changes and floodplain transformations are other factors that could be affecting estuarine processes.

The physicochemical processes (hydrodynamic, chemical and sedimentological) largely determine the biological components (e.g. vegetation composition/distribution, health and the habitat types) in the estuary. For example, (i) wetland plant communities vary across estuarine salinity or water quality gradients (Sand-Jensen and Borum 1991), and (ii) mangroves have been adversely affected by sediment burial of roots (Ellison 1999). Furthermore, changes in composition and condition of estuarine habitats could influence the spatial distribution of faunal populations including amphibians, fish, birds, reptiles and mammals (Adams *et al*., 2012). Therefore, the spatio-temporal monitoring of estuarine vegetation should be considered as an integral part of understanding estuarine biological processes and detecting changes in particular and by proxy, the underlying physicochemical

processes. Vegetation sampling coupled with remote sensing data and other ancillary information e.g. topographic and land use data will provide a regional, temporal, seasonal and spatial understanding of estuarine processes. Change detection over space and time could inform integrated management of estuaries.

The paucity of exhaustive spatial-temporal information on estuarine vegetation composition, distribution and health in South Africa undermines a holistic understanding of estuarine processes and potential threats to their functioning. The development of new Earth Observation (EO) methods is essential to providing time-cost effective ways of assessing wetland or estuarine processes. Conventional field-based surveys are laborious, time-consuming, expensive and risky in the wetland environment. Monitoring of protected tree species under the National Forest Act (Act no. 84 of 1998; RSA, 1998b), is challenging in such environments. Remote sensing, using current or anticipated space-borne sensors is widely viewed as a time- and cost-efficient way to proceed with inventorying of estuarine vegetation, water quality and processes such as channel development. Conventional EO techniques are however inadequate because of the low spectral/spatial resolutions of commonly available sensors. According to the National Estuary Biodiversity plan for South Africa (Turpie *et al*., 2012) rapid assessment methods are required to assess estuarine processes more regularly. The uMfolozi/ uMsunduzi/St Lucia estuarine system (Figure 1.1), being the largest estuary in South Africa (50% of estuarine area in SA) would benefit from a space-borne rapid-assessment for conservation and management purposes.

The iSimangaliso Wetland Park (uMfolozi/uMsunduzi/St Lucia estuaries) is situated in the largest fluvial coastal plain in South Africa (Van Heerden, 2011) and the largest estuarine system in Africa (155 000 Ha) and hosts the highest diversity of wetland habitat types for its size in the whole of southern Africa (Cowan, 1999). In November 2000 an extended area to the Ramsar site was declared as a World Heritage Site, according to the World Heritage Convention Act, Act 49 of 1999 (RSA, 1999). Management resorted to both the local KwaZulu-Natal Parks authority, Ezemvelo KwaZulu-Natal Wildlife (EKZNW) Management, as well as the iSimangaliso Wetland Park Authority.

The most recent National Biodiversity Plan (NBP) of 2011 (Turpie *et al*., 2012) found that Lake St Lucia represents more than 50% of estuarine area of South Africa, yet is in a very poor condition regardless of being situated in a formal protected area. Historically the uMfolozi/uMsunduzi/St Lucia estuaries were interconnected, and with sufficient run-off from the catchment, the estuary mouth scoured open in a natural way (WRC report no. KV 255/10

(Bate *et al*., 2011)). Since 1920, much of the water which previously fed directly into the various lake compartments has been diverted for agriculture and other uses, thus affecting biophysical processes in the estuary (Bate *et al*., 2011).

However, a review of studies on the above estuary (Bate *et al*., 2011), showed that research has focused mainly on hydrological assessments, sediment processes, faunal diversity as well as an economical assessment of the ecosystem services, with insufficient information on the estuarine vegetation. Nondoda *et al*. (2011) (in Bate *et al*. 2011) present vegetation distribution maps based on aerial photography of the uMfolozi swamp. However, information on the vegetation health/condition or the distribution of macrophyte species has not been derived from panchromatic aerial images. Recently the uMfolozi River was reconnected to the St Lucia estuary (Bate *et al*. 2011). This could have important repercussion on the estuarine physicochemical and biological processes. Therefore, more exhaustive baseline data is needed to monitor changes in the estuary.

The development of Earth Observation (EO) approaches for mapping vegetation composition, distribution and condition in the uMfolozi/uMsunduzi/St Lucia estuaries is crucial to understanding spatio-temporal dynamics in estuarine processes following the reconnection of St Lucia to the uMfolozi, particularly in this large and mostly inaccessible region. Compared to traditional fieldwork methods, EO can offer regular spatially continuous “snap-shots” of large accessible and otherwise inaccessible areas. Regional mapping of biochemical and biophysical parameters of vegetation is possible, and with regular revisits over the area, provides a multi-temporal view of directed changes or phenological characteristics of the ecosystem. These advantages of EO make it a key tool for understanding the ecosystem at large, and provides a means to assess and monitor the impact of global change on estuarine systems.

To date, only a few studies have explored the feasibility of applying EO techniques to the vegetation in the particular study area (Adam & Mutanga, 2009; Mafuratidze, 2010; Adam *et al.*, 2012; Mutanga *et al*., 2012). These studies assessed a number of wetland vegetation types at canopy and image level scale to assess species separability and biomass. Further work is required at regional scale to provide spatio-temporal information of the study area. Therefore, this study aims at extending on EO data and methods for vegetation assessment, as basis for the understanding of estuarine processes in the region of the uMfolozi/uMsunduzi/St Lucia estuaries.

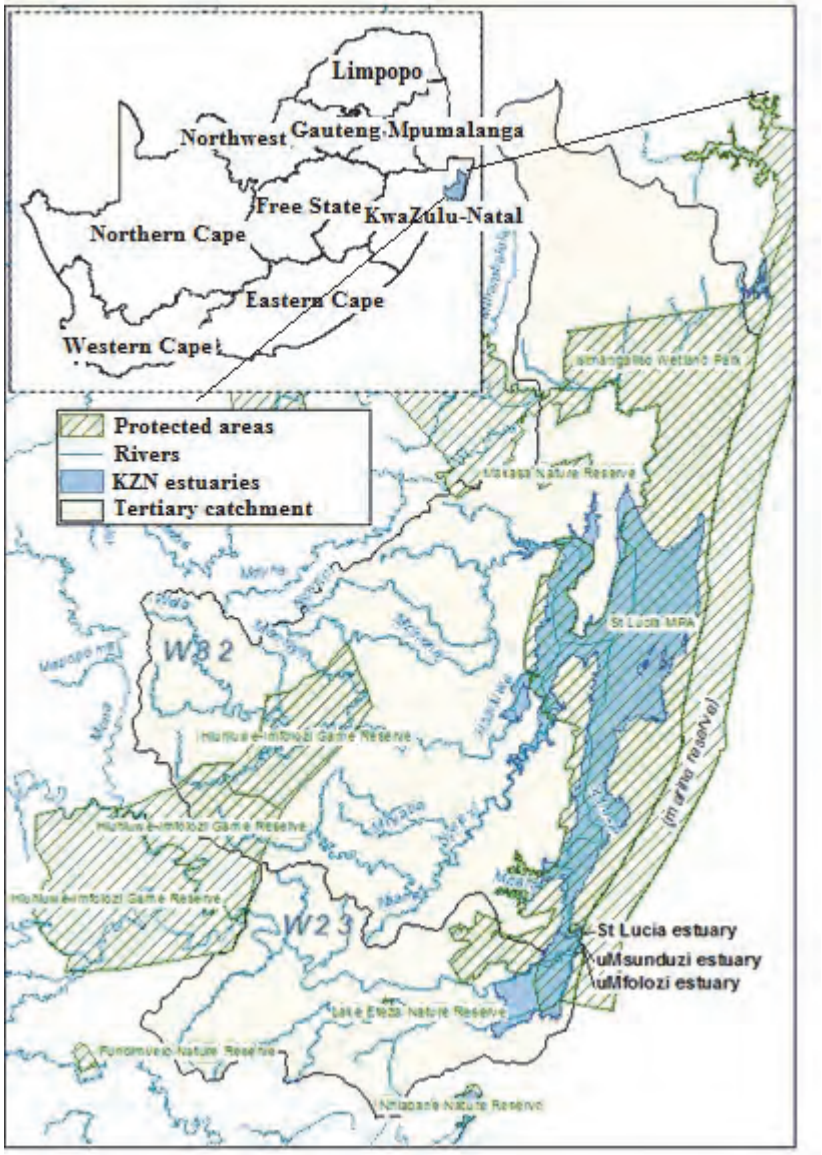

Figure 1.1: Location of the uMfolozi, uMzunduzi and St Lucia estuaries within tertiary catchments W32 and W23.

1.2 Project Aims

The following are the aims of the project:

1. To spectrally discriminate and map estuarine tree and grass/reed species
2. To accurately map estuarine habitat types, habitat heterogeneity and land use/land cover (LULC) types
3. To assess the estuarine vegetation condition/health using new multispectral imagery such as RapidEye and WorldView-2

4. To explain the physiochemical processes underlying the composition and distribution of vegetation
5. To ensure that the knowledge generated serves to inform sustainable management of the uMfolozi/uMsunduzi/St Lucia estuary by developing a data dissemination system based on a geoportal consisting of a data viewer for relevant stakeholders and conservation managers and to train key personnel in EO methods (ensuring uptake) and interpretation of results.

1.3 Structure of the report

The report is structured as follows:

Chapter	Description	Relevant Aim
1. Introduction and objectives	The background, motivation and aims of the study are outlined in this section	
2. Spectral discrimination of six evergreen wetland tree species at leaf-level scale	This chapter investigates the utility of hyperspectral data across four seasons for discriminating six wetland tree species at the leaf scale.	1
3. Mapping estuarine habitat types	This chapter evaluates the use of very high resolution multispectral satellite imagery and LiDAR for classifying estuarine habitat/vegetation types.	2
4. Remote sensing models for predicting leaf nitrogen and phosphorus across four seasons for six subtropical forest evergreen tree species	This chapter investigates the capability of hyperspectral models, developed from leaf spectra of selected spectral regions and seasons, to predict nutrient concentration across season and species. Foliar nutrients showed a variation across seasons. The results suggest that spectral measurements can be potentially be used to quantify nutrient phenology at regional scale and monitor the impacts of global change on nutrient phenology and photosynthesis.	3
5. Assessing the effects of Dukuduku forest fragmentation on leaf nitrogen distribution using remote sensing data	This chapter explores the utility of new remote sensing tools to model the spatial distribution of leaf N in a forested landscape undergoing deforestation. Leaf N was mapped using models developed from a relatively new spaceborne sensor, RapidEye (5 m spatial resolution). A detailed land-cover map derived from another new spaceborne sensor, WorldView-2 (2 m resolution) was used to assess differences in leaf N between land-cover types.	3

6. Physiochemical processes underlying the composition and distribution of vegetation	This chapter investigated three objectives: (i) the present state and distribution of the macrophytes of the St. Lucia and uMfolozi estuaries; (ii) the present state / health of the mangroves at four sites along the Narrows by assessing sediment condition and population structure of the trees; and (iii) the feasibility of linking the uMfolozi River back to the St Lucia Estuary and the responses of these systems to different management scenarios.	4
7. Geoportal data dissemination	Data produced through this project were compiled in a Web Map Services (WMS) viewer accessible through the CSIR's geoportal. Data available include the vegetation and habitat types and species maps.	5
8. Conclusion	Summarises the implication of the study.	

1.4 Participating organisations

- Council for Scientific and Industrial Research (CSIR)
- University of KwaZulu-Natal (UKZN)
- Nelson Mandela Metropolitan University (NMMU)
- Stellenbosch University (Cikizwa Mbolambi)

1.5 Capacity Building

A number of MSc and PhD students benefitted from this project (Table 1.1).

Table 1.1: Students who benefitted from this WRC project.

Surname	First name	Gender	Race	Degree	University	Final year
Davhula	Azwifaneli	Male	African (Black)	Masters	University of Kwa-Zulu Natal (UKZN)	2013/2015
Van Deventer	Heidi	Female	White	Doctorate	University of Kwa-Zulu Natal (UKZN)	2013/2015
Rautenbach	Kelly	Female	White	Masters	Nelson Mandela Metropolitan University	2013/2014
Mbolambi	Cikizwa	Female	African (black)	Masters	Stellenbosch University (SU)	2014/2015

1.6 References

Adam E & Mutanga O. 2009. Spectral discrimination of papyrus vegetation (*Cyperus papyrus L*.) in swamp wetlands using field spectrometry. ISPRS Journal of Photogrammetry and Remote Sensing, 64, 612-620.

Adam E, Mutanga O, Rugege D. 2010. Multispectral and hyperspectral remote sensing for identification and mapping of wetland vegetation: a review. Wetlands Ecological Management, 18, 281-296.

Adam E, Mutanga O, Rugege D, Ismail R. 2012. Discriminating the papyrus vegetation (*Cyperus papyrus L*.) and its coexistent species using random forest and hyperspectral data resampled to HYMAP, International Journal of Remote Sensing, 33(2): 552-569.

Adams JB, Snow GC and Veldkornet DA. 2012. Estuarine habitat. In: Turpie, J.K., Wilson, G. & Van Niekerk, L. 2012. National Biodiversity Assessment 2011: National Estuary Biodiversity Plan for South Africa. Anchor Environmental Consulting, Cape Town. Report produced for the Council for Scientific and Industrial Research and the South African National Biodiversity Institute.

Artigas FJ and Yang J. 2006. Spectral discrimination of marsh vegetation types in the New Jersey Meadowlands, USA. Wetlands, 26(1), 271-277.

Balls, P.W., 1994. Nutrient Inputs to Estuaries from Nine Scottish East Coast Rivers; Influence of Estuarine Processes on Inputs to the North Sea. Estuarine, Coastal and Shelf Science, 39(4): 329-352.

Bartlett DS and Klemas V. 1980. Quantitative Assessment of Tidal Wetlands Using Remote Sensing. Environmental Management, 4(4), 337-345.

Bate GC, Whitfield AK and Forbes AT (Eds.). 2011. A review of studies on the Mfolozi estuary and associated flood plain, with emphasis on information required by management for future reconnection of the river to the St Lucia system. Report to the Water Research Commission. WRC Report No. KV 255/10. Pretoria: WRC.

Belluco E, Camuffo M, Ferrari S, Modenese L, Silvestri S, Marani A and Marani M. 2006. Mapping salt-marsh vegetation by multispectral and hyperspectral remote sensing. Remote Sensing of Environment, 105, 54-67.

Cho MA, Mathieu R, Asner GP, Naidoo L, Van Aardt J, Ramoelo A, Debba P, Wessels K, Main R, Smit IPJ, Erasmus B. 2012. Mapping tree species composition in South African savannas using an integrated airborne spectral and LiDAR system. Remote Sensing of Environment 125:214-226.

Cho MA, Debba, P, Mutanga, O, Dudeni-Tlhone, N, Magadla T, and Khuluse SA, 2012. Potential utility of the spectral red-edge region of SumbandilaSat imagery for assessing indigenous forest structure and health. International Journal of Applied Earth Observation and Geo-information,16:85-93.

Cho MA, Naidoo L, Mathieu R and Asner GP. 2011. Mapping savanna tree species using Carnegie Airborne Observatory hyperspectral data resampled to WorldView-2 multispectral configuration. The International Symposium on Remote Sensing of Environment (ISRSE 2011)-34th ISRSE. 10-15 April 2011, Sydney, Australia.

Cho MA, Debba P, Mathieu R, Van Aardt J, Naidoo L and Asner GP. 2010. Improving discrimination of Savanna tree species through a multiple endmember spectral angle mapper approach. IEEE Transaction on Geoscience and Remote Sensing, 48(11), 4133-4142.

Cowan GI. 1999. The St Lucia System. Available online at: [http://hdl.handle.net/1834/460]. Last date accessed 1 June 2011.

Elliott M and McLusky DS, 2002. The Need for Definitions in Understanding Estuaries. Estuarine, Coastal and Shelf Science, 55(6): 815-827.

Ellison JC. 1999. Impacts of Sediment Burial on Mangroves. Marine Pollution Bulletin, 37(8-12): 420-426.

Gond V, De Pury SGG, Veroustraete F and Ceulemans R. 1999. Seasonal variations in leaf area index, leaf chlorophyll, and water content; scaling-up to estimate fAPAR and carbon balance in a multilayer, multispecies temperate forest. Tree Physiology, 19, 673-679.

Hestir EL, Khanna S, Andrew ME, Santos MJ, Viers JH, Greenberg JA, Rajapakse SS and Ustin SL. 2008. Identification of invasive vegetation using hyperspectral remote sensing in the California Delta ecosystem. Remote Sensing of Environment, 112, 4034-4047.

Laba M, Tsai F, Ogurcak D, Smith S and Richmond ME. 2005. Field Determination of Optical Dates for the Discrimination of Invasive Wetland Plant Species Using Derivative Spectral Analysis. Photogrammetric Engineering and Remote Sensing, May 603-611.

Lück-Vogel M, Barwell L and Theron A. 2011. Transferability of a remote sensing approach for coastal land cover classification. Proceedings of CoastGIS 2011 Conference, 6-8 September.

Mafuratidze P. 2010. Discriminating wetland vegetation species in an African savanna using hyperspectral data. M.Sc. Thesis, University of KwaZulu-Natal, South Africa.

Mutanga O, Adam E and Cho MA. 2012. High density biomass estimation for wetland vegetation using WorldView-2 imagery and random forest regression algorithm. International Journal of Applied Earth Observation and Geoinformation, 18, 399-406.

McCarthy J, Humbricht T and McCarthy TS. 2005. Ecoregion classification in the Okavango Delta, Botswana from multitemporal remote sensing. International Journal of Remote Sensing, 26(19), 4339-4357.

Potter IC, Chuwen BM, Hoeksema SD and Elliott M, 2010. The concept of an estuary: A definition that incorporates systems which can become closed to the ocean and hypersaline. Estuarine, Coastal and Shelf Science, 87(3): 497-500.

Rebelo LM, Finlayson CM and Nagabhatla N. 2009. Remote sensing and GIS for wetland inventory, mapping and change analysis. Journal of Environmental Management, 90, 2144-2153.

Republic of South Africa (RSA). 1998a. National Forests Act, Act no. 84 of 1998. Pretoria: Government Printers. Available online at: [http://www.dwaf.gov.za/Documents/Forestry/Tact84.pdf]. Last date accessed 14 June 2011. Republic of South Africa (RSA). 1999. World Heritage Convention Act, Act 49 of 1999. Pretoria: Government Printers.

Republic of South Africa (RSA). 1998b. National Water Act, Act 36 of 1998. Pretoria: Government Printers.

Sand-Jensen K and Borum J, 1991. Interactions among phytoplankton, periphyton, and macrophytes in temperate freshwaters and estuaries. Aquatic Botany, 41(1-3): 137-175.

Schmidt KA and Skidmore AK. 2003. Spectral discrimination of vegetation types in a coastal wetland. Remote Sensing of Environment, 85, 92-108.

Smith KL, Steven MD and Colls JJ. 2004. Use of hyperspectral derivative ratios in the red-edge region to identify plant stress responses to gas leaks. Remote Sensing of Environment, 92(2): 207-217.

Turpie JK, Wilson G & Van Niekerk L. 2012. National Biodiversity Assessment 2011: National Estuary Biodiversity Plan for South Africa. Anchor Environmental Consulting, Cape Town. Report produced for the Council for Scientific and Industrial Research and the South African National Biodiversity Institute.

Ustin SL, Gitelson AA, Jacquemoud S, Schaepman M, Asner GP, Gamon JA, Zarco-Tejada PJ. 2009. Retrieval of foliar information about plant pigment systems from high resolution spectroscopy. Remote Sensing of Environment, 113(Supplement 1): S67-S77.

Van Heerden IL. 2011. Management concepts for the Mfolozi flats and estuary as a component of the management of the iSimangaliso Wetland Park. In: Bate GC, Whitfield AK and Forbes AT (Eds.). 2011. A review of studies on the Mfolozi estuary and associated flood plain, with emphasis on information required by management for future reconnection of the river to the St Lucia system. Report to the Water Research Commission. WRC Report No. KV 255/10. Pretoria: WRC.

Wang L, Sousa WP, Gong P and Biging GS. 2004. Comparison of IKONOS and QuickBird images for mapping mangrove species on the Caribbean coast of Panama Remote Sensing of Environment, 91, 432-440.

Weepener HL, Van den Berg HM, Metz M and Hamandawana H. 2012. The development of a hydrologically improved Digital Elevation Model and derived products for South Africa based on the SRTM DEM. Water Research Commission (WRC) Report No. 1908/1/11. Pretoria: WRC.

Zomer RJ, Trabucco A and Ustin SL. 2009. Building spectral libraries for wetlands land cover classification and hyperspectral remote sensing. Journal of Environmental Management, 90, 2170-2177.

2 SPECTRAL DISCRIMINATION OF SIX EVERGREEN WETLAND TREE SPECIES AT LEAF-LEVEL SCALE

This chapter has been published as Van Deventer H, Cho M.A, Mutanga O. 2013, Do seasonal profiles of foliar pigments improve species discrimination of evergreen coastal tree species in KwaZulu-Natal, south Africa? In Conference proceedings of the 35th International Symposium on Remote Sensing of Environment, ISRSE, Beijing, China. Pp.1-12.

2.1 Introduction

The separability of six wetland tree species was assessed at leaf-level scale using biochemical and leaf reflectance measurements. First, we assessed whether foliar pigments (carotenoids and chlorophyll) and nutrients (nitrogen and phosphorous) for the six species were significantly different from one another using chemical laboratory analysis (Van Deventer et al. 2015a). If the foliar pigments and nutrients were to be significantly different, it was likely that absorption features related to these in the reflectance of the leaves could capture these differences and be optimised for species discrimination. Thereafter we investigated whether seasonal profiles of certain absorption features were unique to species and therefore enhance the separability of tree species using pigment profiles inferred from leaf spectra (Van Deventer et al. 2013; Van Deventer et al. 2015a). Important absorption features for species discrimination were determined through the selection of absorption features, which relate to plant properties, which showed a high coefficient of determination between leaf spectra and nutrients (Van Deventer et al. 2015a; Van Deventer et al. 2015c). These absorption features were effectively used to reduce the high dimensionality of the hyperspectral data for the tree species classification (Van Deventer et al. 2015b). Methods for transforming the data to remove the correlation between bands showed that the PLS-RF method was preferable above the PCA-RF method (Van Deventer et al. 2015b). The study further investigated which season achieved the highest accuracy to separate between tree species with no data reduction and transformation (Van Deventer *et al*. 2014). Lastly we investigated which are the most important spectral bands for separating tree species across seasons to improve the classification accuracies with data reduction, transformation and band selection, as well as whether combined seasonal information would improve the classification above a single season (Van Deventer et al. Submitted).

2.2 Study area

The iSimangaliso Wetland Park is situated in a sub-tropical coastal region with mean annual precipitation ranging from 1000 to 1500 mm on the coast, to below 1000 mm inland (Middleton and Bailey 2008). In summer, temperatures range from 23-30°C and can decrease to about 10°C during the winter (Sokolic 2006). A section of the park has been assessed in this part of the study, located between Catalina Bay in the north and the Maphelane node in the south, and from east of the DukuDuku forest in the west up to the coast in the east.

2.3 Methods

Six evergreen wetland tree species from the subtropical coastal, swamp and mangrove forests in the iSimangaliso Wetland Park, South Africa, were sampled along the uMsunduzi, uMfolozi and St Lucia estuarine systems over four seasons (winter, spring, summer and autumn) between 2011 and 2012 (Table 2.1).

Table 2.1: Number of tree species sampled across four seasons in the iSimangaliso Wetland Park, South Africa*.

Tree species	Common name	Acronym	Trees Winter (*n* =)	Trees Spring (*n* =)	Trees Summer (*n* =)	Trees Autumn (*n* =)	Total number of trees per species (*n* =)
Avicennia marina	White mangrove	AM	23 (21)	23 (21)	22 (21)	22 (21)	90 (84)
Bruguiera gymnorrhiza	Black mangrove	BG	20 (19)	19	20 (19)	20 (19)	79 (76)
Ficus sycamorus	Sycamore fig	FSYC	15	15	15	15	60
Ficus trichopoda	Swamp fig	FT	12 (11)	11	11	11	45 (44)
Hibiscus tiliaceus	Lagoon hibiscus	HT	31 (30)	31 (30)	30	30	122 (120)
Syzygium cordatum	Waterberry	SC	17	17	17	17	68 (68)
Total per season			118 (113)	116 (113)	115 (113)	115 (113)	464 (452)

** Species and number of trees were equalised for regression and classification purposes.*

Five leaves were sampled from the sun-exposed canopy of mature trees which are more than 2x2 m in size. Spectral measurements were taken from each leaf using an Analytical Spectral Device spectroradiometer (FieldSpec Pro FR, Analytical Spectral Device, Inc, USA.) according to the procedures previously published (Van Deventer et al. 2013; Van

Deventer et al. 2015c). The pigment concentrations of each leaf were determined using the Datt1998 index for carotenoids and Vogelman3 index for chlorophyll (Van Deventer *et al.* 2013). The foliar concentration of nitrogen and phosphorus were extracted for each season (Van Deventer et al. 2015c).

A One-way ANalysis Of VAriance (ANOVA), with a post-hoc Tukey Honest Significant Difference (HCD) multiple comparisons test, was undertaken to assess whether pigment concentrations differed significantly between seasons and species. The uniqueness of the mean seasonal pigment profile of species was assessed visually and with two similarity measures, including the Spectral Angle Mapper (SAM) and Sum of Euclidian Distances (ED). Thereafter we assessed whether seasonally-combined content of either carotenoids or chlorophyll improves the number of separable combination above a single season.

The varying relationship between nutrients and reflectance data was assessed through a linear regression between nutrient concentration and an NDVI-based vegetation index (Van Deventer et al. 2015c). The maximum coefficient of determination (R^2) for bands, which represent either the centre of known absorption features or established indices of plant properties, were compared between seasons to assess how the relationship changes and how the nutrients co-vary with other plant properties. The selected bands were then used for tree species classification, using a random forest (RF) classification algorithm, and comparing the accuracies of untransformed, as well as Principal Component Analysis (PCA) and Partial Least Square (PLS) transformations (Van Deventer et al. 2015b). RF was also used in assessing the season which achieved the highest classification accuracies using all the bands (Van Deventer *et al.* 2014), as well as for assessing the classification accuracies across seasons when using only selected bands (Van Deventer et al. Submitted). The importance of the selected bands was determined with RF for each of the seasons, with subsequent analysis of the accuracies of the band combinations according to importance rank (Van Deventer et al. Submitted).

2.4 Results

The concentrations of carotenoid and chlorophyll varied across the seasons for species (Van Deventer *et al.* 2013). While many species showed similarities of pigment profiles, exceptions were noted for some species. *Bruguiera gymnorrhiza*, for example, showed distinctly low levels of pigments compared to the other tree species (Figure 2.1). Visually, the mean seasonal profiles of the pigments for each species were unique (Figure 2.1), yet the

similarity measures attained accuracies < 52%. The combination of the pigment content of all four seasons, showed an improvement in species separability of between 27 and 29% compared to a single season (Van Deventer *et al.* 2013). Spring showed the highest percentage of separability for the concentration of pigments, whereas the combined seasons improved separability for carotenoids (Table 2.2).

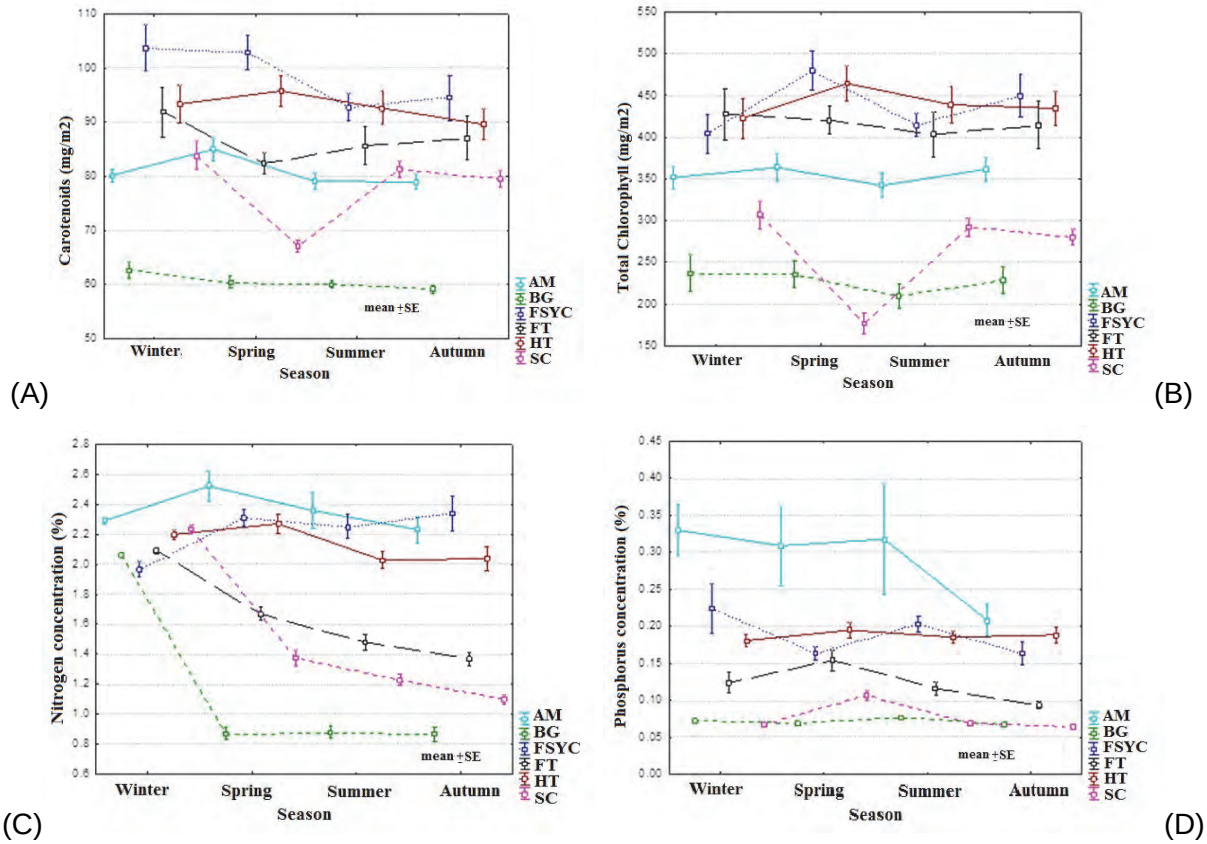

Figure 2.1: Mean seasonal profiles per species over four seasons for (A) carotenoids, (B) chlorophyll, (C) nitrogen and (D) phosphorous. Abbreviations of tree species: AM = *Avicennia marina*; BG = *Bruguiera gymnorrhiza*; FSYC = *Ficus sycamorus*; FT = *Ficus trichopoda*; HT = *Hibiscus tiliaceus*; SC = *Syzygium cordatum*.

Table 2.2: Percentage of comparable pairs that are significantly different ($p < 0.003$ Bonferroni corrected for 15 comparable pairs) between the foliar chemical content of six tree species across the four and combined seasons.

Season:	Carotenoids	Chlorophyll	Nitrogen	Phosphorous
Winter	47	27	40	53
Spring	67	67	73	20
Summer	40	47	67	20
Autumn	40	47	60	53
Combined	73	67	73	60

Foliar nutrient content also showed a high variability among the species, similar to the pigments. Similar to the pigments, the foliar nitrogen content showed the highest separability in the spring season and the highest separability of > 60% for the spring, summer and autumn seasons, compared to the foliar pigments and phosphorous content. The combined-seasonal data improved the separability for the carotenoids and nutrients. Twenty-two bands were selected which represented pigments, nutrients, foliage biomass, leaf water content, starch, lignin, tannins, pectin, protein and cellulose plant properties (Van Deventer et al. 2015c). Of all the seasons, winter showed the highest mean N content and lowest variability, whereas the other three seasons showed lower mean nitrogen values, and an increase in variability. In contrast, foliar P showed no significant differences between seasons (Van Deventer et al. 2015c). The relationship between foliar nutrient concentrations and N was lowest in the winter season, and highest for spring for many regions associated with co-varying organic constituents (Van Deventer et al. 2015c). The highest R^2 for N was recorded in the shortwave infrared (SWIR) for the band combination 2130 and 2240 nm. Across the seasons, P showed very low R^2 values, with the highest value recorded in autumn (R^2 = 0.38, $p < 0.01$) (Van Deventer et al. 2015c).

The classification of tree species using only the 22 bands (untransformed) at leaf level in spring resulted in an accuracy of 84%, a mere 2% less than the accuracy attained by 421 hyperspectral bands (Van Deventer et al. 2015b). The optimisation of the data through transformation and component reduction, showed the PLS-RF to outperform the PCA-RF model for both the overall and individual accuracies of the tree species (Van Deventer et al. 2015b).

Using all bands with no data reduction or transformation, the spring season was found to be the best season amongst the four to use for species discrimination (Van Deventer et al. Submitted). The highest overall accuracy was attained for spring, and the lowest for winter (Van Deventer et al. Submitted). The overall accuracy increased when the combined seasons were used.

The twenty-two bands relating to plant properties and used effectively for data reduction, showed variation in importance for species classification (Van Deventer et al. Submitted). A number of Shortwave Infrared region (SWIR) bands showed scaled conditional variable importance values of > 50% for all four individual seasons, including 2240, 2250 and 2300 nm, which are associated with absorption features relating to protein, starch and nitrogen. Bands associated with foliage biomass (740, 780 nm) and leaf water content (860 nm) achieved > 40% importance values in the winter and autumn seasons, though were ranked < 35% for the spring and summer seasons, with the exception of 740 nm in the spring season (near 70%). The bands associated with pigments (510, 680 nm) and leaf water content (1240 nm), lignin, tannins, pectin and protein (1630, 1690 nm) contributed the least (< 20%) to the classification. The band with the lowest importance value across all four seasons, was 1900 nm, related starch. In the combined seasons data, the foliage biomass band (740 nm) and leaf water content band (860 nm) also had importance values > 50% in addition to the three SWIR bands 2230, 2250 and 2300 nm, found important in the four individual seasons. For the combined seasons data, the pigment bands 510 and 680 nm increased in importance rank from < 20% for the individual seasons to > 50%. In all seasons the band 1900 nm, associated with starch, ranked the lowest in importance.

Using the 22 selected bands for data reduction and transforming the data to remove correlation using the PLS-RF algorithm, the overall accuracy (OA) showed variation across seasons from spring with the highest OA (90±0.6%) to winter with the lowest OA (83±0.9%) (Van Deventer et al. Submitted). The combined season showed a significant (p < 0.005, Bonferroni corrected) increase in the OA compared to the winter (increase of 9%) and summer (increase of 6%) seasons (Van Deventer et al. Submitted). No significant difference was noted between the OA of the combined season when compared to the spring and autumn seasons (< 2.7% difference). The OA of the spring and autumn seasons were also significantly (p < 0.005, Bonferroni corrected) higher to the winter and summer seasons respectively 8%, 6%, 5% and 4% (Van Deventer et al. Submitted).

2.5 Discussion

The six wetland tree species showed a high separability at foliar chemical level for nitrogen content across the spring, summer and autumn seasons (≥60% of the comparable pairs were separable). The tree species were separable for the pigments carotenoids and chlorophyll only during the spring season (67% of the comparable pairs were separable) however not in the other three seasons. Foliar phosphorus showed the lowest capability of

separating between the species across the four seasons. Secondly, the pigment content indicated that the spring season is the best season for separating between the six tree species (≥67% comparable pairs were separable), whereas a low separability was noted for leaf pigments in the winter, summer and autumn (< 47% of the comparable pairs were separable). Thirdly, tree species were more separable using the combination of the carotenoid and phosphorus content of the four seasons. The combination of seasonal biochemical content of chlorophyll and nitrogen resulted in similar number of separable comparable pairs achieved in the spring season. The biochemical results raised the expectation that absorption features which relate to these leaf chemicals will therefore be useful in the classification of tree species, mostly using nitrogen and to a lesser degree the foliar pigments (carotenoids and chlorophyll). Furthermore, the results also indicate that the spring season may be optimal for species discrimination and that combined seasonal information may improve species discrimination.

The study furthermore demonstrated that a changing relationship exists between leaf spectra and leaf nutrients across seasons and spectral regions. The co-variants of leaf nitrogen, chlorophyll and foliage biomass, did however not co-vary in spring and autumn. These results raised the question whether absorption bands of nitrogen would be more successful in separating between the six tree species during spring and autumn.

The leaf-level reflectance data resulted in an overall classification accuracy of > 83±0.9% across the individual and the combined seasons (Van Deventer et al. Submitted). Spectral bands from the SWIR region, relating to protein, starch and nitrogen contributed most to the separability of the tree species in a decision-tree classifier, whereas the other biochemical and biophysical parameters, such as pigments, foliage biomass and leaf water content varied in importance across the seasons. Similar to the results at leaf chemical level, the spring season showed the highest overall accuracy (90%±0.6) of all four individual seasons, and the combined seasonal information improved the classification accuracy (92±1.3) significantly compared to the winter and summer seasons.

Our results therefore suggest that tree species may be more separable when many plant properties, other than pigments, are considered. Both the foliar chemical data and classification of reflectance data indicated that nitrogen, lignin, protein, starch, cellulose, waxes, pectin, tannins, foliage biomass and leaf water content may contribute more to the separability of tree species compared to carotenoids or chlorophyll only. Many other studies

also suggested that the SWIR region, which relate to leaf structural components, has value in tree species classification (Van Deventer *et al*. 2015a).

The combination of data across phenological phases may capture unique phenological or growth patterns of species. Our study was however limited in spatial and temporal extent, the climatic region represented as well as in the number of species sampled. Further work is therefore required to assess whether these findings are relevant at image level, for other species and other regions.

2.6 References

Brus, DJ, Hengeveld, GM, Walvoort, DJJ, Goedhart, PW, Heidema, AH, Nabuurs, GJ & Gunia, K 2011. Statistical mapping of tree species over Europe. *European Journal of Forest Research,* 131(1): 145-157.

Cho, MA, Ramoelo, A, Debba, P, Mutanga, O, Mathieu, R, Van Deventer, H & Ndlovu, N 2013. Assessing the effects of subtropical forest fragmentation on leaf nitrogen distribution using remote sensing data. *Landscape Ecology,* 28(8): 1479-1491.

Middleton BJ, Bailey AK 2008. Water resources of South Africa, 2005 Study (WR2005) and Book of Maps. WRC Research Reports No.TT381/08 & TT382/08.

Nabuurs GJ, Brus DJ, Hengeveld GM, Walvoort DJJ, Goedhart PW, Heidema AH, Gunia K 2015, , *Tree species maps for European forests.* Available: http://www.efi.int/portal/virtual_library/information_services/mapping_services/tree_species_maps_for_european_forests/ [2015, March 6].

Sokolic F 2006. The use of satellite remote sensing to determine the spatial and temporal distribution of surface water on the Eastern Shores of Lake St Lucia. M.Sc. thesis. Durban, South Africa UKZN.

Van Deventer, H, Cho, MA & Mutanga, O In review. Improving tree species classification across four phenological phases with multi-seasonal data and band combinations: six subtropical evergreen trees as case study. *Manuscript submitted for publication,* .

Van Deventer, H., Cho, M.A. & Mutanga, O. 2015a. Using remote sensing for tree species discrimination in the narrow coastal forests of KwaZulu-Natal, South Africa. *XIV World Forest Congress.* WFC, Durban, South Africa, 7-11 September 2015.

Van Deventer H, Cho MA, Mutanga O, Mutanga O 2013. *Do seasonal profiles of foliar pigments improve species discrimination of evergreen coastal tree species in KwaZulu-Natal, South Africa?* in *Conference proceedings of the 35th International Symposium on Remote Sensing of Environment (ISRSE).* ISRSE, Beijing, China, pp. 1-12.

Van Deventer H, Cho MA, Mutanga O, Naidoo L, Dudeni-Thlone N 2014. *Identifying the best season for mapping evergreen swamp and mangrove species using leaf-level spectra in an estuarine system in KwaZulu-Natal, South Africa.* in , eds. F.A. Ahmed, O. Mutanga & E. Zeil-Fahlbusch,*10th International Conference of the African Association of Remote Sensing of the Environment (AARSE).* , http://www.aarse2014.co.za/programme.html#programme edn, AARSE, University of Johannesburg, South Africa.

Van Deventer, H, Cho, MA, Mutanga, O, Naidoo, L & Dudeni-Tlhone, N 2015b. Reducing leaf-level hyperspectral data to 22 components of biochemical and biophysical bands optimises tree species discrimination. *IEEE-JSTARS,* January.

Van Deventer, H, Cho, MA, Mutanga, O & Ramoelo, A 2015c. Capability of models to predict leaf N and P across four seasons for six subtropical forest evergreen trees. *ISPRS Journal of Photogrammetry and Remote Sensing,* 101: 209-220.

3 MAPPING ESTUARINE HABITAT TYPES

M. Lück-Vogel, C. Mbolambi, K. Rautenbach, J. Adams, L. van Niekerk .

3.1 Introduction

The St. Lucia estuary is part of the uMfolozi/uMsunduzi/St Lucia estuarine system which forms the largest fluvial coastal plain in South Africa (Van Heerden, 2011) and the largest estuarine system in Africa (155 000 Ha). As part of the iSimangaliso Wetland Park it hosts the highest biodiversity of wetland habitat types for its size in the whole of southern Africa (Cowan, 1999). However, the paucity of spatial-temporal information on estuarine vegetation composition and distribution in South Africa currently undermines a holistic understanding of estuarine processes and functioning and subsequently the prediction of impacts of major environmental changes. Mapping of the estuarine vegetation would provide a baseline for understanding and monitoring of estuarine biological processes.

Remote sensing is widely viewed as an effective way to spatially-continuously undertake inventories of vegetation composition, distribution and condition, particularly in large and inaccessible regions in many regions of the world. However, in coastal and estuarine environments, the very small scale of the habitats, frequently in form of narrow bands along the shore, prohibited the application of remote sensing until recently, as most of the “conventional” satellite images successfully used in other environments did not provide enough spatial detail. Examples are the Landsat 4 to 8 series and the MODIS and NOAA AVHRR sensors. Only with the recent upcoming of very high resolution (VHR) imagery e.g. from the SPOT-6, RapidEye and Worldview-2 sensors which provide multispectral imagery with pixel sizes between 2 and 6 meters, remote sensing of coastal regions has become more feasible. In addition, topographic information derived from airborne LiDAR (Light Detection and Ranging) technology has proven to improve coastal vegetation mapping significantly, in particular when used in combination with multispectral imagery.

The aim of this work was therefore to test and compare the use of VHR SPOT-6, RapidEye and WorldView-2 (WV2) satellite imagery with and without combination of LiDAR data for mapping relevant vegetation types in the St. Lucia estuary.

In order to add value to real-world estuarine management conditions, the classes to be mapped were aligned with existing habitat keys (e.g. from the National Biodiversity Assessment, 2012). The intention was to provide guidance on which sensor or sensor

combination provides the most accurate spatial information for informing mapping and estuarine management, including those areas not under formal protection. The methods, results and challenges are presented below.

3.2 Study area

The St. Lucia system is divided into False Bay, North Lake, South Lake and the Narrows. Five rivers drain into the system, in order from north to south, the uMkuze, Mzinene, Hluhluwe, Nyalzi and Mpate Rivers. In the south the estuary mouth is connected to the Indian Ocean by the 21 km long Narrows channel. The lake system is separated from the sea by high coastal dunes that flank its eastern bank (Taylor, 2006). The focus of this project component however was on the estuarine areas below the 10 metre contour.

The predominant natural estuarine vegetation in the region can be divided into 8 habitat units, namely permanently flooded macroalgae and submerged macrophytes, partly flooded reeds and sedges and salt marshes, mangroves and swamp forests, and grass and shrub vegetation, and lastly floating macrophytes. Table 3.1 below summarises the dominant species and gives a brief description of these habitat types.

Table 3. 1: Habitat units and their dominant species (Rautenbach, 2015).

Habitat Unit	Dominant Species	Description
Macroalgae	*Ulva intestinalis*, *Chaetomorpha* sp., *Cladophora* sp., *Bostrychia* sp. and *Polysiphonia* sp.	Found at estuary margins, as epiphytes and associated with mangrove pneumatophores
Submerged macrophytes	*Ruppia cirrhosa*, *Zostera capensis* and *Stuckenia pectinata*	Plants rooted in substrata whose leaves and stems are completely submersed. Found predominantly in the Narrows
Reeds and sedges	*Phragmites australis*, *Juncus kraussii* and *Schoenoplectus scirpoides*	Observed at sites with freshwater input at the margins, rooted in submerged substrata. *Juncus kraussii* is observed at the vicinity of the Forks and the Narrows.
Mangroves	*Avicennia marina* and *Bruguiera gymnorrhiza*	Observed in the brackish to saline intertidal areas at the Narrows and mouth area
Grass and shrubs	*Sporobolus virginicus*, *Paspalum vaginatum* and *Stenotaphrum secundatum*	Sedge grass and shore slope lawn, observed in areas where there is no freshwater input, freshwater is provided by rainfall
Salt marsh	*Sarcocornia* sp., *Salicornia meyeriana* and *Atriplex patula*	Succulent species colonize exposed saline soils in False Bay and in the mudflats of North Lake and are not tolerant to long periods of inundation
Swamp forest	*Ficus trichopoda*, *Barringtonia racemosa* and *Voacanga* sp.	Observed on the banks of uMfolozi Estuary, in the vicinity of the back channel and Narrows and along the Eastern Shores under freshwater conditions.
Floating macrophytes (not used in this study)	*Nymphaea nouchal*, *Azolla filiculoides*	Floating leaved species are commonly associated with submerged and deepwater aquatics and occur at water depths from 0.5 to 2m

Land use in the vicinity of the estuarine system is diverse. It includes commercial (sugarcane) crop production, subsistence agriculture, mining, tourism, commercial and subsistence forestry, conservation as well as residential areas. While each of these activities benefits from the ecosystem services of the estuarine systems, they also impact on the condition in a cumulative way.

The land use in the area changed dramatically during the last 2 decades. Before the establishment of the Wetland Park, large areas have been used for commercial forestry, introducing alien Eucalypt and Pine species. Since the creation of the Wetland Park, forestry is receding, and international eco-tourism is becoming more important. On the abandoned forestry units, a quick succession of natural vegetation can be observed. Furthermore, an expansion of rural settlements into the area due to a massive population increase (immigration from Mozambique and other areas), puts another pressure on natural environments.

3.3 Input data

3.3.1. Reference habitat map

As reference map for this study an existing GIS map based on aerial imagery from 2008 was used. The map delineates habitats below the 5m contour. This map was originally generated by Nondoda (2012). A modified version of this map as presented by Rautenbach (2015) has been used for this study which aggregates some of Nondoda's original classes. Accuracy and spatial detail was considered suitable for our purpose. The habitat classes derived from this data set are summarised in Table 3.2:

Table 3.2: Estuarine habitat types used by Rautenbach (2015).

Submerged Macrophytes
Salt Marsh
Reeds
Swamp Forest
Grass and Shrubs
Groundwater-fed communities
Juncus
Mangroves

These classes are largely the same as in Table 3.2 above, with the only difference that the class "Reeds and sedges" in Table 3.2 here is subdivided into the individual classes Reeds, Groundwater-fed communities and Juncus.

Figure 3.1 below shows a subset of Rautenbach's classification for the area around St Lucia town. Note however that some of the classes, e.g. submerged macrophytes, did not occur in the displayed region.

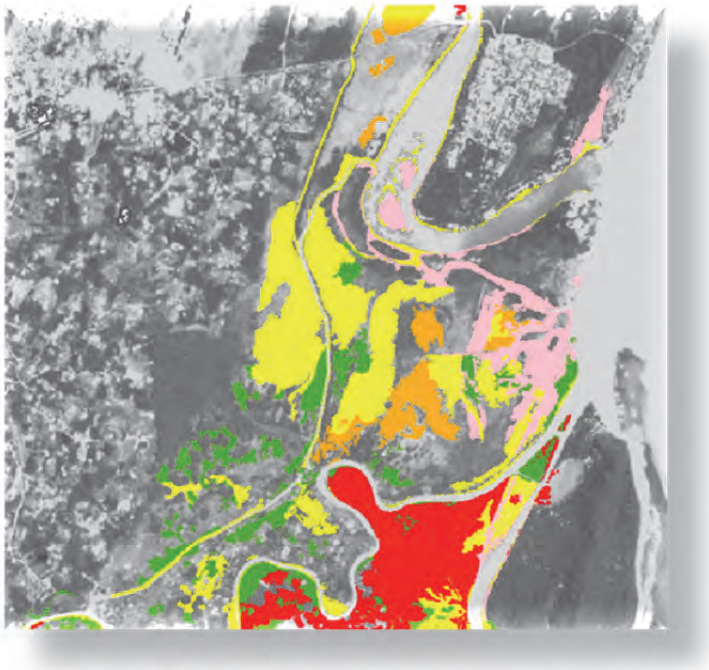

Figure 3. 1: Subset of 2008 habitat classification map (Rautenbach 2015). Colours correspond to classes as in Table 3.2. Grey-scale background: RapidEye band 4 (red edge).

3.3.2. LiDAR data

In 2013, the company AAM developed for the iSimangaliso Wetland Park's GEF project "Development, Empowerment and Conservation in the iSimangaliso Wetland Park and Surrounding Region Project" a Digital Terrain Model (DTM)[1] covering the iSimangaliso Wetland Park area. The data consist of high accuracy (1 Sigma) point data of LiDAR derived surface information, which has been provided in xyz ASCII format as well as in 0.25 m contours in SHP file format. The ASCII format contains very detailed surface information. However, files tend to be huge, and require special software to access. In contrast, the SHP format is a format that most GIS practitioners can readily use, however, the generalisation of the information to derive 25 cm contours means a loss of detail. In order to assess the impact of this loss of detail on the habitat classification accuracy, in this project, we used both the SHP file contour product and the raw, unthinned xyz point cloud data binned to 1 meter.

3.3.3. Satellite imagery

For this project, a series of high resolution data was acquired from the respective commercial satellite data providers. Table 3.3 below gives an overview of the respective

[1] *A digital surface model represents the highest elevation at a point, including also tree canopies and buildings. In contrast, digital terrain models represent only soil surface elevation.*

sensors, the spatial resolution, the available spectral bands and the respective acquisition dates.

While the listed SPOT-6 and RapidEye images are covering about the entire area which has been mapped by Rautenbach (2015), the available WorldView-2 imagery unfortunately only covers the southern part of that area, as the purchase of the more images would have exceeded the project budget (Figure 3.2).

Table 3.3: Satellite data used and their specifications

Sensor	Resolution (m)	Spectral bands	Acquisition Date
WorldView-2	2.0	8: Coastal, B, G, Y, R, RedEdge, NIR1, NIR2	9 Apr. 2010
RapidEye	5.0	5: B, G, R, RedEdge, NIR	18/20 July 2011
			13 Jan. 2012
SPOT6	5.0*	4: B, G, R, NIR	8 Feb. 2014
LiDAR	Rasterised to match above	"1"	ca. July/Aug. 2013

3.3.4. Areas used for classification approach

For the supervised classification approach, not the full coverage of available images was used, but only subsets of the total satellite coverage which corresponded largely with the extent of the Wetland Park and Rautenbach's habitat map. In this way, land cover and habitat classes were largely excluded for which no reference data were available and whose accuracy could not have been assessed (e.g. any agriculture and other transformed areas). Included in the accuracy assessment however, were only areas below the 5 metre contour (the Estuary Functional Zone as required for the development of Estuary Management Plans and Estuary Water Requirement studies).

Figure 3.2 shows the full spatial extent of Rautenbach's map. The available RapidEye and SPOT-6 data cover about the full extent of Rautenbach's area (the coloured patches), while for WorldView-2, only for the southern part of Rautenbach's data imagery was available.

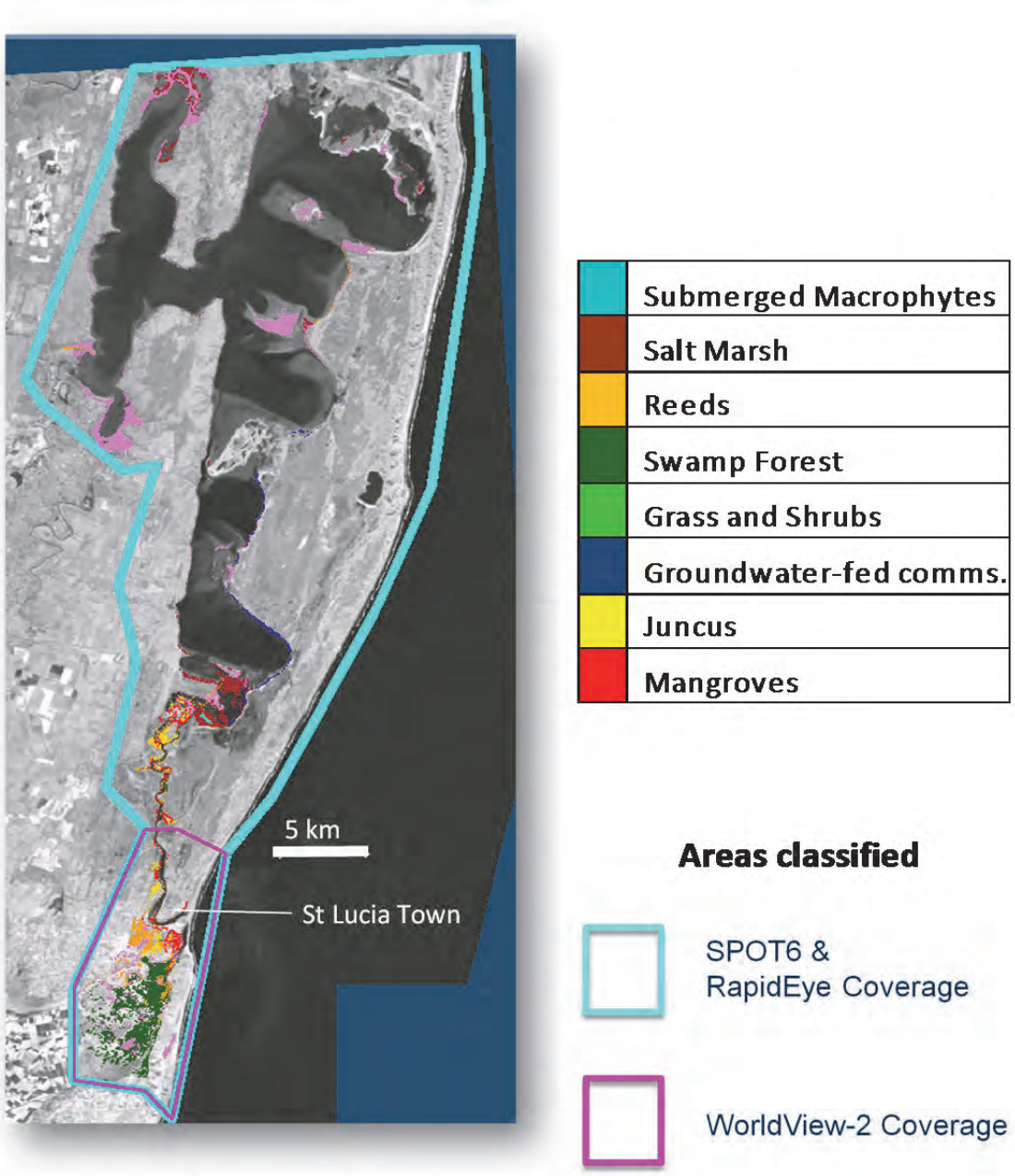

Figure 3. 2: Outline of Study area. Discontinuous colour patches: 2008 habitat reference map (Rautenbach, 2015) and the outline of the high resolution image areas (subsets) assessed in this project. Grey-scale background: NIR band of RapidEye 2011 image.

3.4 Methods

3.4.1. Data pre-processing

The final goal of comparing habitat classifications derived from different combinations of input data has been achieved following several pre-processing, data conversion and data generation steps. The individual pre-processing, classification and post-processing steps are unpacked in the following sections.

As a first step, all 15 satellite image files were corrected for radiometric and atmospheric effects using ATCOR-2 software, version 8.3.1, implemented in IDL (Richter & Schläpfer, 2014). This correction allowed for better analysis of the spectral signatures in the actual classification approach as described below.

The RapidEye image for July 2011 was provided as seven individual tiles from two separate acquisition dates (18 and 20 July 2011), the RapidEye image for 13 January 2012 as six individual tiles. The mosaicking of the individual RapidEye tiles allows for an easier handling of the data in the following work steps (two images instead of 13, plus one SPOT-6 and one WorldView-2 image).

Some of the satellite images originally came in UTM projection with WGS84 Datum, while others were provided in Transverse Mercator projection. It was decided to reproject all images to the projection of the 2008 reference data: Transvers Mercator, Meridian 33, Hartebeesthoek 1994 Datum, Scale factor 1.0. In this way, the best possible geographical match was achieved. It is important that the images to be classified overlay with high geographic accuracy to the reference data, as spatial misalignments can easily lead to misclassifications and reduced accuracies (Townshend *et al*., 1992).

The LiDAR data for that area were provided in individual small tiles as well. Therefore, in a first step, those tiles were identified which cover the SPOT-6, RapidEye and WV-2 mosaics. For those, both, the 25cm contour SHP files as well as the unthinned xyz ASCII files binned to 1m resolution were converted into a raster format matching the spatial resolution of the respective multispectral images (2m, 5m resp.). The individual raster tiles were then mosaicked and reprojected to match the projection of the multispectral mosaics. Figure 5.3 below illustrates the differences in details in the 1m, 2m and 5m rasters derived from the unthinned ASCII point cloud, the 25 cm contours and unthinned point clouds respectively.

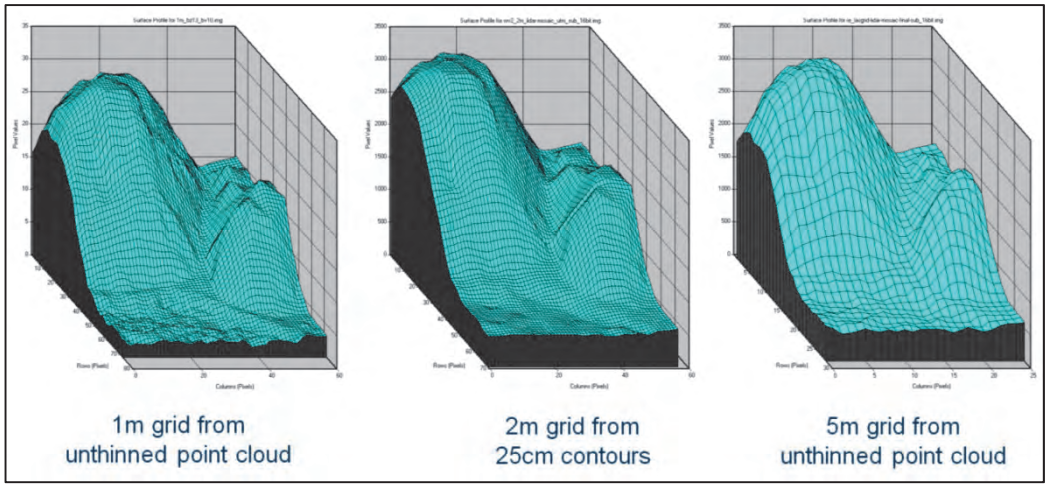

Figure 3. 3: differences in details in the 1m, 2m and 5m rasters derived from the unthinned ASCII point cloud, the 25 cm contours and unthinned ASCII point clouds respectively (from left to right). Displayed is a 28 metre high coastal dune with its landward slope south of the St Lucia estuary.

The data format was then changed from the original float range to unsigned 16bit. This was done to enable the stacking of the LiDAR data with the unsigned 16 bit format of the multispectral data. During this step, the value range of the LiDAR data has also been "stretched" to better match the value range of the multispectral bands.

In a final pre-processing step, the multispectral mosaics were then combined with the respective re-scaled LiDAR data. The bands of the resulting data stacks are illustrated in Table 3.4 below.

Table 3. 4: Bands of the respective layer stacks used for the supervised classification process.

Band No	WV-2	RapidEye 2011/12	SPOT-6
1	Coastal	Blue	Blue
2	Blue	Green	Green
3	Green	Red	Red
4	Yellow	RedEdge	NIR
5	Red	NIR	LIDAR
6	RedEdge	LIDAR	
7	NIR1		
8	NIR2		
9	LIDAR		

Altogether 8 (4x2) data stacks were produced as input for the classification process:

1. the multispectral bands plus the “degraded” 25cm contour-based LiDAR information
2. the multispectral bands plus the original xyz data based LiDAR information.

3.4.2. Generation of ground reference data

The training and validation data were extracted from the 2008 reference map (section 3.3), consisting of 8 habitat classes:

- Grass and shrubs
- Ground water fed communities
- Juncus (sedge)
- Reeds
- Salt marsh
- Submerged macrophytes
- Swamp forest
- Mangroves

Stratified random points were extracted for all 8 classes. It was aimed to create a minimum of 20 points per class. This approach was run twice, first for the whole extent of the reference map (and covered by the RapidEye and SPOT-6 images) and secondly only for the southern part which was covered by the WV-2 image, in order to create a sufficient number of points for that smaller area, too. The resulting points were then evenly split and the one half saved for use as training points for the classification process and the other half for use in the validation of the classification results.

For all resulting points it was visually verified if any of them was in an area impacted by clouds or cloud shadows in any of the 4 images. Impacted points were deleted to avoid biases in the classification and validation approach. This approach circumvents the approach of masking out cloud-infested areas in the satellite images.

Further, it was decided to create additional random points for the land cover classes open water and bare soil, as we believed that these classes are 1. highly important in an estuarine and coastal context and 2. as the inclusion of training points for these classes would improve the overall accuracy of the supervised maximum likelihood classification in narrowing the actual feature space for all classes.

For the identification of open water and bare soil area, the normalised Difference Vegetation Index (NDVI) was calculated for all four images, following the formula NDVI = (NIR- Red) / (NIR + Red). The value range for NDVI data is from -1 to +1. It is generally accepted that NDVI values for open water are lower than 0, and values for bare soil are in the positive range, just above 0, if images are derived from radiometrically corrected images, as in our case.

Visual inspection of the actual NDVI data confirmed this rule, only for the RapidEye-derived NDVI data the threshold between water and bare soil had to be slightly modified for a proper distinction between the two classes.

Table 3.5 below shows the value ranges that were used in the next step, the generation of binary masks for water and bare soil respectively, using the ERDAS Spatial Modeller.

Table 3. 5: Value ranges used for stratification of NDVI data for the classes water and bare soil.

Land cover type	NDVI range WV-2	NDVI range SPOT-6	NDVI range RapidEye
Water	< 0	< 0	< 0.1
Bare soil	0-< 0.4	0-< 0.4	0.1-< 0.4

The threshold of 0.4 for delineating bare soil from vegetation has been defined visually from the image, using fallow fields, roads and the beach as reference. Strictly spoken though, our class “Bare Soil” is likely to include some sparse vegetation, too.

From the derived binary masks, 50 random points per class were extracted, split into two subsets and added to the respective training and validation point SHP files generated for the habitat data. Points impacted by clouds and cloud shadows were removed for these classes as well. For the resulting 10 habitat classes (2008 habitats plus water and bare soil), between 170 (WV-2) and 295 (RapidEye) training and validation points respectively were used. The variation in point numbers is related to the amount of points which had to be deleted due to cloud and cloud shadow impact.

3.4.3. Maximum Likelihood classification

For all four images spectral training signatures were created for all respective training points for all eight respective layer stacks (MS plus 25cm contour-derived DSM, and MS plus xyz-derived DSM). The resulting spectral signatures were cleaned from obvious spectral outliers that would have contributed to biased spectral statistics in the following classification

process. Outliers were caused mainly by changes in land cover in the time between the reference data (2008) and the actual image acquisition date, such as forest plantation to grass and shrubs, or grass and shrubs to swamp forest. Where the analysis of the spectral signatures revealed that there are spectral subgroupings within one of the reference classes, these subclasses were treated as individual classes during the classification process. As an example, the class “Grasses and Shrubs” consisted of areas which were clearly dominated by shrubs, while other areas were dominated by grasses, resulting in more tree or grass dominated spectral signatures. Here subclasses “Grass and shrubs-woody” and Grass and shrubs-grassy” were created. Or some of the reeds were obviously flooded during the image acquisition date and looked spectrally different from non-flooded reeds. Keeping these spectrally different subgroups of a class separate in the actual classification process has shown to produce higher classification accuracies.

The classification process was then run on both LiDAR-version stacks for each image, first including all spectral bands per image stack, i.e. including the LIDAR band, and then excluding the LiDAR band. For all classifications, Feature Space was selected as non-parametric rule and Maximum Likelihood as parametric rule in ERDAS’ Supervised classification tool.

3.4.4. Post-Processing

Given the high spatial resolution of the satellite images, the eight classification results looked very “noisy”. This means that the vegetation types were disrupted by single classes or groups of pixels of another class, mainly as a result of shadow effects in the vegetation canopy. It was therefore decided to filter the classification outputs to eliminate those miss-classified single pixels or small pixel groups consisting of < 8 pixels (Figure 3.4).

Further, where existing, the interim subclasses (e.g. Juncus-flooded and Juncus-non-flooded) were merged again to the original class types. This had to be done to have the same level of class detail as Rautenbach’s habitat map for accuracy assessment purposes.

As the accuracy assessment showed frequent confusion between the classes Juncus and Reeds (section 3.4.5), both classes in the classification results of the four stacks including the xyz-LiDAR DSM were merged into one new class “Juncus and Reeds”. In order to allow for accuracy assessment, these classes were also merged in the ground validation points.

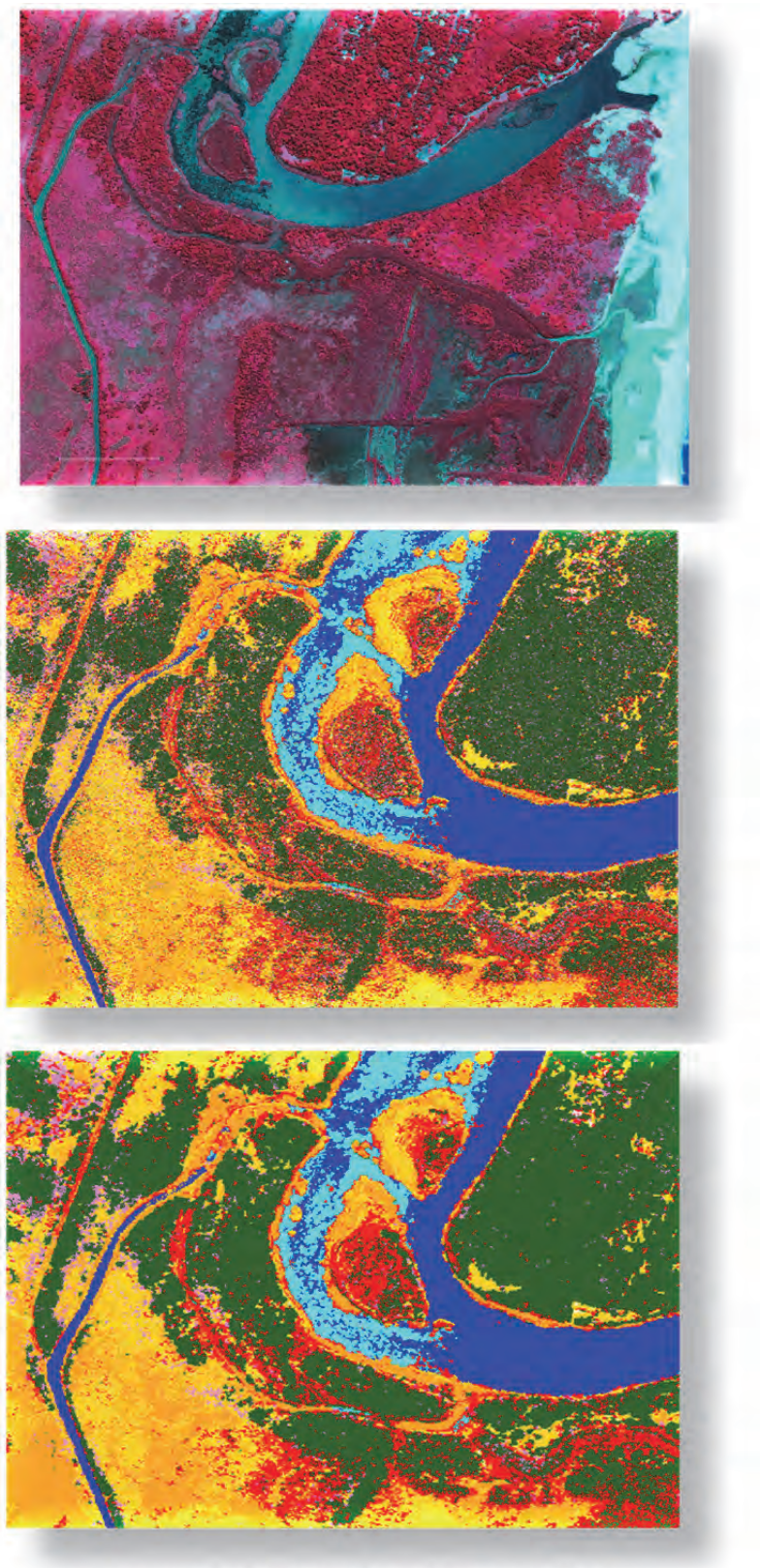

Figure 3. 4: Illustration of filtering effects.
Top: Multispectral WV-2 image for the estuary mouth.
Centre: raw classification output with lot of "noise".
Bottom: classification results for same area, after filtering process.

3.4.5. Accuracy Assessment

Using ERDAS's Classification accuracy assessment tool, error matrices including the Overall Accuracy, the User's and Producer's Accuracy, the Errors of commission and omission for each class as well as the Kappa coefficient were produced and analysed, based on the accuracy analyses with the validation points.

3.5 Results & Discussion

Table 3.6 below gives an overview of the Overall Accuracies and Kappa values for all 20 classification runs.

Table 3. 6: Overview of accuracies of all classifications

	WV-2 2010		RE 2011		RE 2012		SPOT6 2014	
	overall accuracy	kappa	overall accuracy	kappa	overall accuracy	kappa	overall accuracy	kappa
multispectral (MS)	65.8	0.58	51.1	0.45	52.2	0.46	65.1	0.61
MS + LiDAR from 25 cm contours	68.4	0.61	56.1	0.51	56.7	0.51	63.6	0.59
MS	72.4	0.66	50.0	0.44	52.2	0.47	64.9	0.61
MS+ LiDAR from raw xyz	72.4	0.66	61.4	0.57	50.9	0.45	70.7	0.67
MS+ LiDAR from raw xyz fused*	79.0	0.73	64.6	0.60	51.9	0.45	73.7	0.70

*: fused = classes Juncus and reeds merged

3.5.1. Impact of LiDAR DSMs on classification accuracies

Table 3.6 shows the overall accuracies and kappa values for all 20 classification runs. Generally overall accuracies above 70% are considered satisfactory. The Kappa value is another frequently used accuracy indicator. It indicates to which probability the derived classification is different from a random classification. This means that a kappa of 0.5 indicates that with 50% probability this class is different from a random classification. Compensating for differences in sizes of validation sample numbers, kappas are frequently lower than producer's, user's and overall accuracies.

Table 3.6 shows that in 5 out of the 8 classifications the additional use of the LiDAR derived DSM information improved the classification accuracies (rows 1 to 4 in Table 3.6). In the case of the second run of the WorldView-2 image, while causing differences in individual class accuracies, the LiDAR did not change the overall accuracy (rows 3 and 4). The LiDAR deteriorated the classification results for the first run of the SPOT-6 image (rows 1-2) and the second run of the 2012 RapidEye image (rows 3-4).

The overall accuracies and kappas for the purely multispectral based classifications of the first and second run are about the same for the RapidEye and SPOT-6 images, which was to be expected (rows 1 and 3). However there is a significant improvement in the second run of the WorldView-2 image (row 3). This might be caused by a slightly better selection of training signatures in otherwise identical classification sets.

Accuracies for three of the four classifications including the detailed LiDAR information in the second run (row 4) are higher than the respective accuracies for the contour-derived LiDAR stacks (row 2). This indicates that the use of more detailed surface data improves vegetation classification accuracies.

3.5.2. Classification anomalies between Juncus, Reeds and Grass and Shrubs

Table 3.7 shows the error matrix for the second run classification result of the WorldView-2 classification (row 4 in Table 3.7) including the detailed xyz-derived LiDAR data. This matrix below shows how many of the reference samples have been classified correctly. For example, of the 21 validation points for the class Reeds, 6 points have been classified correctly, 9 have been classified as Grass and Shrubs and 6 as Juncus. Altogether, 11 points have been classified as Reeds (Row total), 6 of which are in fact Reeds, but for the 11 should have been classified as Juncus and 1 as Grass and Shrubs. The last columns give the respective Producer's and User's Accuracy and Kappa value per class.

Table 3. 7: Error matrix for the WorldView-2 classification on the stack including the xyz-derived LiDAR information. Strikingly bad accuracies highlighted in red.

LASGRID LIDAR			Overall Classification Accuracy = 72.37%								
test-all-sigs-2_recode.img			Overall Kappa Statistics = 0.6571								
									Producers	Users	
Classified Data	Reeds	Sw. for.	Gr. & Shr.	Juncus	Mangr.	Water	Bare	Row Total	Accuracy	Accuracy	Kappa
Reeds	6	0	1	4	0	0	0	11	28.6%	54.6%	0.47
Swamp forest	0	45	2	0	1	0	0	48	81.8%	93.8%	0.90
Grass and Shrubs	9	9	13	1	1	0	0	33	68.4%	39.4%	0.31
Juncus	6	0	1	3	0	0	0	10	37.5%	30.0%	0.26
Mangroves	0	1	1	0	7	0	0	9	70.0%	77.8%	0.76
Open water	0	0	0	0	0	22	0	22	88.0%	100.0%	1.00
Bare soil	0	0	1	0	1	3	14	19	100.0%	73.7%	0.71
Column Total	21	55	19	8	10	25	14	152			

Table 3.7 shows that the accuracies for 4 of the 7 classes with Kappas > 0.7 are quite good, including the classes bare soil and water, which, because of their spectral distinctness from any vegetation classes, in most land cover classifications yield very high accuracies. However, the classes Grass and Shrubs, Juncus and Reeds got confused with each other to

a great extent, leading to Kappas as low as 0.26 and Accuracies as low as 28.6% (red values in Table 3.13). The analysis of the other 7 classifications of the first and second runs shows the same confusion between these three classes.

The reasons for this low representation could not establish with a high degree of certainty during this study but could be contributed to the following:

1. True vegetation change: the estuary experienced significant water level and salinity changes during the observation period. This might have led to true vegetation changes if compared to the situation in the reference data in 2008. This would mean that the WV-2 image from 2010 should be the least affected by this aspect, given the greatest temporal “proximity” to the 2008 reference data, and the SPOT-6 image from 2014 being the worst. This gradient in accuracy could not be observed though, as the effect of some obvious changes have been eliminated during the selection of training and reference data (exclusion of points where obvious changes were visible in the images, see section 3.4.2). High dynamics in the estuarine vegetation have also been reported by Rautenbach (2015) for the period 2008-2013.
2. Spectral similarity between the classes: The more grassy areas of the class Grass and Shrubs might have been misclassified with the non-woody sedges and reeds. And reeds might have been confused with sedges.
3. Small scale vegetation mosaic: in case that the vegetation on the ground appears in form of a mosaic of small patches of different vegetation types and that this patchiness had been “generalised” in the 2008 reference map, this might misdirect the classification in that either the classifier picked variations up correctly but the generalised reference data wrongly negated it, or in the form of spectral mixed pixels, which are “blurry” and do not pick up boundaries between patches correctly.
4. Different water levels: All three vegetation types are bound to sites which are low lying and prone to (and dependent on) various levels of flooding. So even if the vegetation itself did not change between the image and the reference date, various levels of flooding, spatially and temporally, might have biased the spectral signatures and lead to confusion between these classes.
5. Accuracy of the reference data: Unfortunately the confidence/resolution of the reference vegetation map over the entire study area could not be established. Nondoda (2012) however mentioned some problems with the 2008 aerial images due to smoke plumes for the northern Lake area. It can therefore not be excluded, that those three classes have been confused in the original data by Nondoda (2012).

However, for the purpose of estuarine environmental management and reporting, in South Africa a distinction is not always made between the classes Juncus (or sedges) and Reeds (NBA: Turpie et al., 2012, Van Niekerk and Turpie, 2012). Therefore we found it legitimate to merge these two classes in an additional post processing step (section 3.4.4) and validated these classifications as well. This aggregation has been done in the final version of Rautenbach (2015) as well. As the results in row 5 in Table 3.7 show, this step improved all classification results significantly, apart from the 2012 RapidEye result, where the improvement was incremental. This leads to the conclusion, that in those cases where the merging of the two classes did not significantly improve the overall classification accuracies, these were not the (only) problematic classes and that the reasons for the low accuracy have to be sought elsewhere.

3.5.3. Analysis of accuracies of other classes

Out of all classes over all 20 classifications, the classes Submerged macrophytes and Swamp forest were the only classes with consistently high accuracies. While in the case of Swamp forest, being spectrally very distinct from all other classes, this result is not surprising, is it unexpected for Submerged macrophytes. The reasons for this result will have to be further investigated. Further, the classes Bare soil and Open water have been delineated largely accurately – as expected, apart from the RapidEye classifications, which are analysed in more detail in the following sections.

As discussed above, accuracies for Grass and Shrubs were consistently low, the same as for Groundwater fed communities. The latter is a summary class for various different classes (i.e. it includes a range of plant/habitat types that are ground-water dependant). This habitat type can also be patchy in nature. Therefore, the botanical and spectral heterogeneity of this class, as well as different water/flood levels, could be a reason for the misclassifications.

Accuracies of the remaining classes, Salt marsh, Reeds, Juncus, Mangroves, Juncus & Reeds either provided consistently moderately satisfactory results or varied between very high and very low accuracies between the individual runs.

3.5.4. Comparison of accuracies between sensors

Generally, WorldView-2 produced the best accuracies and SPOT-6 the second best results, while all the RapidEye classifications produced strikingly low accuracies (Table 3.7) with overall accuracies between 50.0 and 64.6% and Kappas as low as 0.44 to 0.60. The good

WV-2 performance is as expected, given the greatest temporal “proximity” to the 2008 reference data.

Surprisingly, the 2014 SPOT-6, being the furthest away from the 2008 reference data and only having only 4 spectral bands and a pixel size of 5 meters, yielded the second highest accuracies. This is unexpected, as misclassification due to habitat change during the 6 years between reference data and image acquisition might have been expected to lead to misclassification. This again points out the merit of the visual filtering for temporal effects during the generation of the reference points (section 3.4.2).

It might be premature though to conclude that WorldView-2 with its highest spectral and spatial resolution (8 bands, 2m pixel size) is the most appropriate sensor for estuarine habitat classification, as, given to the smaller extent of the available image, the total number of classes was lower than in the other images with Submerged macrophytes, Salt marsh and Groundwater fed not occurring in that area. A lower number of classes usually increase classification accuracies.

RapidEye however, with 5 spectral bands and also 5 meter pixel size produced unsatisfactory results for many classes for both images. The reasons for the bad RapidEye performance are analysed further in the following section.

3.5.5. Analysis of RapidEye results using environmental data

Table 3.8 shows the error matrix of for the 2011 RapidEye classification on the stack including the xyz-derived LiDAR information as a typical example for the RapidEye results. Strikingly bad accuracies are highlighted in red.

Table 3. 8: Error matrix for the 2011 RapidEye classification on the stack including the xyz-derived LiDAR information. Juncus and Reeds merged into one class. Strikingly bad accuracies highlighted in red.

LASGRID LIDAR__FUSED					Overall Classification Accuracy =	64.55%							
2011-07-18_re_plus-lasgrid-lidar_ml-no-dunes-no-flooded_recode-fus					Overall Kappa Statistics = 0.5964								
											Producers	Users	
Classified Data	Submerged	Salt Marsh	Sw. forest	Gr. & Shr.	GW. Fed	Mangr.	Water	Bare Soil	Juncus & R.	Row Total	Accuracy	Accuracy	Kappa
Submerged Macroph.	20	0	0	0	0	0	0	0	0	20	87.0%	100.0%	1.00
Salt Marsh	0	20	0	4	5	0	1	0	2	32	83.3%	62.5%	0.58
Swamp forest	0	0	22	5	0	2	0	0	3	32	75.9%	68.8%	0.64
Grass & Shrubs	0	2	0	7	0	3	0	7	6	25	33.3%	28.0%	0.20
Groundw. Fed comms.	0	0	0	1	7	1	0	0	3	12	58.3%	58.3%	0.56
Mangroves	0	0	3	0	0	17	0	0	1	21	68.0%	81.0%	0.79
Open Water	0	0	0	0	0	0	9	0	0	9	39.1%	100.0%	1.00
Bare Soil	3	1	0	0	0	0	13	11	1	29	61.1%	37.9%	0.32
Juncus & Reeds	0	1	4	4	0	2	0	0	29	40	64.4%	72.5%	0.65
Column Total	23	24	29	21	12	25	23	18	45	220			

The merged class Juncus & Reeds produces better accuracies than the individual classes, but – as expected – still gets confused with Grass and Shrubs. However, in this image, Grass and Shrubs also got confused with Bare soil. It has to be remembered though, that the Bare Soil mask was produced using an NDVI threshold of 0.4, which is likely to include sparsely vegetated areas as well (compare section 3.4.2). It is therefore possible that some open Grass and Shrub areas, maybe areas recovering after vegetation die-back/removal wrongly fell into the bare soil class. Further, probably the more woody fraction of the Grass and Shrubs class got confused to a greater extent with the other two woody classes Swamp forest and Mangroves. Apparently RapidEye's spectral resolution was not good enough to distinguish between these spectrally relatively similar classes.

Really striking however is the high degree of misclassification of the Bare Soil and Water classes in both, the 2011 and the 2012 RapidEye images. In the literature (and own experience), these classes usually produce accuracies of 75-80% or better.

Figure 3.5 and Figure 3.6 might explain the results. At the bottom of Figure 3.6 subsets of the Lakes area of the RapidEye and SPOT-6 images are displayed in natural (true) colour. The WorldView-2 image unfortunately did not cover this area (compare Figure 3.4). The Lakes look very different in all three images. In the July 2011 image, the water level appears to be moderately high, in the January 2012 image the water level is very low, and in the 2014 SPOT-6 image the water level appears to be very high. These observations are supported by the measured water levels at the St Lucia Bridge (Figure 3.6). In 2008 at the time of the imagery used for the reference map, the water level of the estuary was low, too

(Figure 3.6). Therefore, the water level in the WV-2 and RE 2011 image probably represents best the water level conditions at the time of the 2008 reference data. The flood events in January July and December 2011 might explain the misclassification which is to be found close to the water edge in 2011 and 2012, as these flood events might have washed away the vegetation in those areas. This result is supported by Rautenbach (2015) who noted: *"The biggest change in vegetation composition was the overall decrease in salt marsh (by 57%) and increase in submerged macrophytes (by 96%). After the drought, water level rose rapidly as rainfall returned to normal and the Mfolozi River connected to the sea and St. Lucia Estuary. This caused an increase in surface area of the water column (which includes the Lakes, Narrows, Back Channel, Link Canal and Mfolozi River) from 30 498 ha in 2008 to 32 624 ha in 2013. The increase in water level and the reduction in salinity in False Bay and the lakes (North and South) caused flooding and inundation of the salt marsh habitat, reducing the area covered."*

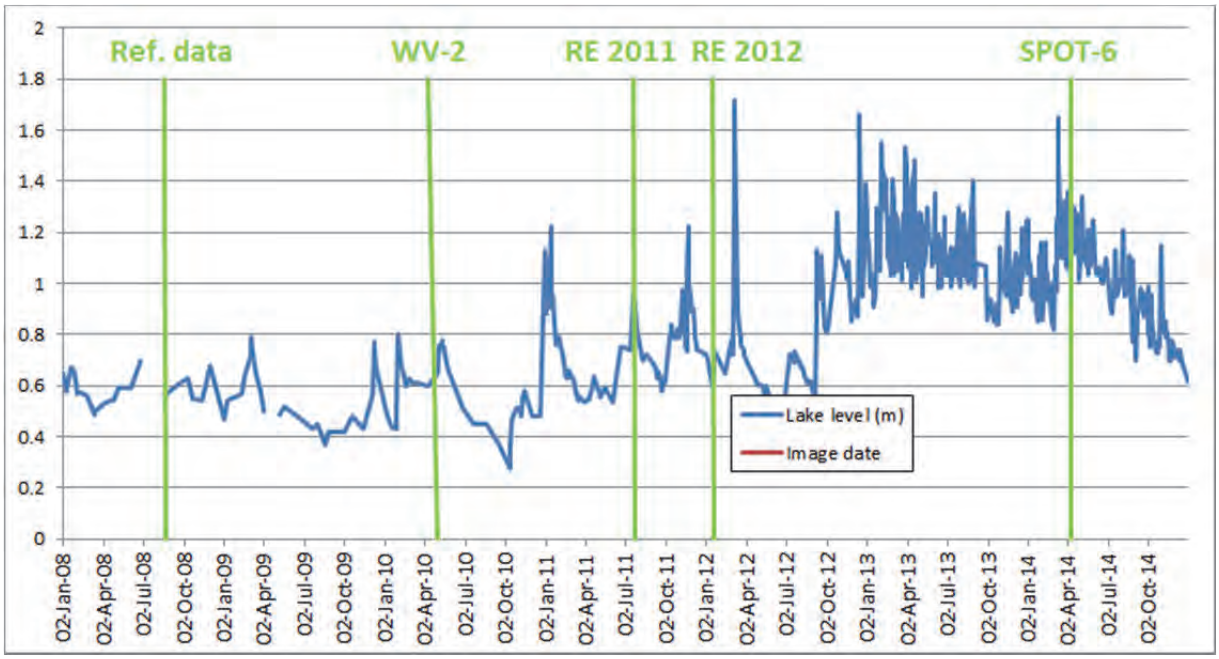

Figure 3. 5: Water level at the St Lucia Estuary, measured at the St Lucia Bridge (Source: C. Fox of EKZNNW). Green bars: 4x image acquisition dates and 1x Kelly's 2013 reference date.

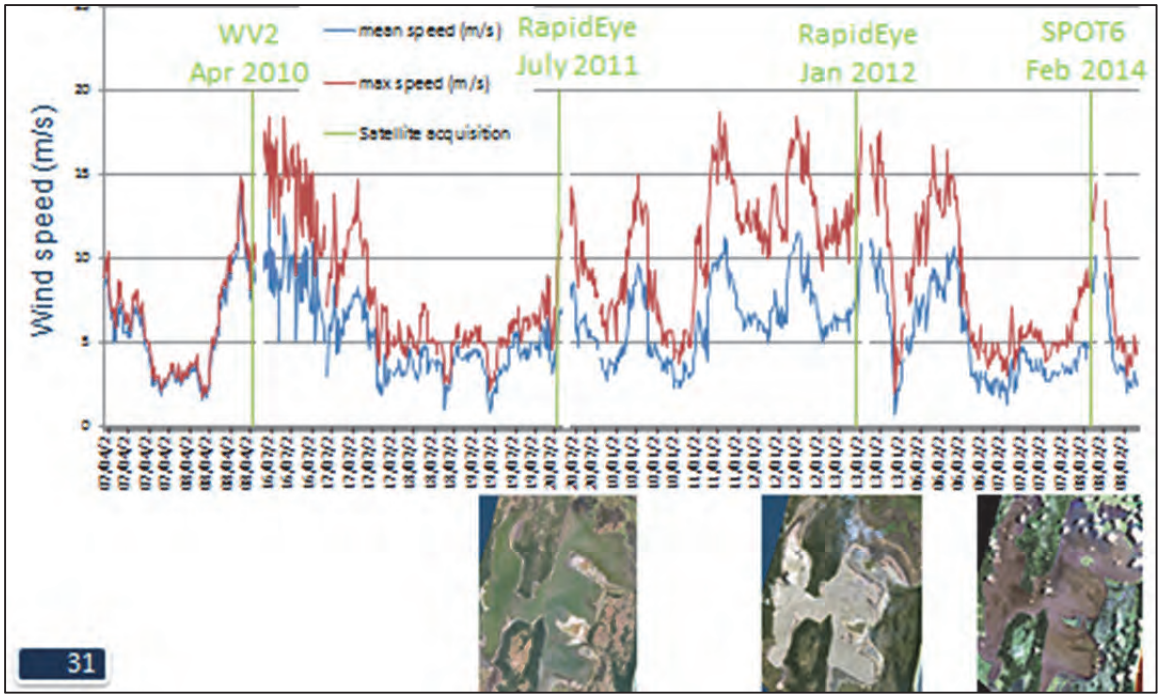

Figure 3. 6: Top: Hourly wind speed, measured at Richards Bay, for three days prior to respective satellite image acquisition dates. Bottom: true colour image of respective RapidEye and SPOT-6 images.
Wind data source: SADCO.

The colour of the water at the image acquisition dates is another potential source for misclassification. In the SPOT-6 image the water looks as water “should look like”. The visible slightly brown discolouration indicates some small degree of turbidity, maybe as a result of the mixing of the strong winds two days before the image was taken (Figure 3.6, top) and the recent flood at that date (Figure 3.5).

In the 2012 RapidEye image, the water looks very turbid and rugged. Figure 3.5 and Figure 3.6 show that the water level at that time was very low and that the three days preceding the image capture a strong (south-easterly) wind was blowing. Under these conditions the water column would have been mixed up and very turbid and the water surface very rough with wind waves. (The waves are actually visible when zooming into the image.) This explains the massive confusion between bare soil and water in this image.

3.6 Conclusions

This project component examined the value of very high resolution multispectral satellite imagery acquired between 2010 and 2014 and LiDAR derived digital surface information for classifying estuarine vegetation types. Ground truthing reference was a GIS-based vegetation map from 2008. Supervised maximum likelihood classification produced

satisfactory overall accuracies between 63.6% and 79.0% for the WorldView-2 and the SPOT-6 image, while the RapidEye-based classifications produced overall accuracies between 50.0% and 64.6%. Analysis of the results showed that the reasons for the misclassifications may have been mainly based on environmental conditions rather than on technical or sensor-related issues. Therefore, we conclude that all three sensors assessed in this project are suitable for mapping coastal and estuarine vegetation.

It is mainly the inherent high dynamic nature of the estuarine environment with massive fluctuations in water levels and salinity which cause swift turn-over of vegetation types, temporally and spatially. Examples include turnover from Salt marsh to Reeds, or Grass and Shrubs to Swamp forest on abandoned Forest plantations. This leads to misleading low accuracies in vegetation classifications if the acquisition dates of satellite imagery and validation data are too far apart. In the St Lucia estuary, even a 6-12 months difference turned out to lead to major vegetation change and hence misclassification, if a major flood eradicated entire vegetation patches or a recent wind event biased the image quality. This impact was aggravated by the fact that the available reference data were entirely taken below the 5m contour (estuary functional zone), i.e. the inherently dynamic estuarine zone which are most prone to impacts of changing water level and salinity. For future approaches it would be advisable to include some data from higher and environmentally more stable sites which are less prone to change over time as reference sites, however it should be noted that this will not include the target estuarine habitats.

Further negative impact on the results was caused by physiognomic and thus spectral similarity of certain vegetation types, such as grass and reeds, and shrubs and forests. This misclassification is technically expected. The additional use of LiDAR-derived Digital Terrain Models improved the separability of those classes and improved 5 out of 8 classification runs. Further improvement would be achieved with the use of more sophisticated LiDAR-derived products, such as the combined use of Digital Surface Model (which includes vegetation canopy height and Digital Terrain Models (which only include soil surface height) to derive the actual vegetation height or LiDAR return intensity information.

Further solutions could include either the use of a sensor with a better (hyperspectral) resolution of the satellite imagery or possibly by a more conscience choice of the image acquisition date, in cases where spectral separability between classes varies over the seasons. The other project components will inform on this aspect.

Apart from true vegetation change, we experienced that weather impacts (high water levels inundating fringe vegetation and wind events mixing up the water column) cause bias in the reflective properties of the satellite imagery and impair the accurate identification of surface and vegetation types.

However, as imagery from the optimal observation period is often not available, our research also showed that it is essential to also analyse ancillary environmental data such as flood levels, wind and weather data to interpret results appropriately.

The results show that the spatial and spectral resolution of modern very high resolution imagery is sufficient to satisfactorily map and monitor small scale estuarine vegetation. They emphasize however the importance of synchronisation of ground truthing data with actual image acquisition times in these highly dynamic environments.

3.7 References

Adams, J. B., and Bate, G. C., 1999. Growth and photosynthetic performance of *Phragmites australis* in estuarine waters: a field and experimental evaluation. Aquatic Botany, 64: 359-367.

Cowan G.I., 1999. The St Lucia System. Available online at: [http://hdl.handle.net/1834/460]. Last date accessed 1 June 2011.

Nondoda, S. P., 2012. Macrophyte distribution and responses to drought in the St. Lucia Estuary. MSc, Nelson Mandela Metropolitan University.

Rautenbach K., 2015. Present state of Macrophytes and response to management scenarios at the St. Lucia and Mfolozi estuaries. Nelson Mandela Metropolitan University (NMMU). South Africa.

Richter, R. and Schläpfer, D., 2014. Atmospheric / Topographic Correction for Satellite Imagery – ATCOR-2/3 User Guide, Version 8.3.1, February 2014. DLR Report No. DLR-IB 565-01/13. Available online at www.rese.ch.

Taylor, R. H., 2006. Ecological responses to changes in the physical environment of the St. Lucia Estuary. PhD Thesis, Norwegian University of Life Sciences. Papers 1, 2 and 3.

Taylor, R., Fox, C. & Mfeka, S., 2013. Monitoring the St Lucia Estuarine System: A synthesis and interpretation of the monitoring data for May 2013. Unpublished Ezemvelo KZN Wildlife report. 16 pages.

Townshend, J.R.G., Justice, C.O., Gurney, C., McManus, J., 1992. The Impact of Misregistration on Change Detection. IEEE Transactions on Geoscience and remote sensing. Vol. 30, No. 5, 1054-1060.

Turpie, J.K., Wilson, G. & Van Niekerk, L., 2012. National Biodiversity Assessment 2011: National Estuary Biodiversity Plan for South Africa – Technical Report. Anchor Environmental Consultants Report No. AEC2012/01, Cape Town.

Van Heerden I.L., 2011. Management concepts for the Mfolozi flats and estuary as a component of the management of the iSimangaliso Wetland Park. In: Bate GC, Whitfield AK and Forbes AT (Eds.). 2011. A review of studies on the Mfolozi estuary and associated flood plain, with emphasis on information required by management for future reconnection of the river to the St Lucia system. Report to the Water Research Commission. WRC Report No. KV 255/10. Pretoria: WRC.

Van Niekerk, L. and Turpie, J.K. (eds), 2012. South African National Biodiversity Assessment 2011: Technical Report. Volume 3: Estuary Component. CSIR Report Number CSIR/NRE/ECOS/ER/2011 /0045/B. Council for Scientific and Industrial Research, Stellenbosch.

4 REMOTE SENSING MODELS FOR PREDICTING LEAF NITROGEN AND PHOSPHOROUS ACROSS FOUR SEASONS FOR SIX SUBTROPICAL FOREST EVERGREEN TREE SPECIES

This chapter was published in the journal paper: Van Deventer, H.; Cho, M.A.; Ramoelo, A. 2015. Capability of models to predict leaf N and P across four seasons for six sub-tropical forest evergreen trees. ISPRS Journal of Photogrammetry and Remote Sensing,101: 209-220.

4.1 Abstract

Nutrient phenology of evergreen subtropical forests of southern Africa is poorly understood. Foliar nitrogen (N) and phosphorous (P) forms key components of photosynthesis and are vulnerable to global change stressors. Remote sensing techniques can potentially map and monitor nutrient phenology, yet models to predict across species, seasons and climatic regions are deficient. This study evaluates the capability of various models, developed from leaf spectra of selected spectral regions and seasons, to predict nutrient concentration across season and species. Seasonal differences in foliar N and P were assessed using a one-way ANalysis Of VAriance (ANOVA). The relationship between leaf spectra and nutrients was assessed using linear regressions between the foliar nutrients and spectral indices. The predictive capability of three models was compared using root mean square error (RMSE) values. Amongst the four seasons, winter leaves showed the highest mean N (2.16%, $p < 0.01$). However, winter showed the lowest variability of foliar N (coefficient of variation = 8%) compared to the variability of the other three seasons (coefficient of variance > 35%). In fact, between winter and spring, the variability in foliar N increased by 294%. Foliar P did not significantly differ between the four seasons. Predictive models for leaf N concentration developed for each season showed a higher level of accuracy, particularly for winter, whereas predictive models for leaf P showed low accuracies. Models developed from a single season showed a slight increase in error for the summer and autumn, however a larger increase in error for the winter season for the evergreen trees. The results suggest that spectral measurements can potentially be used to quantify nutrient phenology at regional scale and monitor the impacts of global change on nutrient phenology and photosynthesis.

4.2 Introduction

Global change has shown significant impacts on the periodic behaviour of plants or phenology since the 1970s (Richardson *et al*. 2013). Most noticeably, the onset and duration of the active growth season has been affected across climatic zones, though the impact on

the autumnal season is not well established (Zhou et al. 2003; Richardson et al. 2013). Several authors have argued that global increase in carbon dioxide and temperature may speed up the rates of photosynthesis and respiration in vegetation, though the increased rates are dependent on water and nutrient availability (Evans 1989; Penuelas et al. 1995; Drake and Gonzalez-Meler 1997; Kirschbaum 2000). Predicting the impact of global change on these processes remains difficult, owing to the limitations of simulating regional scale ecosystem responses either in laboratories or *in situ*, particularly for forests (Seppälä et al. 2009; Lukac et al. 2010; Millard and Grelet 2010; Booth et al. 2012; United States Department of Energy (US DOE) 2012; FAO and JRC 2012; Sardans and Peñuelas 2012; Richardson et al. 2013). It is, however, generally recognised that global change is causing changes to vegetation physiology, condition, composition and distribution, and therefore to vegetation phenology, at local to regional scales (Campoy et al. 2011; Sardans and Peñuelas 2012). Phenological expression is however unique to species and climate regions, therefore, to address uncertainties in vegetation response to global change, our understanding of the unique phenology of vegetation types needs to be improved (Reich and Oleksyn 2004; Lukac et al. 2010; Richardson et al. 2013).

Tropical and subtropical forests are considered to be some of the most vulnerable systems to global warming because of their exposure to multiple stressors (Seppälä *et al*. 2009). Tropical forests are nutrient poor (Reef *et al*. 2010) and with limited availability of phosphorus (Jordan 1985), hence may have limitations in adapting to increased temperatures and photosynthesis. In addition, humid subtropical forest areas are highly fragmented and have been extensively converted into commercial plantations (Seppälä *et al*. 2009). Their resilience and adaptive capacity to global change is therefore considered reduced (Seppälä *et al*. 2009). Despite the sensitivity of these forests to global change, seasonal variation of leaf chemicals and translocation in evergreen tropical forests are not well understood and often highly simplified in global ecosystem models (De Weirdt *et al.* 2012). Furthermore, global change impacts on tropical and subtropical forests vary greatly from regional to continental scales (United States Department of Energy (US DOE) 2012). A systematic approach to monitor global changes in a comparable way at regional scale is deficient.

Monitoring foliar nutrients in tropical and subtropical forests using traditional methods of leaf harvesting and transportation to laboratories for analysis implies a number of difficulties. These forests are sometimes inaccessible, because of dense overgrowth or located in swamp wetlands (United States Department of Energy (US DOE) 2012). Laboratories are often not close enough to the collection site which risks the loss of nutrients from leaves

during the transportation period. The cost of human resources and laboratory analysis for a high number of foliar chemicals and repetitive time periods can increase beyond affordability. More cost-effective methods would be required to monitor global change impacts at the physiological leaf level and at the regional scale in the long term. Remote sensing, using air- or spaceborne imagery has been utilised as a cheaper alternative for assessing foliar nutrients of forest canopies at the broad landscape scale. Furthermore, spaceborne sensors offer continuous repetitive coverage of areas across the globe and are ideal for monitoring nutrients across a number of ecosystems. Various regions of the leaf or canopy electromagnetic spectrum have been associated with leaf water, pigments, nutrients and leaf biomass absorption or scattering of electromagnetic energy (Curran 1989) (Figure 3.1). High spectral (hyperspectral) resolution sensors on airborne and spaceborne platforms have enabled the mapping of foliar nutrients since the late 1990s (Smith et al. 2002; Townsend et al. 2003; Huang et al. 2004; Mutanga and Kumar 2007; Huber et al. 2008; Kokaly et al. 2009; Schlerf et al. 2010; Skidmore et al. 2010; Knox et al. 2011). However, the high cost of hyperspectral sensors has restricted their routine utilisation for forest nutrient analysis. New spaceborne multi-spectral sensors such as WorldView-2 and RapidEye with fewer bands adapted for foliar pigment assessment also offer promise for assessing canopy nutrients such as leaf N. These multi-spectral sensors have proved successful in mapping foliar nutrients at regional scale (Ramoelo et al. 2012; Ullah et al. 2012; Clevers and Gitelson 2013; Ramoelo et al. 2013; Cho et al. 2013).

The successful employment of remote sensing in monitoring the impact of global change across phenologically-unique climate regions requires; (a) the ability to detect and characterise the unique patterns of nutrient phenology of various climate regions and (b) capable models that can be used to predict nutrients across species, seasons and regions. Regardless of the advances made in mapping foliar nutrients with remote sensing at small regional scales, a few challenges remain. First, the relationship between foliar nutrient concentration and spectral reflectance across species, season and ecosystems remains poorly understood. Foliar nutrients are known to vary over seasons, yet it is not well established how the empirical relationship between foliar nutrients and spectral information reflects seasonal variation. Variations in foliar nitrogen, chlorophyll and carotenoids were positively related to seasonal variation of the photochemical reflectance index (PRI) for deciduous spruce over two seasons in Japan (Nakaji *et al*. 2006). The relationship between foliar chlorophyll *a* and leaf spectral vegetation indices varied between the wet and dry season for evergreen mangrove tree species in Mexico (Flores-de-Santiago *et al*. 2013). Similarly, a changing relationship between foliar nitrogen and leaf reflectance in the red-edge was also found to vary with carboxylation rates for two deciduous species in the growth

season of the United States of America (Dillen *et al*. 2012). In Canada, the relationship between chlorophyll predicted from vegetation indices and observed chlorophyll for deciduous maple leaves varied over the spring, summer and autumn seasons (Zhang *et al*. 2007). The relationship between foliar nutrient and leaf spectral data across different seasons has therefore not been well established for evergreen trees or subtropical forests. Secondly, models for predicting nitrogen and phosphorus remain difficult as they co-vary with related biochemical and biophysical parameters such as chlorophyll, leaf structure, foliage biomass and leaf water content (Elvidge 1990; Yoder and Pettigrew-Crosby 1995). The relationship between the nutrients and co-varying parameters are however known to change over seasons and time (Yoder and Pettigrew-Crosby 1995; Zhang et al. 2007). The chlorophyll red-edge position, for example, has often been used as a reliable co-variant in the mapping of nitrogen (Cho and Skidmore 2006; Mutanga and Skidmore 2007; Ramoelo et al. 2012), yet if the varying relationship between chlorophyll and nitrogen across seasons is poorly understood, the mapping and monitoring of nutrient phenology will potentially be erroneous. The ability to use the Near Infrared (NIR) and Shortwave Infrared (SWIR) bands to decouple nutrients from other co-variants across seasons, remains to be tested. A changing relationship between chlorophyll content estimated from leaf spectra and foliar chlorophyll content, for example, was observed for the maple species in Canada, where the relationship was highest in the spring season for the maple species in Canada, though decreased in correlation and accuracy towards summer and autumn (Zhang *et al*. 2007). The ability of nutrient models developed from single-season data to predict across phenological phases should be evaluated in model development. Currently, models to predict nutrients across species, seasons and climatic zones are deficient (Ferwerda et al. 2005; Ollinger et al. 2008; Knyazikhin et al. 2012; Ollinger et al. 2013).

This study compared the capability of predictive nutrient models, developed from single-season and multiple-seasons leaf spectra, to predict nutrient concentration across seasons and species. Six evergreen tree species, in a subtropical environment in South Africa, were sampled over four seasons (winter, spring, summer and autumn) to assess how the nutrient-spectral relationship changes over seasons. Thereafter, predictive models were developed using the linear regression between leaf spectra and nutrient concentration of the season with the highest coefficient of determination (R^2) as well as those of a combined-seasons data set, and compared to the predictive model of each individual season, to assess the capability of the various models to predict nutrients across the seasons.

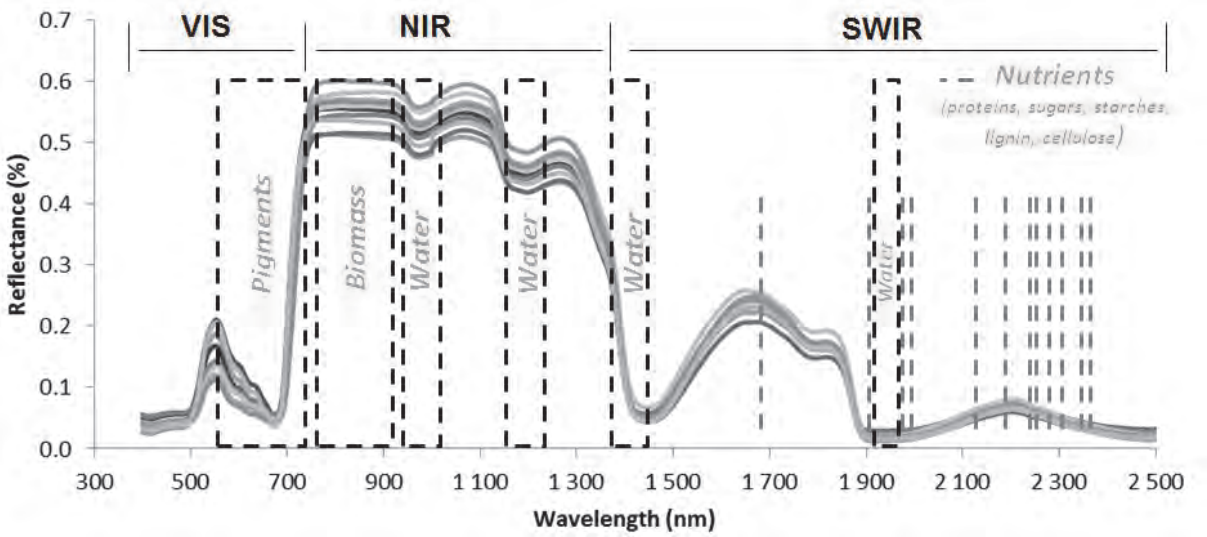

Figure 4.1: Regions of the electromagnetic spectrum known to relate to leaf pigments, foliage, biomass, leaf water content, proteins, starches and structural components.

4.3 Materials and Methods

4.3.1. Study area

The iSimangaliso Wetland Park (28°S, 32°30'E) is located on the east coast of the KwaZulu-Natal province in South Africa. The area has a humid sub-tropical climate with strong seasonal variation in rainfall and temperature (Figure 4.2). Mean Annual Precipitation (MAP) ranges between 1 000-1 500 mm (Middleton and Bailey, 2008) and the mean temperatures in summer ranges from 23-30°C, with winter temperatures decreasing to approximately 10°C (Sokolic 2006). The Park is situated on a coastal plain (Partridge et al. 2010) with sandy undulating hills between 10 m to 20 m above mean sea level (a.m.s.l.). The vegetation types include wooded grassland, dune vegetation and dune forests, to swamp forests and critically endangered mangrove forests (Mucina and Rutherford 2006). A number of evergreen tree species are found in the St. Lucia and Maphelane nodes of the iSimangaliso Wetland Park (Table 4.1; Figure 4.3).

Table 4.1: Number of trees sampled per species and season in St. Lucia, KwaZulu-Natal, South Africa.

Tree species	Common name	Trees Winter (*n*)	Trees Spring (*n*)	Trees Summer (*n*)	Trees Autumn (*n*)	Total number of trees per species (*n*)
Avicennia marina	White mangrove	21	21	21	21	84
Bruguiera gymnorrhiza	Black mangrove	19	19	19	19	76
Ficus sycamorus	Sycamore fig	15	15	15	15	60
Ficus trichopoda	Swamp fig	11	11	11	11	44
Hibiscus tiliaceus	Lagoon hibiscus	30	30	30	30	120
Syzigium cordatum	Waterberry	17	17	17	17	68
Total per season:		113	113	113	113	***452***

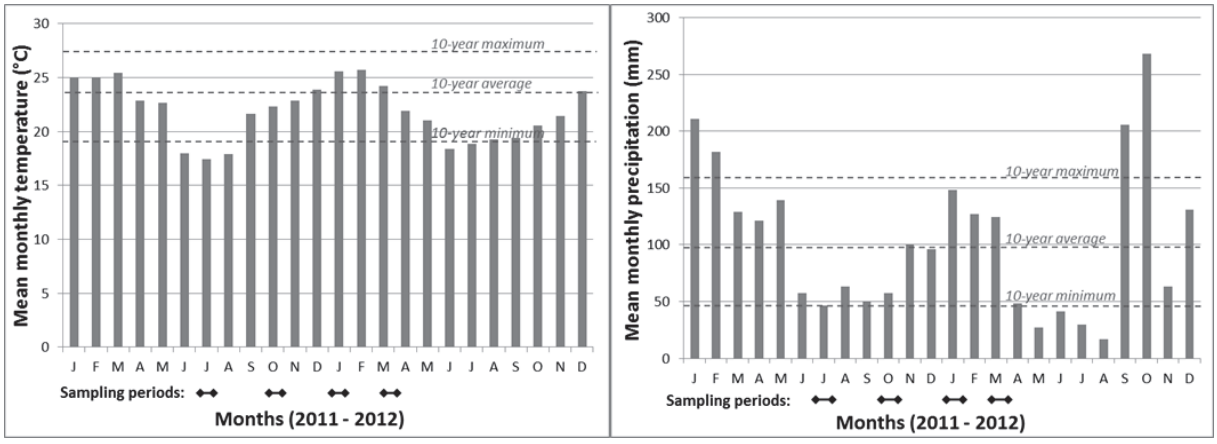

Figure 4.2: Mean monthly temperature and rainfall between January 2011 and December 2012 for the St. Lucia study area, KwaZulu-Natal, South Africa (Harris *et al*. 2013).

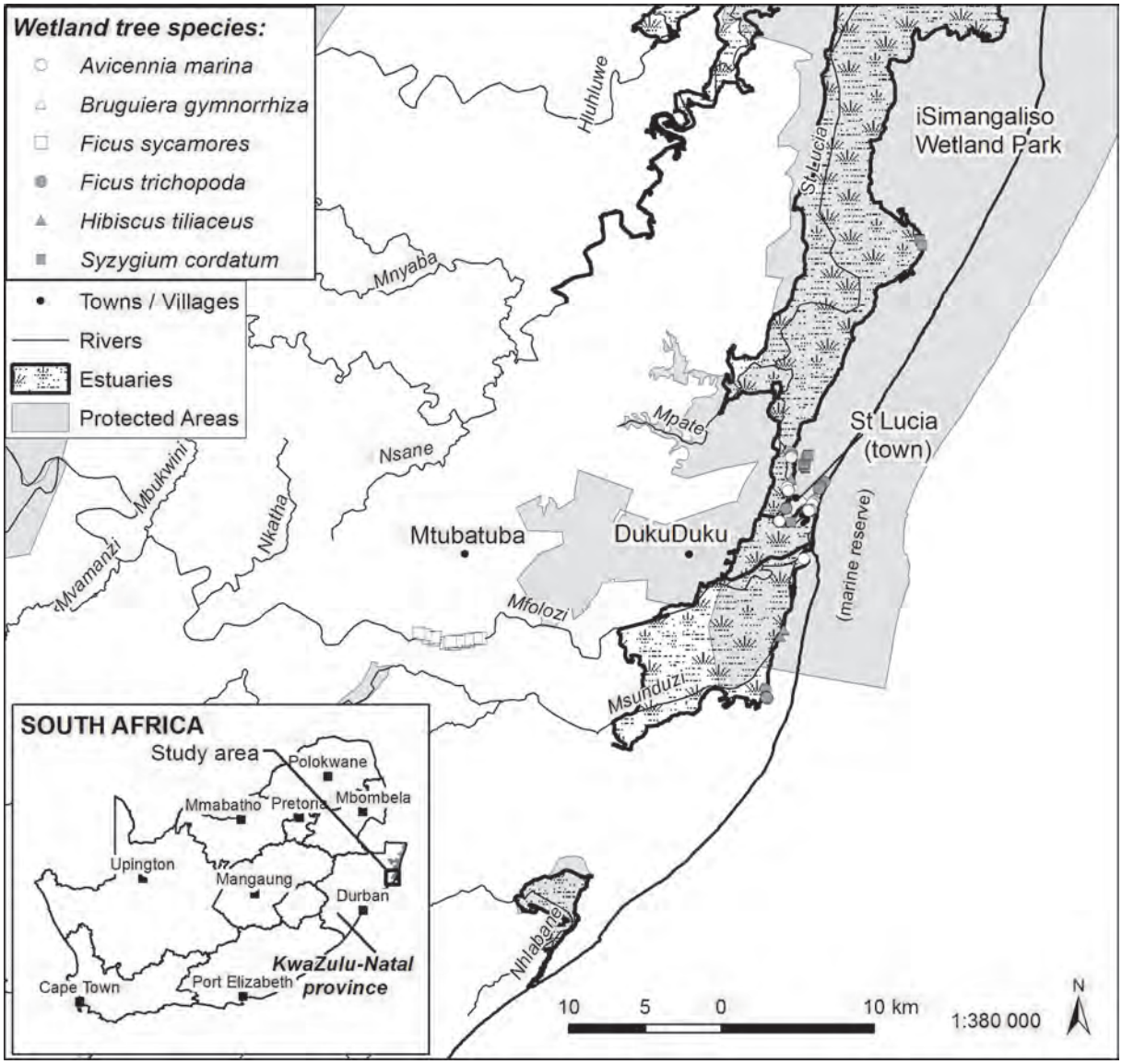

Figure 4.3: The St. Lucia study area is located northeast of the city of Durban in the KwaZulu-Natal Province of South Africa. Six wetland and estuarine tree species were sampled in the study area along the uMfolozi River, as well as the St. Lucia, uMfolozi and uMsunduzi estuaries.

4.3.2. Leaf sampling, spectral measurements and laboratory analysis of foliar N and P

Field campaigns were conducted for four seasons (winter, spring, summer and autumn) across 2011 and 2012. Sample sites were selected along wetlands and estuaries where tree canopies were accessible, mature and sun exposed. Five sunlit leaves were randomly sampled across the canopy of each tree (*n* trees = 452, Table 1). Leaf spectral reflectance measurements of the adaxial surface of each leaf were made using the Analytical Spectral Device (ASD) plant probe accessory connected to an ASD spectroradiometer (FieldSpec Pro FR, Analytical Spectral Device, Inc, USA), with the average scan time set at 10. The ASD covers the spectral range between 350 and 2500 nm with a 1.4 nm sampling interval

between 350 and 1050 nm range, and ±2 nm between 1050 and 2500 nm. The plant probe provides a direct-contact probe which limits ambient light. The radiance measurements were converted to reflectance against scans of a white spectralon reference panel. The five leaf specimens per tree were combined for nutrient analysis (N and P). The leaves were oven-dried at 65°C until constant weight was reached. Bemlab Pty Ltd analysed nitrogen concentration using a Leco FP528 nitrogen analyser (Horneck and Miller 1998) and phosphorus through Inductively Coupled Plasma Optical Emission Spectrometry (ICP-OES) analysis (Isaac and Johnson 1998).

4.3.3. Data analysis

Differences in leaf N or P concentration between seasons were assessed using one-way ANalysis Of VAriance (ANOVA). The alpha levels were corrected for Bonferroni effects to decrease the likelihood of committing type 1 error as a result of multiple comparable pairs (McDonald 2008). The adjustment is made to ensure that the alpha level (p = 0.05) is not merely a reflection of the differences between the dependent (nutrient concentrations) and independent variables (combined seasons), but adjusted downwards to assess the differences between each combination of individual seasons. The comparison of four seasons to one another results in six comparable pairs and therefore the alpha level (p < 0.05) is adjusted by dividing 0.05 by the six comparable pairs = p < 0.01. Thereafter, the linear relationship between foliar nutrients and leaf spectral reflectance was assessed using a spectral vegetation index (VI), based on the normalised difference vegetation index (NDVI). NDVI is one of the most commonly used vegetation indices where two bands are combined and normalized through their difference (Rouse et al. 1973;Tucker 1979). One band is traditionally located at the absorption feature of the vegetation parameter in question and the other band is used to normalize the absorption band. VI values were computed for all possible band combinations (Cho *et al*. 2009) (Eq. 1). First, the 1 nm spectral reflectance ASD data were resampled using a Gaussian model (full-width half-maximum equal to every 10 nm band spacing between 400 and 2 500 nm) in the Environment for Visualizing Images (ENVI) software (v.4.8, ITT Visual Information Systems) to reduce complexity and redundancy in the data. Subsequently, the 10 nm data were used to compute VIs for all possible band combinations (210! = 22 155) from the visible (400 nm) to the SWIR (2500 nm). This was done to assess the behaviour of the relationship between leaf N or P and VIs for various spectral regions associated with pigments, foliage biomass, leaf water content, proteins, starch as well as lignin across seasons. A simple linear regression was used to determine the strength of the relationship (coefficient of determination (R^2)) between

each foliar nutrient and the VIs. For each nutrient, the season which attained the highest R^2 between the VI and nutrient concentration, was selected as one of the predictive models for evaluation.

$$VI_{(i,j,n)} = \frac{(R_{(i,n)} - R_{(j,n)})}{(R_{(i,n)} + R_{(j,n)})} \quad (1)$$

Where $R_{(i,n)}$ and $R_{(j,n)}$ are the reflectance of any two bands for each sample $_n$.

Foliar N or P was predicted from known absorption regions of the electromagnetic spectrum which yielded the highest coefficient of determination (R^2) for each nutrient. Absorption regions were selected for pigments (500, 510, 670, 680, 700 and 760 nm), foliage biomass (740 and 780 nm), leaf water content (860 and 1240 nm), as well as for starch, lignin, tannins, pectin, protein and cellulose (1630, 1690, 1900, 2000, 2050, 2060, 2130, 2180, 2200, 2210, 2240, 2250, 2300 and 2380 nm).

The model with the best predictive capability for each nutrient was selected through comparing the root mean square error (RMSE) and percentage error of prediction or relative RMSE per season. Model comparison was done to assess the capability of models to predict across seasons. RMSE values were calculated for three different predictive models for each nutrient across seasons: (a) a model using predicted values for each season (individual-season model); (b) a model developed from the season providing the highest R^2 for the particular nutrient and applied to all four seasons; and (c) a model developed combining data from all four seasons for each nutrient (multiple- or combined-seasons model). The RMSE (Eq. 2) was calculated for each model, season and nutrient to compare accuracies.

$$RMSE = \sqrt{\frac{1}{n}\sum_{i=1}^{n}(\hat{y}_i - y_i)^2} \quad (2)$$

Where $\hat{y}_i$ is the predicted nutrient content, y_i is the observed nutrient content, and n is the number of samples.

For the combined-seasons model, a third of the data for each season was retained as an independent data set, whereas the remaining 2/3 of each season was combined into a single data set. An iterative bootstrap process (1 000 iterations) using R software (RStudio v. 0.98.507, © 2009-2013 RStudio, Inc.) divided the combined data set randomly into a training (2/3) and test (1/3) data set. A linear model was fit to the training data set between the observed nutrient concentration and the vegetation index, and then applied to the test data set. The RMSE was then calculated for both the training and test data set and recorded with the model coefficients, before each new reiteration. The mean coefficients were thereafter

applied to the independent data sets of each season and the RMSE calculated and reported per season. The percentage of error was calculated using the mean observed nutrient concentration per season for model comparison. The change in percentage error between the models was compared to evaluate the capability of each model to predict across seasons.

4.4 Results

4.4.1. Foliar nutrient variations per season

Amongst the four seasons, winter leaves showed the highest mean N ($p < 0.01$, Bonferroni corrected $p = 0.008$) (Table 4.2; Table 4.3). However, winter showed the lowest variability of foliar N (standard deviation = 0.17) when compared to the other three seasons (standard deviation > 0.6). In fact, between winter and spring, the variability increased by 294% whereas the variability over the active growth season showed little difference.

Contrary to what was observed with foliar N, foliar P showed no significant differences between the four seasons. The transition from winter to spring showed a slight increase in variability (8%) for foliar P compared to 294% observed for foliar N. The variability of foliar P actually declined by 71.5% between summer and autumn, whereas the variability of foliar N showed very little change between these two seasons.

Table 4.2: Descriptive statistics for laboratory-analysed foliar nitrogen (N) and phosphorus (P) concentration (%) of the six species over four seasons.

Foliar nutrient (%)	Statistic	Winter	Spring	Summer	Autumn
N	Min	1.47	0.69	0.57	0.55
	Mean	2.16	1.89	1.75	1.71
	Max	2.51	3.33	3.37	3.37
	Stdev	0.17	0.67	0.63	0.67
P	Min	0.05	0.05	0.03	0.04
	Mean	0.17	0.17	0.17	0.14
	Max	0.59	0.93	1.14	0.41
	Stdev	0.13	0.14	0.17	0.08

Table 4.3: Intra-season ANalysis Of VAriance (ANOVA) for foliar N and P concentration (%) of the six species.

Nutrient	Seasons	Winter	Spring	Summer	Autumn
N	Winter				
	Spring	0.003293 *			
	Summer	0.000008 *	0.246426		
	Autumn	0.000008 *	0.075883	0.947032	
P	Winter				
	Spring	0.999999			
	Summer	0.996919	0.996201		
	Autumn	0.244360	0.237694	0.346901	

* –significant ($p < 0.01$), Bonferroni corrected $p = 0.008$

4.4.2. Assessing the seasonal relationship between foliar nutrient concentration and leaf spectra

The relationship between foliar N and leaf spectra varied across seasons (Figure 4.4; Table 4.4). Winter showed the lowest correlations between foliar N and leaf spectra compared to the other three seasons. The highest R^2 for winter was recorded in the SWIR with a two-band combination associated with protein and starch ($R^2 = 0.22$, $p < 0.01$) (Table 4.4). In contrast, spring showed an increase in correlation between foliar N and leaf spectra across spectral regions associated with foliar pigments, foliage biomass, leaf water content, protein, starches, cellulose and lignin (Figure 4.4; Table 4.4). The region with the highest average R^2 across seasons (0.59) was recorded in the SWIR associated with protein absorption bands (2130, 2240), yielding the highest R^2 in spring ($R^2 = 0.80$, $p < 0.01$), followed by summer ($R^2 = 0.77$, $p < 0.01$) and autumn ($R^2 = 0.71$, $p < 0.01$) (Table 4.4). The second highest region was also located in the SWIR associated with protein and cellulose (2180, 2210), followed by foliage biomass in the red-edge region (740, 780), lignin, tannins, pectin and protein in the SWIR (1630, 1690), and then the chlorophyll bands in the red-edge region (700, 760). The relationship in the carotenoid pigment region remained relatively constant from spring to summer and autumn ($R^2 = 0.37$, 0.37, 0.34, $p < 0.01$), though the relationship between foliar N and spectra showed a slight increase (30%) in the bands associated with chlorophyll from spring to autumn, as well as for lignin, waxes, protein and nitrogen (16%). The relationship showed a decrease from spring to autumn in the region associated with foliage biomass (-21%), leaf water content (-57%) and the region of lignin, tannins, pectin and protein (-50%). Bands associated with protein or protein bond absorption features showed an average decrease from spring to autumn of < 22%), whereas bands associated with starch showed a decrease by > -90% from spring to autumn.

Compared to leaf N, the relationship between foliar P and leaf spectra also varied over the four seasons, but with lower R^2 values over all four seasons (Figure 4.4; Table 4.4). High R^2 values ($R^2 > 0.25$) between foliar P and leaf spectra were recorded for all four seasons in the SWIR, compared to the high diversity of regions noted for N. In the winter, the highest average coefficient of determination (R^2) across the four seasons ($R^2 = 0.25$, $p < 0.01$) was recorded in the SWIR region associated with lignin, waxes, protein and nitrogen (2050, 2380), followed by protein, nitrogen and lignin (2060, 2380). Other high average R^2 regions were mainly associated with protein (2130, 2240), protein and cellulose (2180, 2210) and lignin, tannins, pectin and protein (1650, 1690). The SWIR region with the highest average R^2 across all four seasons (2050, 2380), also showed the highest R^2 in autumn ($R^2 = 0.38$, $p < 0.01$). The pigment region showed a marked increase from winter to spring and spring to summer (> 110%). An increase in the relationship was observed from winter to spring (> 150%), in the regions associated with chlorophyll, foliage biomass and starch, though a decrease was noted from spring to summer (> -66%) for these regions. The band combinations protein, protein bonds with cellulose, nitrogen and starch, in general, showed a decrease from winter to spring (by > -27%) and spring to summer (by > 6%), though increased between summer and autumn between 13-93%.

Spring showed the highest R^2 between foliar N and leaf spectra and winter the lowest. In contrast, the highest relationship between foliar P and leaf spectra was recorded in the winter, summer and autumn, and the lowest in spring. Foliar nitrogen and phosphorus showed higher R^2 values with the SWIR region, except for nitrogen in the red-edge regions associated with chlorophyll and foliar biomass (Table 4.4).

Table 4.4: Maximum linear regression coefficient of determination (R^2), extracted from a matrix showing the relationship between nutrient concentrations and leaf spectra of the six species, for band regions known to relate to leaf features, given per season and nutrient.

Foliar nutrient	VI Band combination •	Associated parameter	Winter	Spring	Summer	Autumn	*Average*
N	510, 680	Carotenoids	0.00	0.37*	0.37*	0.34*	*0.27*
	700, 760	Chlorophyll	0.09*	0.40*	0.44*	0.52*	*0.36*
	740, 780	Foliage biomass	0.08*	0.62*	0.49*	0.49*	*0.42*
	860, 1240	Leaf water content	0.00	0.37*	0.15*	0.16*	*0.17*
	1630, 1690	Lignin, tannins, pectin & protein	0.06*	0.66*	0.47*	0.33*	*0.38*
	1900, 2250	Starch	0.01	0.33*	0.13*	0.01	*0.12*
	2000, 2250	Starch	0.01	0.40*	0.13*	0.03	*0.14*
	2050, 2380	Lignin, waxes, protein & nitrogen	0.02	0.38*	0.48*	0.44*	*0.33*
	2060, 2300	Protein & nitrogen	0.02	0.22*	0.00	0.01	*0.06*
	2060, 2380	Protein, nitrogen & lignin	0.00	0.47*	0.47*	0.37*	*0.33*
	2130, 2240	Protein	0.09*	0.80*	0.77*	0.71*	*0.59*
	2180, 2210	Protein & cellulose	0.06*	0.60*	0.63*	0.59*	*0.47*
	2180, 2240	Protein & nitrogen	0.21*	0.42*	0.41*	0.27*	*0.33*
	2200, 2240	Protein & starch	0.22*	0.31*	0.30*	0.18*	*0.25*
P	500, 670	Carotenoids	0.06*	0.17*	0.37*	0.10*	*0.18*
	700, 760	Chlorophyll	0.02*	0.05*	0.00*	0.14*	*0.05*
	740, 780	Foliage biomass	0.02	0.06*	0.02	0.13*	*0.06*
	860, 1240	Leaf water content	0.01	0.01	0.00	0.04	*0.02*
	1650, 1690	Lignin, tannins, pectin & protein	0.17*	0.19*	0.30*	0.19*	*0.21*
	1900, 2250	Starch	0.04*	0.18*	0.06*	0.06*	*0.09*
	2000, 2250	Starch	0.01	0.13*	0.03	0.05	*0.06*
	2050, 2380	Lignin, waxes, protein & nitrogen	0.28*	0.24*	0.09*	0.38*	*0.25*
	2060, 2300	Protein & nitrogen	0.02	0.02	0.00	0.00	*0.01*
	2060, 2380	Protein, nitrogen & lignin	0.20*	0.25*	0.13*	0.36*	*0.24*
	2130, 2240	Protein	0.23*	0.16*	0.15*	0.29*	*0.21*
	2180, 2210	Protein & cellulose	0.29*	0.15*	0.14*	0.25*	*0.21*
	2180, 2240	Protein & nitrogen	0.31*	0.20*	0.17*	0.21*	*0.22*
	2200, 2240	Protein & starch	0.26*	0.19*	0.15*	0.17*	*0.19*

• Two-band combinations yielding high correlations were extracted from regions known to be related to pigments (Gitelson et al. 2002;Gitelson and Merzlyak 2004;Gitelson et al. 2006); foliage biomass (Mutanga and Skidmore 2004;Cho et al. 2007); leaf water content (Gao, 1996); proteins & starches (Curran, 1989); waxes & protein/enzyme *D*-ribulose 1-5-diphosphate carboxylase@2050, tannic acid@1660, lignin, pectins & protein/enzyme *D*-ribulose 1-5-diphosphate carboxylase@1680, lignin@2380 (Elvidge 1990).

* –significant ($p < 0.01$)

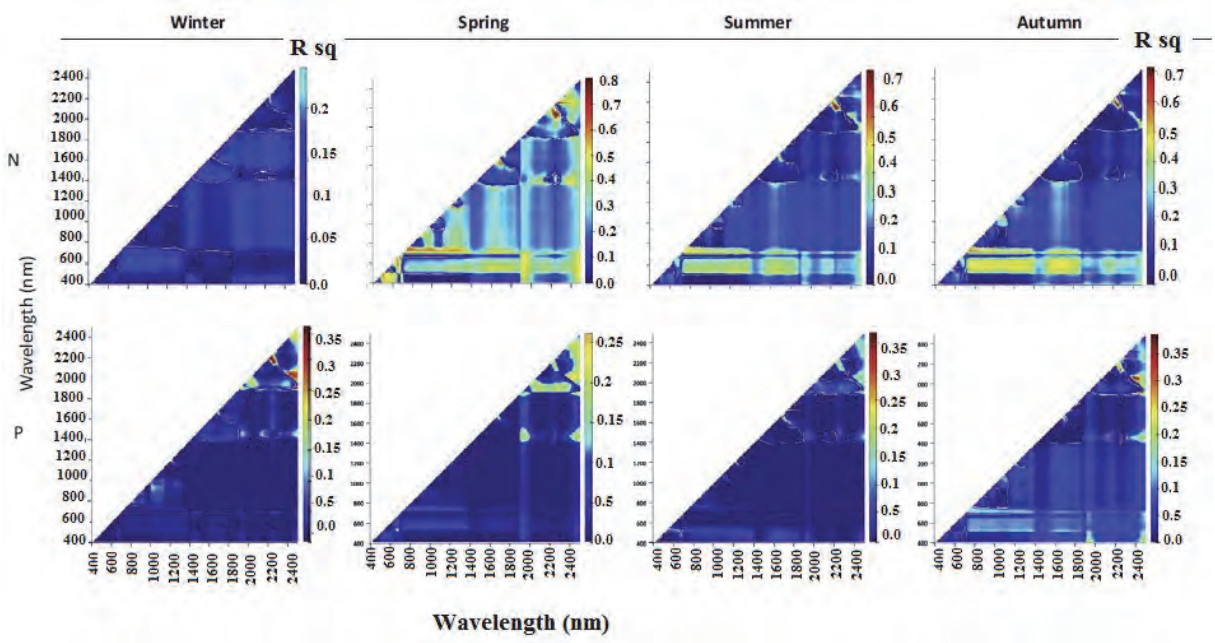

Figure 4.4: Contour plots showing the regression (R^2) between selected vegetation indices calculated from all possible waveband combinations (vertical and horizontal axes) in the 400-2500 nm range (at 10 nm intervals) and leaf N or P concentrations (%) for the six species.

4.4.3. Comparison of predictive models across seasons

The individual-seasons model showed the lowest prediction error of leaf N for the winter season for the indices developed in the red-edge (chlorophyll and foliage biomass) and SWIR regions (protein) of the spectrum (Table 4.5). For the spring, summer and autumn seasons, the individual-seasons model of N showed lower error of prediction (%) in the SWIR, compared to the red-edge region. When the spring-season model (the spring season recorded the highest R^2 between the VI and N concentration) was used to predict N for the other three seasons, the error of prediction (%) increased by 1-5% for the summer and autumn seasons for the VIs in both the red-edge and SWIR regions. Applying the spring-season model to the winter leaf spectra resulted in an increase of the error of prediction by 11-18%. The combined-seasons model for N, compared to the individual-seasons model, showed an increase in error of between 4-7% for the three VIs in winter, a slight decrease in error (≤ 4%) for the spring season, though no major changes for the summer and autumn seasons.

The accuracy of the predictive models for leaf P when compared to the leaf N models was very low (Error > 46%; Table 4.6). The VI for the lignin, waxes, protein and nitrogen bands in the SWIR showed the lowest error of prediction (46%). The combined-season model, on the other hand, decreased the error in prediction by 12-28%, though for the SWIR region in autumn, only by 3%.

Table 4.5: Assessing the capability of the three different predictive models for predicting foliar nitrogen across four seasons. The capability of the spring-season model and combined-seasons model is evaluated in the change of percentage error from the individual-seasons model.

		Winter			Spring			Summer			Autumn		
Model:	VI-band combination	700, 760	740, 780	2130, 2240	700, 760	740, 780	2130, 2240	700, 760	740, 780	2130, 2240	700, 760	740, 780	2130, 2240
	Associated parameter	Chlorophyll region	Foliage biomass	Protein	Chlorophyll region	Foliage biomass	Protein	Chlorophyll region	Foliage biomass	Protein	Chlorophyll region	Foliage biomass	Protein
Individual-seasons	Linear regression:	y = 0.6229x +1.7924	y = 3.7848x +2.0208	y = -1.7299x +2.2936	y = 3.9682x -0.41	y = 34.17x +0.7901	y = -19.06x +3.4246	y = 5.0957x -1.2398	y = 39.447x +0.5076	y = -22.107x +3.9439	y = 5.6791x -1.659	y = 40.194x +0.4004	y = -26.185x +4.3275
	RMSE	0.16	0.17	0.17	0.51	0.41	0.30	0.46	0.44	0.30	0.45	0.48	0.35
	% Error	7.61	7.66	7.68	26.94	21.45	15.92	26.45	25.08	16.90	26.25	27.80	20.67
Spring-season model	Linear regression:	y = 3.9682x -0.41	y = 34.17x +0.7901	y = -19.06x +3.4246	y = 3.9682x -0.41	y = 34.17x +0.7901	y = -19.06x +3.4246	y = 3.9682x -0.41	y = 34.17x +0.7901	y = -19.06x +3.4246	y = 3.9682x -0.41	y = 34.17x +0.7901	y = -19.06x +3.4246
	RMSE	0.40	0.44	0.55	0.51	0.41	0.30	0.50	0.46	0.38	0.53	0.52	0.43
	% Error	18.69	20.39	25.42	26.94	21.45	15.92	28.64	26.17	21.41	30.82	30.28	25.39
Combined-seasons	Mean linear regression:	y = 3.767x -0.3291	y = 29.29x +0.9075	y = -16.04x +3.318	y = 3.767x -0.3291	y = 29.29x +0.9075	y = -16.04x +3.318	y = 3.767x -0.3291	y = 29.29x +0.9075	y = -16.04x +3.318	y = 3.767x -0.3291	y = 29.29x +0.9075	y = -16.04x +3.318
	Mean RMSE training data	0.47	0.44	0.39	0.47	0.44	0.39	0.47	0.44	0.39	0.47	0.44	0.39
	Mean SD training data	0.01	0.01	0.01	0.01	0.01	0.01	0.01	0.01	0.01	0.01	0.01	0.01

	Mean SEP	0.48	0.45	0.39	0.48	0.45	0.39	0.48	0.45	0.39	0.48	0.45	0.39
	Mean SD SEP	0.02	0.02	0.02	0.02	0.02	0.02	0.02	0.02	0.02	0.02	0.02	0.02
	Mean SEP Independent dataset	0.26	0.27	0.32	0.43	0.34	0.25	0.47	0.42	0.28	0.49	0.47	0.34
	SD SEP Independent dataset	0.17	0.18	0.23	0.34	0.28	0.18	0.33	0.30	0.23	0.31	0.32	0.27
	Training % error	21.79	20.40	18.08	24.81	23.23	20.59	26.83	25.11	22.26	27.49	25.73	22.81
	Test % error	22.25	20.86	18.08	25.34	23.76	20.59	27.40	25.69	22.26	28.07	26.32	22.81
	Independent % error	12.05	12.52	14.83	22.70	17.95	13.20	26.83	23.97	15.98	28.65	27.49	19.88
Difference in % error between models:	Spring-season model compared to Individual	-11.08	-12.73	-17.74	0.00	0.00	0.00	-2.19	-1.09	-4.51	-4.57	-2.48	-4.72
	Combined compared to Individual	-4.44	-4.86	-7.15	4.24	3.50	2.72	-0.38	1.11	0.92	-2.40	0.31	0.79
	Combined compared to Spring-season model	6.64	7.87	10.59	4.24	3.50	2.72	1.81	2.20	5.43	2.17	2.79	5.51

SD, standard deviation

SEP, standard error of prediction

Table 4.6: Assessing the capability of the three different predictive models for predicting foliar phosphorus across four seasons. The capability of the autumn-season model and combined-seasons model is evaluated in the change of percentage error from the individual-seasons model.

		Winter		Spring		Summer		Autumn	
Model:	VI-band combination	500, 670	1650, 1690	500, 670	1650, 1690	500, 670	1650, 1690	500, 670	1650, 1690
	Associated parameter	Carotenoids	Lignin, waxes, protein & nitrogen	Carotenoids	Lignin, waxes, protein & nitrogen	Carotenoids	Lignin, waxes, protein & nitrogen	Carotenoids	Lignin, waxes, protein & nitrogen
Individual -seasons	Linear regression:	y = 0.9929x +0.1932	y = 3.7752x +0.3748	y = 1.6711x +0.2559	y = 3.726x +0.2359	y = 3.5344x +0.2985	y = 3.701x +0.3398	y = 1.0447x +0.1865	y = 3.0753x +0.2738
	RMSE	0.12	0.11	0.12	0.12	0.13	0.16	0.08	0.06
	% Error	69.90	60.68	68.79	67.80	77.17	94.15	54.37	45.95
Autumn-season model	Linear regression:	y = 1.0447x +0.1865	y = 3.0753x +0.2738	y = 1.0447x +0.1865	y = 3.0753x +0.2738	y = 1.0447x +0.1865	y = 3.0753x +0.2738	y = 1.0447x +0.1865	y = 3.0753x +0.2738
	RMSE	0.12	0.12	0.13	0.14	0.15	0.16	0.08	0.06
	% Error	70.05	71.32	73.53	79.74	90.25	96.85	54.37	45.95
Combined-seasons	Mean linear regression:	y = 1.3777x +0.2077	y = 2.837x +0.3004	y = 1.3777x +0.2077	y = 2.837x +0.3004	y = 1.3777x +0.2077	y = 2.837x +0.3004	y = 1.3777x +0.2077	y = 2.837x +0.3004
	Mean RMSE training data	0.11	0.11	0.11	0.11	0.11	0.11	0.11	0.11
	Mean SD training data	0.01	0.01	0.01	0.01	0.01	0.01	0.01	0.01
	Mean SEP	0.11	0.11	0.11	0.11	0.11	0.11	0.11	0.11
	Mean SD SEP	0.02	0.02	0.02	0.02	0.02	0.02	0.02	0.02
	Mean SEP Independent dataset	0.08	0.08	0.08	0.07	0.09	0.09	0.06	0.06

	SD SEP Independent dataset	0.08	0.08	0.13	0.14	0.15	0.17	0.06	0.04
	Training % error	63.48	63.48	63.39	63.39	64.84	64.84	78.32	78.32
	Test % error	63.48	63.48	63.39	63.39	64.84	64.84	78.32	78.32
	Independent % error	46.17	46.17	46.10	40.34	53.05	53.05	42.72	42.72
Difference in % error between models:	Autumn-season model compared to Individual	-0.15	-10.64	-4.74	-11.94	-13.08	-2.70	0.00	0.00
	Combined compared to Individual	23.73	14.51	22.69	27.46	24.12	41.10	11.65	3.23
	Combined compared to Autumn-season model	23.88	25.15	27.43	39.40	37.20	43.80	11.65	3.23

SD, standard deviation

SEP, standard error of prediction

4.5 Discussion

4.5.1. Foliar nutrient variation compared to other evergreen subtropical trees

Our results of high foliar nitrogen concentration in winter concurred with other evergreen tropical and subtropical trees (Cai et al. 2009; Lin et al. 2010). Evergreen *Quercus* and spruce trees in other climatic zones showed similar trends (Chapin and Kedrowski 1983; Sabaté et al. 1995; Yasamura and Ishida 2011). These findings support the notion that older leaves of evergreen trees are used for storage during the dormant season, and remobilised in spring for leaf growth (Cherbuy et al. 2001; Millard and Grelet 2010). Other studies showed, however, a lower concentration and variability of foliar nitrogen in winter, compared to the other seasons, for evergreen tropical dry and savannah forests (Franco et al. 2005; Chaturvedi et al. 2011). Few studies reported detailed observations of variability with mean nitrogen concentrations over four seasons or a full phenological cycle. Contrary to our findings, Bell and Ward (1984) reported low variability and concentration of foliar nitrogen in winter for evergreen trees in a Mediterranean climate, and a high variability and concentration in spring (Bell and Ward 1984).

In this study, foliar phosphorus showed relatively similar mean concentrations over the four seasons, though the variability was highest in all seasons except autumn. Bell and Ward (1984) also found very little variability in mean foliar phosphorus concentration of mature evergreen leaves of *Eucalyptus wandoo* over the seasons, with a high variability in summer (Bell and Ward 1984). Other tropical evergreen trees also showed high mean concentration and higher variability of foliar phosphorus for the summer season compared to the other seasons (Cai et al. 2009; Lin et al. 2010). In evergreen savanna trees, however, foliar phosphorus showed a slight decrease from winter to spring, and a significant increase towards summer (Franco *et al*. 2005). In the study of the two evergreen *Eucalyptus* spp., the lowest variability of foliar phosphorus was recorded for winter (Bell and Ward 1984), compared to our findings of the lowest variability in autumn. In a tropical forest of Nigeria, foliar phosphorus concentrations showed no seasonal variation (Sharma 1983).

4.5.2. Seasonally varying nutrient-spectral relationship

The relationship between leaf spectra and foliar nutrients varied over seasons and spectral regions. The highest correlation between leaf N and spectra was recorded in spring and the lowest in winter, whereas the highest correlation between leaf P and spectra was recorded in winter, summer and autumn. Co-variants of foliar N, chlorophyll and foliage biomass did not

follow similar patterns of change between spring and autumn, confirming the varying relationship over seasons. The variations recorded in the relationship concur with the variations noted in the seasonal foliar N patterns, associated with the photosynthesis process. Seasonal patterns of N, derived through VIs from leaf spectra, can therefore potentially indicate seasonal changes in photosynthetic activity of subtropical evergreen trees. All spectral regions used in this study were consistent with other studies for regions associated with foliar N, i.e., the red-edge and SWIR, as well as with foliar P, i.e., the SWIR region (Curran 1989; Elvidge 1990; Kokaly and Clark 1999; Johnson 2001; Kumar et al. 2001; Kokaly 2001; Cho and Skidmore 2006; Cho et al. 2010; Ramoelo et al. 2011).

The other high correlation (R^2 = 0.37, p < 0.01) between foliar P and leaf spectra was found between the carotenoid spectral region (500-520 nm) and the red-edge region (680-760 nm) which may be indicative of a possible relationship between foliar carotenoids, foliar chlorophyll and foliar P occurring at peak productivity in summer. The methyl-erythritol phosphate pathway, which is responsible for the production of both carotenoids and foliar abscisic acid, controls stomatal opening which is also associated with foliar P (Barta and Loreto 2006). The correlation between foliar P and this spectral band combination is, however, only high in summer and not in any of the other three seasons.

To our knowledge, our work is the first study noting the variance in the seasonal relationship between foliar nutrients and related leaf spectral absorption features. Changing relationships between foliar chlorophyll *a* and related leaf spectra was also observed for evergreen mangrove species in a subtropical environment between the wet and dry seasons (Flores-de-Santiago *et al*. 2013). Zhang et al (2007) also noted a changing relationship between estimated and observed chlorophyll for a deciduous maple species, showing a decline in the correlation and accuracy from spring to summer, and an increase in correlation and accuracy from summer to autumn.

4.5.3. Monitoring foliar nutrient phenology using remote sensing models

A number of models, developed from leaf-level spectra, was assessed in their capability to predict foliar nutrient concentration across species and seasons. The RMSE values and error of prediction (%) of two models were compared to those of the model developed for each individual season: a predictive model of the season in which the highest R^2 values were recorded between a VI and nutrient concentrations, as well as a predictive model combining all the seasons. To minimise the influence of individual species on the

development of a regression model, a 1000-times iterative bootstrap procedure was used in the evaluation of the combined-seasons predictive model. The maximum error ranges of the various predictive models for leaf N concentration of the evergreen subtropical trees were below 31% and offered relative capable models to predict across species and season. The individual-season leaf N model showed the lowest range of error for leaf N with an error range between 7-28%. The combined-season leaf N model increased in the prediction error range of between 12-29%, while the spring-season model for leaf N showed an increase in prediction error of between 15-31%. The predictive models for foliar P were mostly > 40% and therefore considered inaccurate in predicting P for these evergreen subtropical trees.

The seasons with the lowest error of prediction was mainly the spring, summer and autumn seasons. The error of prediction for these three seasons deviated by < 5.5% from the error of prediction of the individual-seasons model. However, the error of prediction increased by 4-7% when the combined-seasons model was applied to winter, and by > 10% when the spring-season model was applied to the winter season. The winter season showed significantly higher (p < 0.08) mean observed N concentration, and lower variance, compared to the other three seasons. The phenology of these evergreen trees therefore had a definite influence on the error of predicting leaf N concentration when a model developed in spring was applied to the leaf spectra collected in winter.

The bands with the lowest error of prediction for leaf N concentration was found in the SWIR region for the spring, summer and autumn seasons, compared to the bands used in the red-edge region (related to chlorophyll and foliage biomass). The reversed was observed for winter, where the error of prediction was lower in the red-edge region, compared to the SWIR region bands.

The various models and bands were assessed as an initial step to assess the potential of remote sensing techniques to monitor nutrient phenology across regions and species. A number of multi-spectral spaceborne sensors, such as RapidEye (RE) launched in 2008, and WorldView-2 (WV2) launched in 2009, is expected to improve vegetation health and foliar nitrogen monitoring through the incorporation of a band in the red-edge region. A number of multispectral sensors are also planned for deployment, including WorldView-3 (WV3; 2014), and Sentinel-2 (2015), which will improve the spatial resolution of current sensors, and add to the number of red-edge and SWIR bands at higher spectral resolution. These sensors are expected to improve nutrient mapping at the landscape level (Clevers and Gitelson 2013). The improved spatial resolution of these sensors, will further allow

single-canopy species identification and monitoring, overcoming most of the current limitations of multispectral imagery. In support of these developments, further research is required to improve our understanding of whether the relationship between foliar N and P and spectra reflectance features will change annually, under different climatic conditions, at canopy scale or for other species.

4.5.4. Implications for monitoring global change impact on vegetation

The impact of global change on the seasonal dynamics of nutrients can be potentially monitored through the changing relationship of foliar nutrients to spectra, at canopy (satellite image) scale. Seasonal patterns of nutrients are expected to differ across climatic zones. Remote sensing can contribute to the characterization of foliar nutrient phenology at the bioregional scale, and secondly, monitor the impact of global change on these patterns. The quantification of foliar nutrients could potentially provide more information on subtle changes in magnitude of foliar nutrients, in addition to impacts already noted in phenophases. Considering the low photosynthetic activity currently observed in the dormant season, and that temperature increases may increase photosynthetic activity, an increase in the variability of foliar nutrients, particularly nitrogen, may be expected in future.

4.6 Conclusions

This study found a seasonally changing relationship in foliar nutrients (nitrogen and phosphorus) for evergreen subtropical tree species in St. Lucia, South Africa. The relationship between foliar nutrients and leaf spectra also varied over the seasons and across regions associated with known biochemical and biophysical parameters. A high variability in foliar nutrients is assumed to reflect foliar nutrient dynamics, whereas the higher mean concentration of foliar nutrients may indicate storage of nutrients during the dormant season. Predictive models for leaf N concentration developed for each season showed a higher level of accuracy, particularly for winter, whereas predictive models for leaf P showed low accuracies. Models developed from a single season showed a slight increase in error for the summer and autumn, however a larger increase in error for the winter season for the evergreen trees. Global biogeographic patterns of foliar N and P of tropical and subtropical forests are limited. Many studies focus on nutrient dynamics of a few species and locations, yet monitoring the impact of global change at species level may be difficult and time consuming. Remote sensing offers the potential to monitor N and P at canopy level to establish biogeographical patterns at the regional scale. Furthermore, the subtle initial changes of an increased temperature on photosynthetic activity, is possible through the

quantification of nutrient variability over seasons. We recommend further studies on the phenology of foliar nutrients at regional scale for a number of species and climatic zones, using remote sensing.

4.7 Acknowledgements

This work was funded by the South African Department of Science and Technology (DST), the National Research Foundation (NRF), the Council for Scientific and Industrial Research (CSIR) and the Water Research Commission (WRC). We thank the iSimangaliso Wetland Park Authority and Ezemvelo KwaZulu-Natal (KZN) Wildlife for granting access and logistical support. Dr Ricky Taylor, former ecologist at Ezemvelo KZN Wildlife for guidance and advice. We are grateful to the following fieldwork assistants: Mr S. Gumede, Dr F. Durand, Ms R. van Deventer, Mr A. van Deventer, Mr S. Mfeka, Dr E. Adam, Mr T. Colins, Mr K. Barker, Mr O. Malahlela and the iSimangaliso bursary students Ms N. Nkosi, Ms T. Sibiya, Ms N. Gumede, Mr B. Mdamba, Mr B. Gumbi; Dr A. Ramoelo and Ms N. Dudeni-Tlhone for assistance with R code; Dr K. Eatwell for proof reading.

4.8 References

Barta, C., Loreto, F., 2006. The relationship between the methyl-erythritol phosphate pathway leading to emission of volatile isoprenoids and abscisic acid content in leaves. American Society of Plant Biologists 141 (4), 1676-1683.

Bell, D.T., Ward, S.C., 1984. Seasonal changes in foliar macronutrients (N, P, K, Ca and Mg) in *Eucalyptus saligna* Sm. and *E. wandoo* Blakely growing in rehabilitated bauxite mine soils of the Darling Range, Western Australia. Plant and Soil 81, 377-388.

Booth, B.B.B., Jones, C.D., Collins, M., Totterdell, I.J., Cox, P.M., Sitch, S., Huntingford, C., Betts, R.A., Harris, G.R., Lloyd, J., 2012. High sensitivity of future global warming to land carbon cycle processes. Environmental Research Letters 7 (2), 024002-(8).

Cai, Z., Schnitzer, S.A., Bongers, F., 2009. Seasonal differences in leaf-level physiology give lianas a competitive advantage over trees in a tropical seasonal forest. Oecologia 161, 25-33.

Campoy, J.A., Ruiz, D., Egea, J., 2011. Dormancy in temperate fruit trees in a global warming context: A review. Scientia Horticulturae 130 (2), 357-372.

Chapin, F.S. III, Kedrowski, R.A., 1983. Seasonal Changes in Nitrogen and Phosphorus Fractions and Autumn Retranslocation in Evergreen and Deciduous Taiga Trees. Ecology 64 (2), 376-391.

Chaturvedi, R.K., Raghubanshi, A.S., Singh, J.S., 2011. Leaf attributes and tree growth in a tropical dry forest. Journal of Vegetation Science 22 (5), 917-931.

Cherbuy, B., Joffre, R., Gillon, D., Rambal, S., 2001. Internal remobilization of carbohydrates, lipids, nitrogen and phosphorus in the Mediterranean evergreen oak Quercus ilex. Tree physiology 21 (1), 9-17.

Cho, M.A., Ramoelo, A., Debba, P., Mutanga, O., Mathieu, R., Van Deventer, H., Ndlovu, N., 2013. Assessing the effects of subtropical forest fragmentation on leaf nitrogen distribution using remote sensing data. Landscape Ecology 28 (8), 1479-1491.

Cho, M.A., Van Aardt, J., Main, R., Majeke, B., 2010. Evaluating variations of physiology-based hyperspectral features along a soil water gradient in a *Eucalyptus grandis* plantation. International Journal of Remote Sensing 31 (12), 3143-3159.

Cho, M.A., Skidmore, A.K., 2006. A new technique for extracting the red edge position from hyperspectral data: The linear extrapolation method. Remote Sensing of Environment 101 (2), 181-193.

Cho, M.A., Skidmore, A.K., Sobhan, I., 2009. Mapping beech (*Fagus sylvatica L.*) forest structure with airborne hyperspectral imagery. International Journal of Applied Earth Observation and Geoinformation 11 (3), 201-211.

Cho, M.A., Skidmore, A., Corsi, F., Van Wieren, S.E., Sobhan, I., 2007. Estimation of green grass/herb biomass from airborne hyperspectral imagery using spectral indices and partial least squares regression. International Journal of Applied Earth Observation and Geoinformation 9 (4), 414-424.

Clevers, J.G.P.W., Gitelson, A.A., 2013. Remote estimation of crop and grass chlorophyll and nitrogen content using red-edge bands on Sentinel-2 and -3. International Journal of Applied Earth Observation and Geoinformation 23, 344-351.

Curran, P.J., 1989. Remote Sensing of Foliar Chemistry. Remote Sensing of Environment 30, 271-278.

De Weirdt, M., Verbeeck, H., Maignan, F., Peylin, P., Poulter, B., Bonal, D., Ciais, P., Steppe, K., 2012. Seasonal leaf dynamics for tropical evergreen forests in a process-based global ecosystem model. Geoscientific Model Development (5), 1091.

Dillen, S.Y., De Beeck, M.O., Hufkens, K., Buonanduci, M., Phillips, N.G., 2012. Seasonal patterns of foliar reflectance in relation to photosynthetic capacity and color index in two co-occurring tree species, Quercus rubra and Betula papyrifera. Agricultural and Forest Meteorology 160, 60-68.

Drake, B.G., Gonzalez-Meler, M.A., 1997. More efficient plants: A consequence of rising atmospheric CO_2? Annual Review of Plant Physiology and Plant Molecular Biology 48, 609-639.

Elvidge, C.D., 1990. Visible and near infrared reflectance characteristics of dry plant materials. International Journal of Remote Sensing 11 (10), 1775-1795.

Evans, J.R., 1989. Photosynthesis and Nitrogen Relationships in Leaves of C_3 Plants. Oecologia 78 (1), 9-19.

Ferwerda, J.G., Skidmore, A.K., Mutanga, O., 2005. Nitrogen detection with hyperspectral normalized ratio indices across multiple plant species. International Journal of Remote Sensing 26 (18), 4083-4095.

Field, C., Mooney, H.A., 1986. The photosynthesis-nitrogen relationship in wild plants. In: On the economy of form and function. Givinsh, T.J. (Ed.), Cambridge University Press, Cambridge, pp. 25-55.

Fife, D.N., Nambiar, E.K.S., Saur, E., 2008. Retranslocation of foliar nutrients in evergreen tree species planted in a Mediterranean environment. Tree Physiology 28, 187-196.

Flores-de-Santiago, F., Kovacs, J.M., Flores-Verdugo, F., 2013. The influence of seasonality in estimating mangrove leaf chlorophyll-*a* content from hyperspectral data. Wetlands Ecological Management 21, 193-207.

Flores-de-Santiago, F., Kovacs, J.M., Flores-Verdugo, F., 2012. Seasonal changes in leaf chlorophyll *a* content and morphology in a sub-tropical mangrove forest of the Mexican Pacific. Marine Ecology Progress Series 444, 57-68.

Food and Agriculture Organization (FAO) of the United Nations (UN), 2012. Global forest land-use change 1990-2005. 169 59 pp-http://foris.fao.org/static/data/fra2010/FP169En.pdf.

Franco, A.C., Bustamante, M., Caldas, L.S., Goldstein, G., Meinzer, F.C., Kozovits, A.R., Rundel, P., Coradin, V.T.R., 2005. Leaf functional traits of Neotropical savanna trees in relation to seasonal water deficit. Trees 19, 326-335.

Gamon, J.A., Surfus, J.S., 1999. Assessing leaf pigment content and activity with a reflectometer. New Phytologist 143 (1), 105-117.

Gitelson, A.A., Keydan, G.P., Merzlyak, M.N., 2006. Three-band model for noninvasive estimation of chlorophyll, carotenoids and anthocyanin contents in higher plant leaves. Papers in Natural Resources 1-5-http://digitalcommons.unl.edu/natrespapers/258.

Gitelson, A.A., Merzlyak, M.N., 2004. Non-destructive assessment of chlorophyll, carotenoid and anthocyanin content in higher plant leaves: Principles and Algorithms. Papers in Natural Resources. 77-94-http://digitalcommons.unl.edu/natrespapers/263.

Gitelson, A.A., Zur, Y., Chivkunova, O.B., Merzlyak, M.N., 2002. Assessing carotenoid content in plant leaves with reflectance spectroscopy. Photochemistry and photobiology 75 (3), 272-281.

Gond, V., De Pury, D., Veroustraete, F., Ceulemans, R., 1999. Seasonal variations in leaf area index, leaf chlorophyll, and water content; scaling-up to estimate fAPAR and carbon balance in a multilayer, multispecies temperate forest. Tree physiology 19 (10), 673-679.

Harris, I., Jones, P.D., Osborn, T.J., Lister, D.H., 2013. Updated high-resolution grids of monthly climatic observations – the CRU TS3.10 Dataset. International Journal of Climatology 34 (3), 623-642.

Horneck, D.A., Miller, R.O., 1998. Determination of Total Nitrogen in Plant Tissue. In: Handbook of reference methods for plant analysis. Kalra, Y.P. (Ed.), CRC Press, Boca Raton, pp. 81-83.

Huang, Z., Turner, B.J., Dury, S.J., Wallis, I.R., Foley, W.J., 2004. Estimating foliage nitrogen concentration from HYMAP data using continuum removal analysis. Remote Sensing of Environment 93 (1-2), 18-29.

Huber, S., Kneubühler, M., Psomas, A., Itten, K., Zimmermann, N.E., 2008. Estimating foliar biochemistry from hyperspectral data in mixed forest canopy. Forest Ecology and Management 256 (3), 491-501.

Isaac, R.A., Johnson, W.C., 1998. Elemental determination by Inductively Coupled Plasma. In: Handbook of reference methods for plant analysis. Kalra, Y.P. (Ed.), CRC Press, Boca Raton, pp. 165-170.

Johnson, L.F., 2001. Nitrogen influence on fresh-leaf NIR spectra. Remote Sensing of Environment 78 (3), 314-320.

Kirschbaum, M.U.F., 2000. Forest growth and species distribution in a changing climate. Tree Physiology 20, 309-322.

Knox, N.M., Skidmore, A.K., Prins, H.H.T., Asner, G.P., Van der Werff, H.M.A., De Boer, W.F., Van der Waal, C., De Knegt, H.J., Kohi, E.M., Slotow, R., Grant, R.C., 2011. Dry season mapping of savanna forage quality, using the hyperspectral Carnegie Airborne Observatory sensor. Remote Sensing of Environment 115 (6), 1478-1488.

Knyazikhin, Y., Schull, M.A., Stenberg, P., Mõttus, M., Rautiainen, M., Yang, Y., Marshak, A., Carmona, P.L., Kaufmann, R.K., Lewis, P., Disney, M.I., Vanderbilt, V., Davis, A.B., Baret, F., Jacquemoud, S., Lyapustin, A., Myneni, R.B., 2012. Hyperspectral remote sensing of foliar nitrogen content. The Proceedings of the National Academy of Sciences of the United States of America E185-E192.

Kokaly, R.F., 2001. Investigating a Physical Basis for Spectroscopic Estimates of Leaf Nitrogen Concentration. Remote Sensing of Environment 75 (2), 153-161.

Kokaly, R.F., Asner, G.P., Ollinger, S.V., Martin, M.E., Wessman, C.A., 2009. Characterizing canopy biochemistry from imaging spectroscopy and its application to ecosystem studies. Remote Sensing of Environment 113, Supplement 1 S78-S91.

Kokaly, R.F., Clark, R.N., 1999. Spectroscopic Determination of Leaf Biochemistry Using Band-Depth Analysis of Absorption Features and Stepwise Multiple Linear Regression. Remote Sensing of Environment 67 (3), 267-287.
Kumar, L., Schmidt, K.S., Dury, S., Skidmore, A.K., 2001. Imaging spectroscopy and vegetation science, In: Image Spectroscopy, Van der Meer, F.D. and De Jong, S.M. (Eds.), Kluver Academic Publishers, Dordrecht.

Lal, C.B., Annapurna, C., Raghubanshi, A.S., Singh, J.S., 2001. Foliar demand and resource economy of nutrients in dry tropical forest species. Journal of Vegetation Science 12, 5-14.

Lewandowska, M., Jarvis, P.G., 1977. Changes in Chlorophyll and Carotenoid Content, Specific Leaf Area and Dry Weight Fraction in Sitka Spruce, in Response to Shading and Season. New Phytologist 2, 247-256.

Lieth, H., 1974. Phenology and Seasonality Modeling, Springer-Verlag, Berlin- New York.

Lin, Y., Liu, X., Zhang, H., Fan, H., Lin, G., 2010. Nutrient conservation strategies of a mangrove species *Rhizophora stylosa* under nutrient limitation. Plant Soil 326 (1/2), 469-479.

Lukac, M., Calfapietra, C., Lagomarsino, A., Loreto, F., 2010. Global climate change and tree nutrition: effects of elevated CO_2 and temperature. Tree Physiology 30, 1209-1220.

McDonald, J.H., 2008. Handbook of biological statistics. Sparky House Publishing, Maryland, USA.

Millard, P., Grelet, G., 2010. Nitrogen storage and remobilization by trees: ecophysiological relevance in a changing world. Tree Physiology 30 (9), 1083-1095.

Mucina, L., Rutherford, M.C., 2006. The Vegetation of South Africa, Lesotho and Swaziland. South African National Biodiversity Institute (Strelizia), Pretoria.

Mutanga, O., Skidmore, A.K., 2007. Red edge shift and biochemical content in grass canopies. ISPRS Journal of Photogrammetry and Remote Sensing 62, 34-42.

Mutanga, O., Kumar, L., 2007. Estimating and mapping grass phosphorus concentration in an African savanna using hyperspectral image data. International Journal of Remote Sensing 28 (21), 4897-4911.

Mutanga, O., Skidmore, A.K., 2004. Narrow band vegetation indices overcome the saturation problem in biomass estimation. International Journal of Remote Sensing 19, 3999-4014.

Nakaji, T., Oguma, H., Fujinuma, Y., 2006. Seasonal changes in the relationship between photochemical reflectance index and photosynthetic light use efficiency of Japanese larch needles. International Journal of Remote Sensing 27 (3), 493-509.

Niinements, U., Tamm, U., 2005. Species differences in timing of leaf fall and foliage chemistry modify nutrient resorption efficiency in deciduous temperate forest stands. Tree Physiology 25, 1001-1014.

Ollinger, S.V., Reich, P.B., Frolking, S., Lepine, L.C., Hollinger, D.Y., Richardson, A.D., 2013. Nitrogen cycling, forest canopy reflectance and emergent properties of ecosystems. The Proceedings of the National Academy of Sciences of the United States of America 110 (27), E2437.

Ollinger, S.V., Richardson, A.D., Martin, M.E., Hollinger, D.Y., Frolking, S.E., Reich, P.B., Plourde, L.C., Katul, G.G., Munger, J.W., Oren, R., Smith, M.-., Paw U, K.T., Bolstad, P.V., Cook, B.D., Day, M.C., Martin, T.A., Monson, R.K., Schmid, H.P., 2008. Canopy nitrogen, carbon assimilation, and albedo in temperate and boreal forests: Functional relations and potential climate feedbacks. The Proceedings of the National Academy of Sciences of the United States of America 105 (49), 19336-19341.

Partridge, T.C., Dollar, E.S.J., Moolman, J., Dollar, L.H., 2010. The geomorphic provinces of South Africa, Lesotho and Swaziland: A physiographic subdivision for earth and environmental scientists. Transactions of the Royal Society of South Africa 65 (1), 1-47.

Penuelas, J., Baret, F., Filella, I., 1995. Semi empirical Indexes to Assess Carotenoids Chlorophyll-*a* Ratio from Leaf Spectral Reflectance. Photosynthetica 31 (2), 221-230.

Ramoelo, A., Skidmore, A.K., Cho, M.A., Schlerf, M., Mathieu, R., Heitkönig, I.M.A., 2012. Regional estimation of savanna grass nitrogen using the red-edge band of the spaceborne RapidEye sensor. International Journal of Applied Earth Observation and Geoinformation 19, 151-162.

Ramoelo, A., Skidmore, A.K., Schlerf, M., Heitkönig, I.M.A., Mathieu, R., Cho, M.A., 2013. Savanna grass nitrogen to phosphorous ratio estimation using field spectroscopy and the potential for estimation with imaging spectroscopy. International Journal of Applied Earth Observation and Geoinformation 23, 334-343.

Ramoelo, A., Skidmore, A.K., Schlerf, M., Mathieu, R., Heitkönig, I.M.A., 2011. Water-removed spectra increase the retrieval accuracy when estimating savanna grass nitrogen and phosphorus concentrations. ISPRS Journal of Photogrammetry and Remote Sensing 66 (4), 408-417.

Rathcke, B., Lacey, E.P., 1985. Phenological patterns of terrestrial plants. Annual Review of Ecology and Systematics 16, 179-214.

Reef, R., Feller, I.C., Lovelock, C.E., 2010. Nutrition of mangroves. Tree physiology 30 (9), 1148-1160.

Reich, P.B., Oleksyn, J., 2004. Global patterns of plant leaf N and P in relation to temperature and latitude. Proceedings of the National Academy of Sciences of the United States of America 101 (30), 11001-11006.

Richardson, A.D., Keenan, T.F., Migliavacca, M., Ryu, Y., Sonnentag, O., Toomey, M., 2013. Climate change, phenology, and phenological control of vegetation feedbacks to the climate system. Agricultural and Forest Meteorology 169, 156-173.

Rouse, J., Haas, R., Schell, J., Deering, D., 1973. Monitoring Vegetation Systems in the Great Plains with ERTS. Third ERTS Symposium, United States of America, National Aeronautics and Space Administration (NASA) SP-351 I 309-317.

Sabaté, S., Sala, A., Gracia, C.A., 1995. Nutrient content in *Quercus ilex* canopies: Seasonal and spatial variation within a catchment. Plant and soil 168-169 297-304.
Sardans, J., Peñuelas, J., 2012. The Role of plants in the effects of global change on nutrient availability and stoichiometry in the plant-soil system. Plant Physiology 160 1741-1761.

Schlerf, M., Atzberger, C., Hill, J., Buddenbaum, H., Werner, W., Schüler, G., 2010. Retrieval of chlorophyll and nitrogen in Norway spruce (Picea abies L. Karst.) using imaging spectroscopy. International Journal of Applied Earth Observation and Geoinformation 12 (1), 17-26.

Seppälä, R., Buck, A., Katila, P., 2009. Adaptation of Forests and People to Climate Change. A Global Assessment Report. IUFRO World Series Volume 22. Helsinki. 224 p.

Sharma, B.M., 1983. Mineral content of leaves of some common tropical forest trees and their associated soils in Ibadan, Nigeria. Canadian Journal of Forest Research (13), 4-556-562.

Skidmore, A.K., Ferwerda, J.G., Mutanga, O., Van Wieren, S.E., Peel, M., Grant, R.C., Prins, H.H.T., Balcik, F.B., Venus, V., 2010. Forage quality of savannas — Simultaneously mapping foliar protein and polyphenols for trees and grass using hyperspectral imagery. Remote Sensing of Environment 114 (1), 64-72.

Smith, M., Ollinger, S.V., Martin, M.E., Aber, J.D., Hallett, R.A., Goodale, C.L., 2002. Direct estimation of aboveground forest productivity through hyperspectral remote sensing of canopy nitrogen. Ecological Applications 12 (5), 1286-1302.

Sokolic, F., 2006. The use of satellite remote sensing to determine the spatial and temporal distribution of surface water on the Eastern Shores of Lake St. Lucia. M.Sc. thesis. Master of Science, University of KwaZulu-Natal. Durban: UKZN.

Townsend, P.A., Foster, J.R., Chastain, R.A., Jr., Currie, W.S., 2003. Application of imaging spectroscopy to mapping canopy nitrogen in the forest of the central Appalachian Mountains using Hyperion and AVIRIS. IEEE Transactions on Geoscience and Remote Sensing 41 (6), 1347-1354.

Tucker, C.J., 1979. Red and photographic infrared linear combinations for monitoring vegetation. Remote Sensing of Environment 8 (2), 127-150.

Ullah, S., Si, Y., Schlerf, M., Skidmore, A.K., Shafique, M., Iqbal, I.A., 2012. Estimation of grassland biomass and nitrogen using MERIS data. International Journal of Applied Earth Observation and Geoinformation 19, 196-204.

United States Department of Energy (US DOE), 2012. Research Priorities for Tropical Ecosystems Under Climate Change Workshop Report. US Department of Energy Office of Science DOE/SC-0153 U.S. Department of Energy Office of Science. science.energy.gov/ber/news-and-resources/.

Yasamura, Y., Ishida, A., 2011. Temporal variation in leaf nitrogen partitioning of broad-leaved evergreen tree, *Quercus myrsinaefolia*. Journal of Plant Research 124 115-123.

Yoder, B.J., Pettigrew-Crosby, R.E., 1995. Predicting nitrogen and chlorophyll content and concentrations from reflectance spectra (400-2500 nm) at leaf and canopy scales. Remote Sensing of Environment 53 (3), 199-211.

Zhang, Y., Chen, J.M., Thomas, S.C., 2007. Retrieving seasonal variation in chlorophyll content of overstory and understory sugar maple leaves from leaf-level hyperspectral data. Canadian Journal of Remote Sensing 33 (5), 406-415.

Zhou, L., Kaufmann, R.K., Tian, Y., Myneni, R.B., Tucker, C.J., 2003. Relation between interannual variations in satellite measures of northern forest greenness and climate between 1982 and 1999. Journal of Geophysical Research 108 (D1), 1-11.

5 ASSESSING THE EFFECTS OF DUKUDUKU FOREST FRAGMENTATION ON LEAF NITROGEN DISTRIBUTION USING REMOTE SENSING DATA

This chapter includes work done by Dr Moses Azong Cho and team, published in the paper by Cho, M.A.; Ramoelo, A.; Debba, P.; Mutanga, O.; Mathieu, R.; Van Deventer, H.; Ndlovu, N. 2013. Assessing the effects of subtropical forest fragmentation on leaf nitrogen distribution using remote sensing data. Landscape Ecology, 2013, 28, 8, 1479-1491.

5.1 Abstract

Tropical forest loss resulting from conversion of forest to other land-cover types such as grassland, secondary forest, subsistence crop farms and small forest patches affects leaf nitrogen (N) stocks in the landscape. This study explores the utility of new remote sensing tools to model the spatial distribution of leaf N in Dukuduku, St Lucia. Leaf N was mapped using models developed from a relatively new spaceborne sensor, RapidEye (5 m spatial resolution). A detailed land-cover map derived from another new spaceborne sensor, WorldView-2 (2 m resolution) was used to assess differences in leaf N between land-cover types. The results showed that indigenous forest fragmentation in Dukuduku leads to significant losses in leaf N as most of the land-cover types (e.g. pasture and subsistence farmlands) resulting from forest degradation showed lower leaf N when compared to the original indigenous forest. Further analysis of the spatial variation of leaf N revealed an autocorrelation distance of about 50 m for leaf N in the fragmented landscape, a scale corresponding to the average dimension of subsistence fields. The availability of new multispectral sensors such as RapidEye and WorldView-2 thus, moves remote sensing closer to widespread monitoring of the effect of tropical forest degradation on nutrient (e.g. N) cycle.

5.2 Introduction

Tropical forest ecosystems play a major role in nutrient and carbon cycling (Vitousek and Sanford, 1986; Van der Werf *et al*., 2009). For example, tropical forests are a major sink of atmospheric carbon dioxide and several studies have shown that tropical forest deforestation and degradation constituted a major source of global greenhouse emission in the 1990s (Malhi and Grace, 2000; Achard *et al*., 2004; Fearnside and Laurance, 2004; Gibbs et al., 2007; DeFries *et al*., 2002). Gibbs *et al* (2007) put the estimates at about 15-25% of annual global greenhouse gas emissions. Whereas, the effects of forest disturbance on carbon stocks at the broad landscape level have been widely studied, few studies have modelled

the effects of forest degradation on nutrient stocks (e.g. Nitrogen (N) and phosphorus (P)) (e.g. Billings and Gaydess, 2008).

Tropical forest degradation in many parts of Africa is characterised by the clearing of the forest for pasture, agriculture or urban development (Van Wyk *et al*., 1996; Coops *et al*., 2004). In most cases, the forest is fragmented into patches of various sizes and shapes. The forest patches in most degraded landscape are surrounded by a matrix of different vegetation and/or land use types (e.g. mono-crop plantations, small subsistence farms, pasture lands) (Saunders *et al*., 1991; Harrera *et al*., 2011). The immediate environmental consequences of forest fragmentation include soil erosion, loss of biodiversity, invasion by alien species, loss of soil fertility, changes in litter and canopy nutrient stocks and vegetation productivity (Saunders *et al*., 1991; Gibbs, 1998; McDonald *et al*., 2002; Vasconcelos, and Luizão, 2004; Giertz *et al*., 2005; Lauga and Joachim, 1992; Duguay *et al*., 2007; Lizee *et al.*, 2011). Spatially explicit information on the above factors is rare, let alone on changes in foliar nutrient stocks, following forest fragmentation. Saunders et al. (1991) asserted that forest fragmentation affects nutrient cycling processes by increased soil heating and its effect on soil microorganism and invertebrate numbers and activity, on litter decomposition and soil moisture retention. The resulting loss of soil fertility might translate into low foliar nutrient stocks.

Nitrogen is an important nutrient for plant growth (Groffman and Turner, 1995). Nitrogen taken up by plants in the form of nitrates is used in the synthesis of components such as chlorophyll, the carbon fixing enzyme ribulose biphosphate carboxylase (Rubisco) and inert structural components in cell tissue (Mooney, 1986). Leaf nitrogen concentration has been used as a proxy to assess ecosystem productivity (Mooney, 1986; Smith *et al*., 2002). Nitrogen inputs into an ecosystem include lightning and bacteria fixation of atmospheric nitrogen, and decomposition and nitrification of dead organic matter (e.g. litter). Outputs from the system include plant uptake, denitrification, leaching and surface runoff. Thus, forest N pools consist of soil N (ammonium, nitrate, and some dissolved organic nitrogen compounds), nitrogen in litter and that retained in living plant parts (roots, stems and leaves) (Vitousek, 1982). Rates of organic matter decomposition are high in lowland moist tropical forest than in temperate forest (Nye, 1960). Greenland and Kowal (1960) argued that standing biomass is as important as the soil as a storehouse of plant nutrients, particularly in moist tropical forest where vegetation growth is so high and where the reserves of nutrients in the soil may be quite rapidly depleted by leaching or absorbed by plants. Vitousek and Sanford (1986) asserted that foliar chemistry represents a useful indicator of overall nutrient

status of a plant, where nutrient concentrations in leaves are correlated with nutrient concentrations in other plant parts. Leaching and surface runoff of nutrients from moist tropical forest patches in a degraded landscape might serve as important nutrient sources for surrounding vegetation, including grasslands and subsistence farms.

The question is, how does the conversion of indigenous tropical forest into other land cover types e.g. grassland, secondary forest, subsistence crop farms and small forest patches affect foliage N stocks in the fragmented landscape? Another question of interest is, at what scale does leaf N vary in fragmented or disturbed landscape. The ability to adequately tackle the above questions may rely on the capability to accurately map land cover types and leaf N concentration at the broad landscape level, a procedure that was rarely achieved before the advent of high spectral resolution (hyperspectral) remote sensing (Iverson et al., 1989; Groom et al., 2006). Most hyperspectral sensors acquire radiance information in less than 10 nm bandwidths from the visible to the shortwave infrared (400-2500 nm) (Curran, 2001). The narrow bandwidth of hyperspectral data allows for the detection of the subtle absorption features of nitrogen in green vegetation (Curran et al, 2001; Cho et al., 2009). However, the high cost and limited availability of spaceborne hyperspectral imagery has stymied the routine application of this sort of remote sensing for leaf nitrogen analysis at the regional scale. Many hyperspectral studies highlighted the region of the red-edge in the electromagnetic spectrum (700-760 nm) as having a high potential for accurate estimation of leaf chlorophyll and N concentration or content at peak productivity (Horler, 1983; Matson *et al*., 1994; Kokaly and Clark, 1999; Cho and Skidmore, 2006). More recently, new spaceborne sensors such as RapidEye (Ramoelo *et al*., 2012) and Worldview-2 have been launched with new wavebands in the red-edge region, for example at 710 nm for Rapideye and at 725 nm for Worldview-2 (Adam *et al*., 2012). These sensors provide us with new opportunities to assess leaf N stock at the regional scale. Ramoelo *et al*. (2012) have successfully mapped leaf nitrogen concentration over a large area using the red-edge band of RapidEye images in the Kruger National Park, South Africa.

The aims of this study were to (i) ascertain the ability to assess leaf N concentration using RapidEye imagery in a fragmented landscape following indigenous forest deforestation and (ii) assess the effects of forest fragmentation on leaf nitrogen distribution. The above aims were achieved through a detailed land cover classification from WorldView-2 images, mapping of leaf N using RapidEye images, an analysis of the differences in the predicted leaf N among land cover types and an analysis of the spatial heterogeneity of leaf N.

5.3 Material and methods

5.3.1. Study site

The study site is situated in the northern part of KwaZulu-Natal between Mtubatuba town and the Indian Ocean, north of Richard's Bay (Figure 5.1). It consists of three main ecosystem types; intact closed canopy forest (inland coastal forest and dune forest), swamp forest and fragmented landscape. The inland coastal forest is known as the Dukuduku forest (28°25'S, 32°17'E). The Dukuduku forest is the largest patch (6500 ha) of coastal lowland forest along the eastern coastline in KwaZulu-Natal. A total of 29% of the Dukuduku forest was lost to settlement and subsistence farming activities between 1992 and 2005 (Ndlovu 2011). The area forms part of the iSimangaliso Wetland Park which is the largest estuary in South Africa (Van Heerden, 2011). The study area as demarcated by the Map in Figure 5.1 is surrounded by large commercial Eucalyptus (to the North) and Sugarcane (to the South) plantation. Thus, the study area consists of varying land uses including protected areas, commercial farms, communal areas and towns.

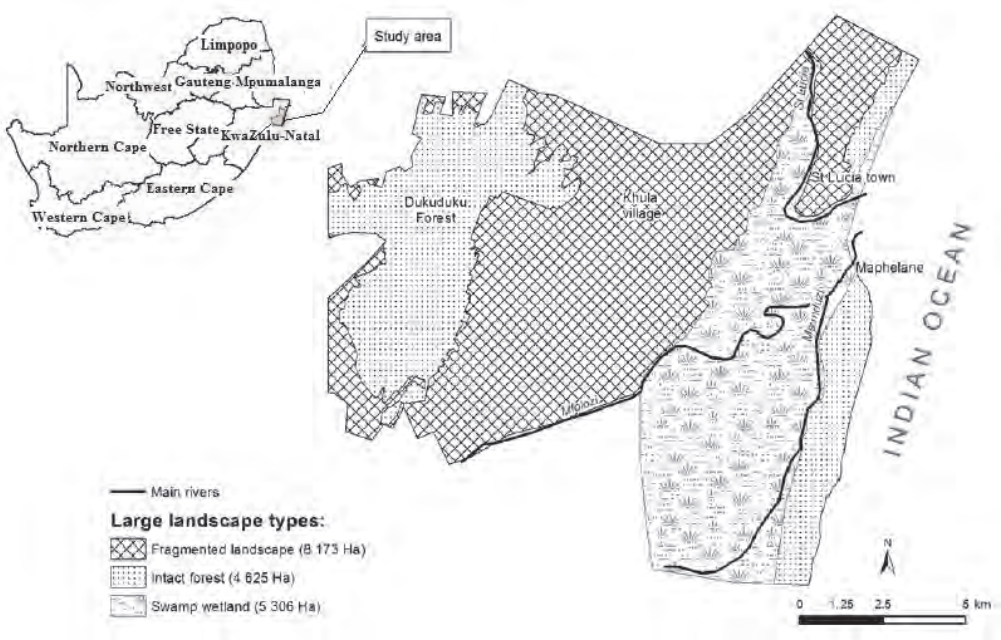

Figure 5. 1: Large landscape types.

5.3.2. Acquisition of satellite images and pre-processing

Rapideye imagery (5 m spatial resolution) of the study site was acquired on 21 March 2011. The sensor consists of five spectral bands (Blue: 440-510 nm; Green: 520-590 nm; Red: 630-685 nm; Red Edge: 690-730 nm; NIR: 760-850 nm). The level 1B RapidEye image (geometrically and radiometrically corrected) obtained from the image provider were atmospherically corrected using ATCOR-2, flat terrain model. ATCOR is based on MODTRAN radiative transfer code (Richter and Schlapfer, 2002). Two archive geometrically corrected WorldView-2 images (2 m spatial resolution) acquired in April and December of 2010 were also used in the study to classify land cover types. Worldview-2 consists of multispectral bands centred at 425 nm, 480 nm, 545 nm, 605 nm, 660 nm, 725 nm, 835 nm and 950 nm. We assessed the geometric accuracies of the two images using ground control points and found the WorldView-2 images more accurately corrected as compared to the RapidEye image. Using the WorldView-2 as the reference image, we corrected the RapidEye image using image-image registration in ENVI software (ITT Visual Information Solution, Boulder Co USA). In this study, the WorldView-2 images were used only for the land cover classification because of the huge time difference between the image acquisition (April and December 2010) and the field campaign to collect leaf N data (March 2011).

5.3.3. Field data acquisition and leaf nitrogen analysis

Fieldwork sampling of leaf specimens was conducted on the 29 and 30 March 2011. Sunlit leaves were collected from 69 randomly selected plots consisting of tree or grass canopies along paths in the intact and fragmented landscape. We ensured that each tree or grass canopy sampled consisted of a homogenous canopy (same species for the trees and similar set of species for the grasses) of about 15 m by 15 m. The sampled trees and grass plots were located between 10 m to about 100 m from the edges of intact forest and paths within the fragmented landscape. The number of plots that were trees and grassland were 44 and 25, respectively. Five and two plots of the grassland plots were wetlands and sugarcane, respectively.

The specimens were oven dried for 24 hours at 70^{o}C on the 31 April 2011. The dry leaf samples were sent to the Agricultural Research Council-Institute for Tropical and Subtropical Crops, South Africa for chemical analysis of leaf N. Leaf N concentration was analysed using acid digestion method. Leaf N concentration was expressed as the percentage nitrogen to the leaf mass.

Additional data were collected for land cover classification in July 2011. The global positioning system (GPS) locations of different land cover (LC) types (intact forest, degraded forest, grassland/subsistence farms, eucalyptus farms, sugarcane farms) were recorded in the field. The points were only collected from homogenous areas (of at least 20 m by 20 m) of the land cover types.

5.3.4. Land cover (LC) classification

The WorldView-2 images were used for the LC classification. A mosaic of the April and December 2010 images were made prior to the classification using ENVI 4.8 software (ITT Visual Information Solution, Boulder Co USA). The classification was also conducted using ENVI 4.8. The GPS point data for the various land cover types (intact forest, degraded forest, grassland/subsistence farms, eucalyptus farms, wetlands and sugarcane farms) were overlaid on the image and a region of interest (ROI) consisting of an array of pixels was created for each point. Additional ROIs were created for the intact forest and wetland grasslands (mainly from the swamp forest) since these were clearly visible on the WorldView-2 image. The ROIs were randomly divided into the training and test datasets in the following ratio: intact forest (44/17), degraded forest (25/10), grassland/subsistence farms (11/6), eucalyptus farms (18/13), sugarcane farms (24/8), wetland grasslands (47/21) bare areas and settlements (22/11). The training dataset was used to train the classifier. The commonly used maximum likelihood classifier was used in this study. The overall, producer's and user's accuracies of classification were derived using the test data on a per pixel basis. The producer's accuracy is a measure of how accurately the analyst classified the image data for each cover-type, while the user's accuracy is a measure of how well the classification performed in the field on a per cover-type basis.

5.3.5. Regression analysis and mapping of leaf nitrogen

The GPS point of the field sample plots were overlaid on the atmospherically corrected RapidEye images and the tree or grass canopy spectral profiles were extracted using an array of 2-by-2 pixels. Several red-edge spectral indices that have shown great promise for leaf nitrogen or chlorophyll estimation in previous studies including normalised difference vegetation index (NDVI) (Rouse *et al*., 1974), Gitelson and Merzlyak index (Gitelson and Merzlyak, 1997), Datt index (Datt, 1998; Datt, 1999) and the MERIS terrestrial chlorophyll index (MTCI) (Dash and Curran, 2007) were computed from the spectral profile. After exploring the relationship between leaf N and the red-edge indices, the MTCI was chosen for

the prediction of leaf N in the study area as it provided the highest coefficient of determination (R^2) with leaf N.

It should be noted that the MTCI was originally derived for leaf chlorophyll estimation. We have used this index to estimate leaf N because leaf chlorophyll is a good correlate of leaf N, particularly at peak productivity (Yoder and Pettigrew-Crosby, 1995). The strength of the linear relationship between leaf N and the MTCI was assessed using a bootstrapped (McGarigal et al., 2000) linear regression (Eq.1) because of the small number of sample points.

$$y = mx + c \tag{1}$$

where *y* is the leaf nitrogen concentration, *x* the vegetation index (i.e. MTCI), *m* the slope and *c* the intercept on the y-axis.

The regression coefficients were computed for 1000 iterative sampling with replacement, i.e. for each iteration, 2/3 of the data were randomly drawn and used for calibration of the regression model and the remaining 1/3 for validation. For each iteration, the root-mean-square error (RMSE, Eq.2) of calibration and validation (termed standard error of prediction (SEP, same as Eq.2)) were computed. The leaf N for each pixel of the vegetation index image was then predicted using Eq.1, whereby, *m* and *c* were the average values for the 1000 iterations in the bootstrapped linear regression.

$$RMSE = \sqrt{\frac{\sum_{i=1}^{n}(y-y\prime)^2}{n}} \tag{2}$$

An MTCI map was derived from the RapidEye image using the ENVI 4.8 bandmaths feature. Using the linear regression equation involving MTCI, a leaf N concentration map was computed from the MTCI map. To evaluate the effect of forest fragmentation on leaf N stock, the land cover map derived from the WorldView-2 imagery was spatially re-sampled to a spatial resolution of RapidEye i.e. to 5 m. Lastly, differences in leaf N concentration between the different land cover classes were assessed. First, ROIs for the different land cover classes were created and overlaid on the leaf N Map using ENVI software. Subsequently, leaf N values for the different land cover classes were extracted from the N map and saved as text files. Tables for the leaf N values were then created. The differences among the various land cover classes were assessed using descriptive statistics including a table of mean and inter-quartile ranges, and box plots.

5.3.6. Characterising spatial heterogeneity of leaf nitrogen concentration

The spatial variation or heterogeneity of leaf N in the intact and fragmented regions were analysed using semivariogram models (Garrigues *et al*., 2006; Murwira and Skidmore, 2006). Semivariogram modelling involves the hypothesis of statistical stationarity i.e. the characteristics of the underlying random function are invariant to the shifting of a group of pixels from one part of the image to another (Garrigues *et al*., 2006). In this study, we proposed to assess the spatial variation of leaf N from exponential models fitted to experimental semivariograms (Eq.3). The exponential model was adopted in this study as it provided the best fit when compared to the spherical and Gaussian models.

$$\gamma(h) = \frac{1}{2n}\sum_{n(h)}\left[z(u) - z(u+h)\right]^2 \quad (3)$$

where *γ(h)* are the semivariances, *z(u)* is the pixel value at position *u* in the input map, *z(u+h)* is the pixel value at position *u+h* in the input map and *h* is the lag vector representing separation (distance) between two spatial points (pixels). We used a lag tolerance of 200 pixels (600 m). Two parameters that describe a semivariogram are of particular importance in this study: (i) the sill represents the point (semivariance) at which a semivariogram levels off and (ii) the range represents the lag distance at which a semivariogram reaches the sill. The range describes the size or scale of the dominant objects in an image that give rise to the semivariogram structure (Jupp *et al*., 1988). The semivariograms were modelled using the Integrated Land and Water Information System (ILWIS) software (ITC, Enchede, The Netherlands).

5.4 Results

5.4.1. Land-cover classification from WorldView-2 imagery

An overall classification accuracy of 85% (kappa coefficient = 0.79) was obtained for the land-cover classification (Figure 5.2). With the exception of the normal grassland class (pasture and farmlands), the producer and user accuracies were in general high (Table 5.1). The low user's accuracy (44%) for the grassland class was due to a miss-classification of wetland grassland pixels (16% of wetland pixels) into other grasslands (pasture and farmlands). Natural forest remains by far the largest (about 7500 ha) land-cover type in the study area followed by wetland grasslands (Table 5.2). The average patch size of natural forest, eucalyptus farm, grasslands (pasture and subsistence farms) and sugarcane farms in

the fragmented landscape are 5900 m^2, 3100 m^2, 1500 m^2 and 625 m^2, respectively; yielding an overall patch size of 2781 m^2.

Table 5. 1: Classification accuracies for land-cover types in the study area using Rapideye imagery

Land cover type	Producer's accuracy (%)	User's accuracy (%)
Natural forest (the intact forest and patches in the fragmented landscape)	96	94
Grasslands (pasture and farmlands)	76	44
Wetland grasslands	79	97
Degraded areas (thickets of shrubs, secondary forest trees and invasive aliens)	88	90
Eucalyptus farms	94	89
Sugarcane farms	95	67
Bare soil and settlements	100	98

Table 5. 2: Surface area of land-cover classes in the study area.

Broad landscape types:					
Land cover class (LC)	Fragmented landscape (ha)	Intact forest (ha)	Swamp wetland (ha)	**Total area (ha)**	% of LC class:
Natural forest	1 821	4 430	1 305	**7 555**	41.7
Grassland/subsistence farms	1 243	5	366	**1 615**	8.9
Wetland grasslands	2 211	94	2 352	**4 657**	25.7
Degraded forest	867	18	310	**1 195**	6.6
Eucalyptus farms	195	18	0	**214**	1.2
Sugarcane farms	683	19	678	**1 380**	7.6
Bare soil and settlements	1 150	38	294	**1 481**	8.2
Total area (ha)	**8 169**	**4 623**	**5 305**	**18 097**	
% of landscape type	45	26	29		

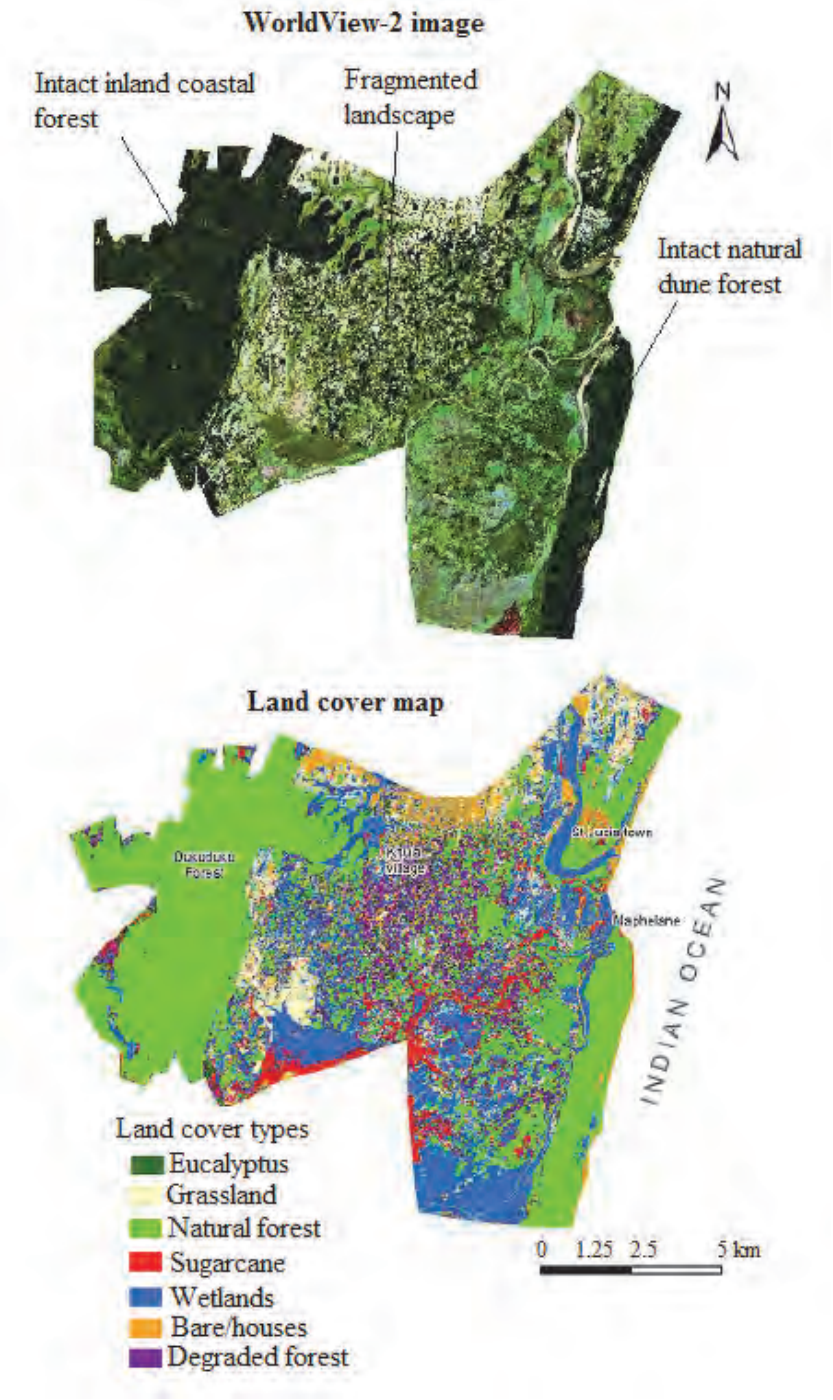

Figure 5. 2: Land cover classes for the study area

5.4.2. Statistics of laboratory measured leaf nitrogen

The laboratory measured leaf N (Figure 5.3) showed the following statistics; mean = 2.19%, maximum = 4.76%, minimum = 0.70% and standard deviation (SD) = 0.94%. The grass leaf N concentration (mean = 1.38%) was significantly (p-value < 0.0001) lower than the tree leaf N (2.66%). Furthermore, a Shapiro-Wilk normality test conducted on the data showed that

the leaf N data for grasses and trees were normally distributed; grass (W = 0.92, p-value > 0.05) and trees (W = 0.98, p-value > 0.05).

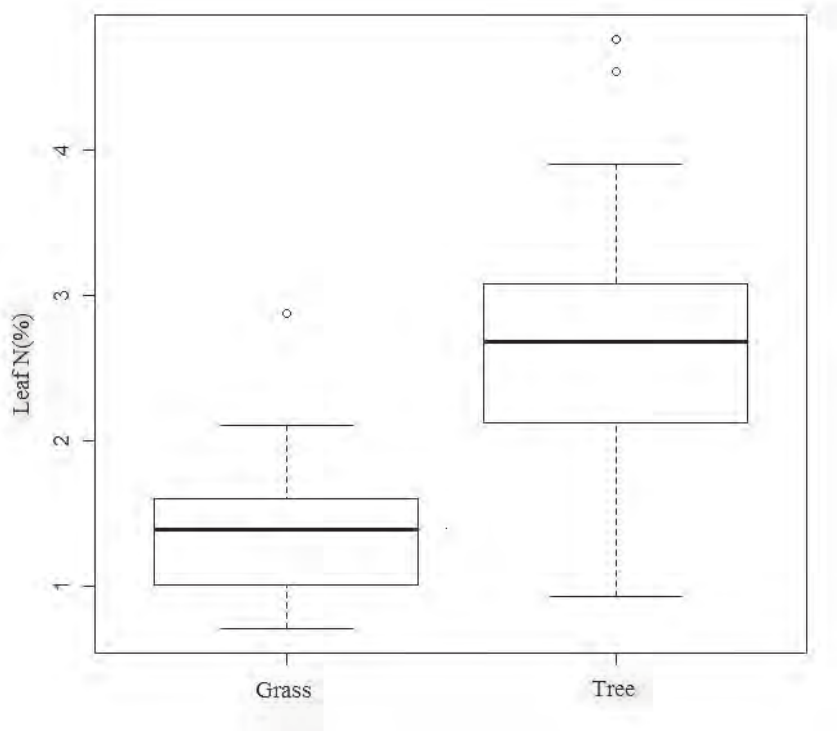

Figure 5. 3: Laboratory measured leaf N for grasses and trees

5.4.3. Mapping leaf nitrogen from RapidEye imagery

Amongst the four vegetation indices investigated, the MTCI yielded the highest linear regression with leaf nitrogen (R^2 = 0.52, SD = 0.05) and the lowest prediction error on the test data (SEP = 0.65% i.e. 29% of mean leaf N, SD = 0.08) (Table 5.3, Figure 5.4). The commonly used NDVI yielded the highest prediction error (SEP = 0.77, SD = 0.1) amongst the indices applied in this study.

The regression model based on the MTCI (Eq. 4) was used to predict leaf N concentration for every pixel on the RapidEye image (Figure 5.5).

$$[N] = 0.8926 * MTCI - 0.6103 \quad \text{Eq.4.}$$

where [*N*] is the leaf N concentration (%). The slope of the line of best fit (0.8926) and the intercept (-0.6103) were the means for 1000 bootstrapped iterations.

Table 5. 3: Training and validation results for predicting leaf nitrogen concentration based on bootstrapped linear regression for 1000 iterations

Index	Formulation (R_λ = reflectance at wavelength (λ nm))	Calibration model				Validation	
		Av R^2	SD R^2	Av RMSE	SD RMSE	Av SEP	SD SEP
NDVI	$(R_{820} - R_{660})/(R_{820} + R_{660})$	0.34	0.05	0.75	0.05	0.77	0.10
Datt	$(R_{820} - R_{710})/(R_{820} - R_{660})$	0.49	0.04	0.66	0.04	0.68	0.08
SR	R_{820}/R_{710}	0.47	0.05	0.67	0.04	0.70	0.08
MTCI	$(R_{820} - R_{710})/(R_{710} - R_{660})$	0.52	0.05	0.64	0.04	0.66	0.08

R^2 = coefficient of determination, RMSE = root mean square error for the calibration model, SEP = standard error of prediction, Av = average, SD = standard deviation, NDVI = normalised difference vegetation index, Datt (named after Datt (1998)), SR = simple ratio, MTCI = MERIS terrestrial chlorophyll index

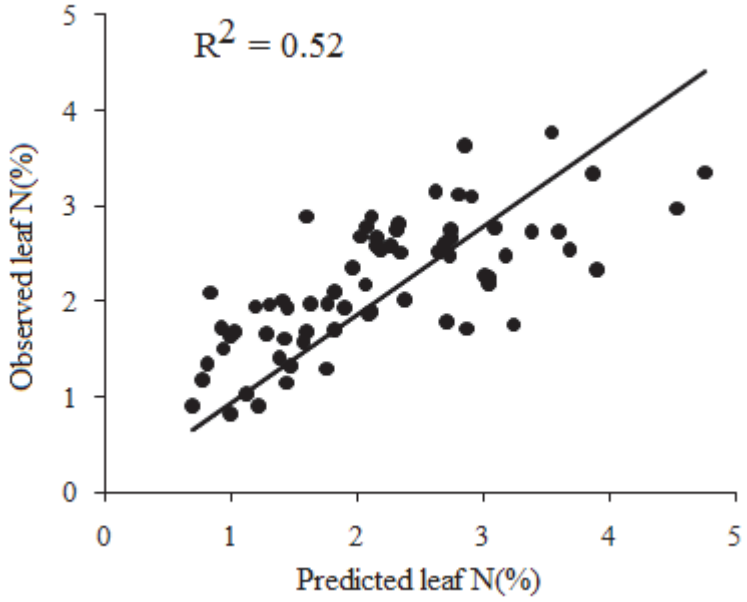

Figure 5. 4: Linear relationship between observed and predicted leaf N concentration using linear regression models for MERIS terrestrial chlorophyll index (MTCI). RMSE = Root mean square error

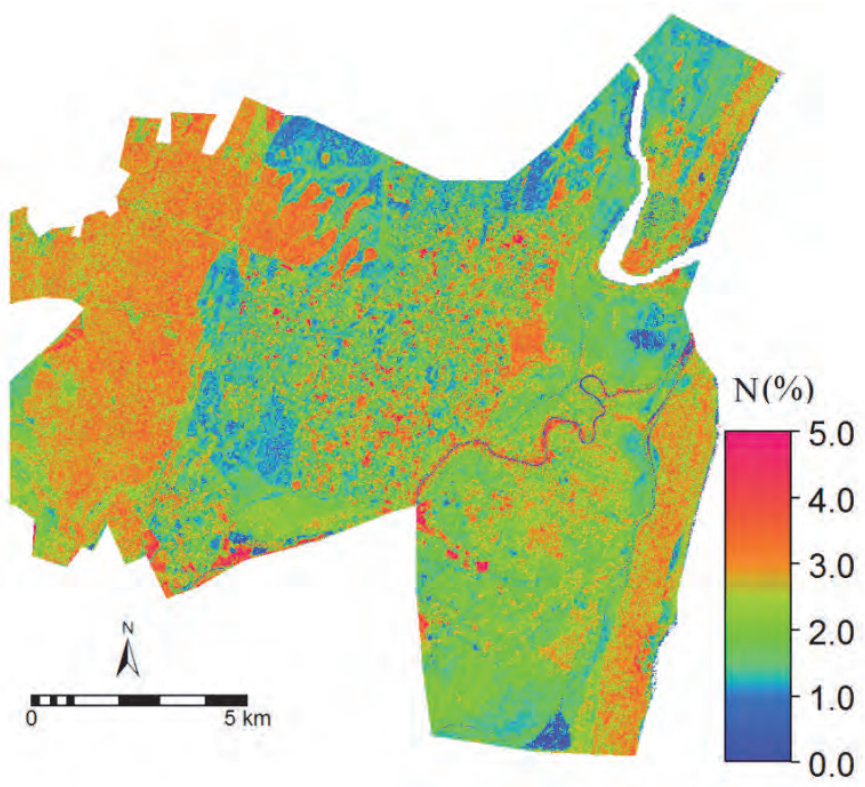

Figure 5. 5: Leaf N concentration in the study area

5.4.4. Differences in predicted leaf nitrogen among land cover types

Table 5.4 shows the descriptive statistics of predicted leaf N for the large intact forest areas (intact inland coastal forest and dune forest) and leaf N of land-cover types in the degraded landscape including small natural forest patches, degraded forest patches, grasslands, eucalyptus and sugarcane farms. Among the cover types, eucalyptus farms showed the highest average leaf N concentration. The conversion of intact forest into grasslands significantly reduces the leaf N stock in the landscape. The Natural forest fragments in the disturbed area still showed leaf N concentrations comparable to those of the large intact forest areas.

Table 5. 4: Statistics of predicted leaf nitrogen

	Intact inland forest	Dune forest	Natural forest in fragmented landscape	Degraded forest in fragmented landscape	Grasslands/ subsistence in fragmented landscape	Eucalyptus	Sugarcane
Mean	2.93	2.77	2.47	2.27	1.45	3.13	2.03
1st quartile	2.59	2.48	1.950	1.82	1.26	2.44	1.53
3rd quartile	3.27	3.09	2.98	2.68	1.56	3.80	2.40
SD	0.52	0.55	0.70	0.61	0.31	0.96	0.69

SD = standard deviation

5.4.5. Scale of leaf nitrogen variability

Leaf N varies at a higher distance (50 m) in the fragmented landscape when compared to the intact forest (25 m) (Table 5.5 and Figure 5.6). The lower autocorrelation distance of leaf N variability in the intact forest probably correspond to tree crown level variability while the autocorrelation distance in the fragmented landscape might depict spatial dependence at the scale of subsistence fields (e.g. crop and eucalyptus farms) in the region (i.e. 2500 m^2 for a rectangular field). It should be recalled that the land-cover classification yielded an average patch size of 2781 m^2 in the fragmented landscape.

Table 5. 5: Exponential model parameters for semivariograms of leaf nitrogen

Land cover type	Nugget	Sill	Range (m)
Intact indigenous forest	0.05	0.26	25
Fragmented landscape	0.05	0.5	50

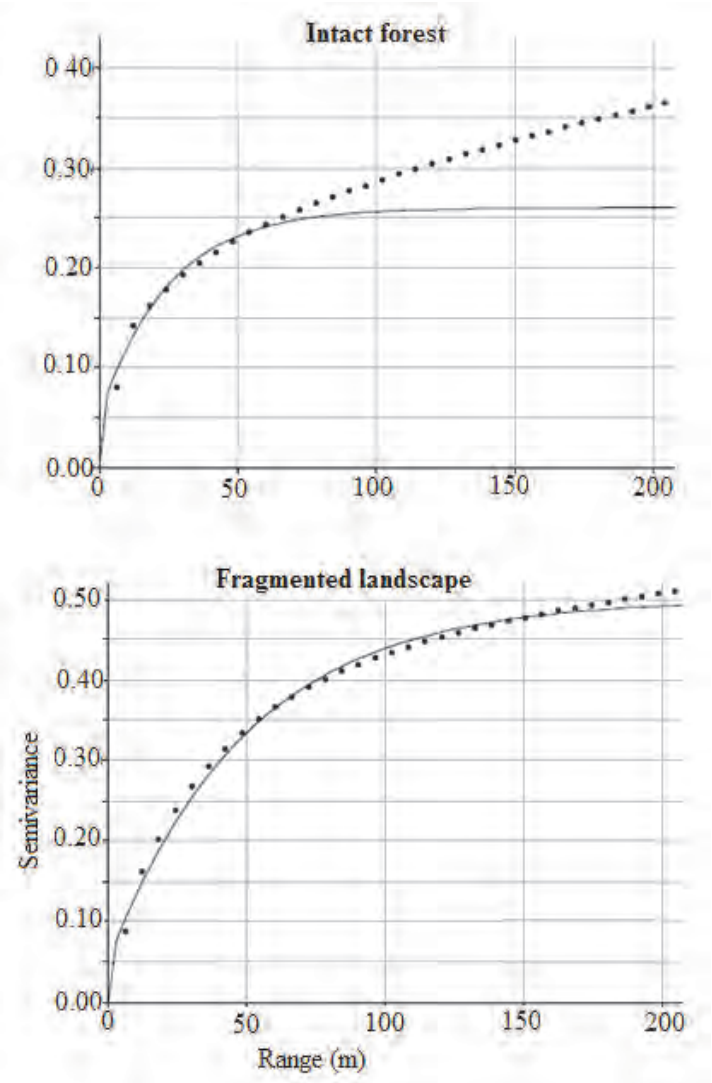

Figure 5. 6: Semivariograms of leaf nitrogen for the intact forest and fragmented landscape

5.5 Discussion

This study has demonstrated the utility of RapidEye imagery for mapping leaf nitrogen concentration at the broad landscape scale, corroborating the results obtained by Ramoelo *et al*. (2012). Leaf N concentration was mapped with a prediction error equal to 29% of mean nitrogen concentration. The accurate mapping of leaf N concentration with Rapideye imagery can be attributed to the presence of the red-edge band at 710 nm. MTCI, an index derived from the red-edge band at 710 nm provided the highest accuracy of estimation of leaf N in this study. Variations in the red-edge reflectance are mostly controlled by differences in leaf chlorophyll concentration. Therefore, the positive correlation between leaf N and MTCI depends on the positive correlation relationship between leaf N and leaf chlorophyll and this relationship has been shown to vary with leaf phenology (e.g. Huang *et al.*, 2004). Low cost spaceborne sensors with strategic bands in the shortwave infrared

(SWIR) might improve on the spatial modelling of leaf N because most of the spectral absorption features of nitrogen are located in the shortwave infrared (Curran, 1989). It is hoped that the Sentinel-2, an upcoming spaceborne sensor to be launched by the European Space Agency (ESA) with strategically located bands in the visible to SWIR would provide new opportunities to routinely assess and monitor leaf N stocks in fragmented and subsistence farming landscapes.

The loss of leaf N stock following forest degradation in the tropics is not an unknown phenomenon. However, the ability to map leaf N at the broad landscape facilitates the task of analysing the effect of forest degradation on the spatial distribution of leaf N on a plot-by-plot level, thus permitting a better understanding of different landscape patterns and processes. This is even more relevant in the tropical forest region of Africa, where more than 80% of the population depends on subsistence farming for their livelihoods. Mapping leaf N at the scale of the RapidEye images (5 m) in the tropical forest systems of Africa would allow for a farm-to-farm assessment of leaf N stocks because of the usual small sizes of subsistence fields. For example, this study shows that leaf N in the degraded landscape varies at a scale (50 m) that might correspond to the size of a subsistence field in the region. Thus, the ability to map leaf N at the farm-size scale might provide a greater understanding of the different land management or farming practices at that scale. Leaf N maps could be used in participatory exercises with the farming communities to create awareness on the consequences of forest degradation on leaf N and hence productivity of subsistence farms.

The results of this study show that deforestation and the subsequent conversion of the degraded area into grasslands leads to loss of nitrogen from the system. However, patches of indigenous forest within the degraded areas still retain relatively high concentration of nitrogen in their foliage. This also applies to eucalyptus trees which are exotic species grown in the degraded area. The cleared areas in the study site are mostly used for farming of crops like sweet potato, maize and sugarcane. The sandy soils in the area are low in fertility. Thus, soil fertility in the area is highly dependent on the decomposition of the dead organic matter, reason for which crop production quickly declines after one to two years of farming on the cleared land. Furthermore, farming methods used in this area are not adequate to maintain soil fertility for long periods of time. Farmers often resort to clearing more forest area to acquire new fertile lands. The vicious cycle of forest clearance and poor farming methods leads to soil depletion and subsequent acquisition of new fertile forest land, resulting in a high rate of forest loss.

Indigenous forest patches in the degraded area can serve as nutrient sources for the surrounding farmlands. Leaching and surface runoff from the forest patches might feed adjacent grasslands and farmlands with nutrients. While both exotic and indigenous trees have the potential to provide nitrogen replenishment in degraded tropical systems, domestication of indigenous tree species has been considered in the past two decades as an alternative to subsistence commercial plantations and slash-and-burn operations associated with the destruction of tropical and sub-tropical indigenous forests (Sanchez *et al*., 1997; Leakey and Simons, 1998; Simons and Leakey, 2004). Although the commercial value of domesticated indigenous trees would not meet those of e.g. *Eucalyptus* spp. for the construction business, agroforestry and non-timber products of domesticated indigenous species offer a number of benefits in comparison to commercial plantations:

- indigenous species sustain greater biodiversity more than subsistence exotic commercial forestry plantations,
- pockets of indigenous trees may provide corridors of faunal migration and floral dispersion,
- indigenous trees use less water (Zhou *et al*., 2002 and are better adapted to soil logging conditions in the swamp wetlands, and
- indigenous forest provide food resources and medicine to poor rural communities.

Thus, mixed farming practices with patches of indigenous tree species should be encouraged in fragmented landscapes to help sustain biodiversity in degraded tropical forest (Prasad, 2003). On the other hand, allelochemicals in eucalyptus leaf litter may suppress growth of understorey vegetation (May and Ash, 1990).

5.6 Conclusions

The following conclusions could be drawn from the study:

- Nitrogen can be mapped at peak productivity using RapidEye sensor.
- Forest fragmentation significantly affects leaf nitrogen concentration.
- Eucalyptus trees tend to accumulate as much leaf nitrogen as the natural forest in the Dukuduku region.

5.7 Acknowledgments

The Council for Scientific and Industrial Research (CSIR), the Department of Science and Technology (DST) and the Water Research Commission (WRC) provided the funding for this study. We wish to thank Oupa Malahlela for atmospherically correcting the RapidEye images used in the study. We also express gratitude to Mr Khanyile MM, the manager of the Dukuduku forest for his wonderful cooperation throughout the project.

5.8 References

Achard F, Eva HD, Mayaux P, Stibig HJ, Belward A (2004) Improved estimates of net carbon emissions from land cover change in the tropics for the 1990s Global Biogeochemical Cycles 18: GB2008

Adam E, Mutanga O, Cho MA **(**2012**)** High density biomass estimation for wetland vegetation using WorldView-2 imagery and random forest regression algorithm International Journal of Applied Earth Observation and Geo-information 366-406

Billings S, Gaydess E (2008) Soil nitrogen and carbon dynamics in a fragmented landscape experiencing forest succession Landscape Ecology 23: 581-593

Cho MA ,Skidmore AK (2006) A new technique for extracting the red edge position from hyperspectral data: The linear extrapolation method Remote Sensing of Environment 101: 181-193

Cho MA, Van Aardt J, Main R, Majeke B (2010) Evaluation of variations of physiology-based hyperspectral features along a soil water gradient in Eucalyptus grandis plantation International Journal of Remote Sensing 31(12): 3143-3159

Coops NC, White JD, Scott NA (2004) Estimating fragmentation effects on simulated forest net primary productivity derived from satellite imagery International Journal of Remote Sensing 25: 819-838

Curran PJ (1989) Remote sensing of foliar chemistry Remote Sensing of Environment 30(3): 271-278

Curran PJ (2001) Imaging spectrometry for ecological applications JAG 3: 305-312

Curran PJ, Dungan JL, Peterson DL (2001) Estimating the foliar biochemical concentration of leaves with reflectance spectrometry: Testing the Kokaly and Clark methodologies Remote Sensing of Environment 76: 349-359

Dash J, Curran PJ (2007) Evaluation of the MERIS terrestrial chlorophyll index (MTCI) Advances in Space Research 39: 100-104

Datt B (1998) Remote Sensing of Chlorophyll *a* Chlorophyll *b* Chlorophyll *a* & *b* and Total Carotenoid Content in Eucalyptus Leaves Remote Sensing of Environment 66: 111-121

Datt B (1999) Visible/near infrared reflectance and chlorophyll content in Eucalyptus leaves International Journal of Remote Sensing 20: 2741-2759

DeFries RS, Houghton RA, Hansen MC, Field CB, Skole D, Townshend J (2002) Carbon emissions from tropical deforestation and regrowth based on satellite observations for the 1980s and 1990s Proceedings of the National Academy of Sciences 99: 14256-14261

Duguay S, Eigenbrod F, Fahrig L (2007) Effects of surrounding urbanization on non-native flora in small forest patches Landscape Ecology 22: 589-599

Fearnside PM, Laurance WF (2004) Tropical Deforestation and Greenhouse-Gas Emissions Ecological Applications 14: 982-986

Garrigues S, Allard D, Baret F, Weiss M (2006) Quantifying spatial heterogeneity at the landscape scale using variogram models Remote Sensing of Environment 103: 81-96

Gibbs HK, Brown S, Niles JO, Foley JA (2007) Monitoring and estimating tropical forest carbon stocks: making REDD a reality Environmental Research Letters 2:1-13

Gibbs JP (1998) Distribution of woodland amphibians along a forest fragmentation gradient Landscape Ecology 13(4): 263-268

Giertz S, Junge B, Diekkrüger B (2005) Assessing the effects of land use change on soil physical properties and hydrological processes in the sub-humid tropical environment of West Africa Physics and Chemistry of the Earth Parts A/B/C 30: 485-496

Gitelson AA, Merzlyak MN (1997) Remote estimation of chlorophyll content in higher plant leaves International Journal of Remote Sensing 18: 2691-2697

Greenland DJ, and Kowal JML (1960) Nutrient content of the moist tropical forest of Ghana Plant and Soil 12: 154-173

Groffman PM, Turner CL (1995) Plant productivity and nitrogen gas fluxes in a tallgrass prairie landscape Landscape Ecology 10(5): 255-266

Groom G, Mücher C, Ihse M, Wrbka T (2006) Remote Sensing in Landscape Ecology: Experiences and Perspectives in a European Context Landscape Ecology 21: 391-408

Herrera J, García D, Morales J (2011) Matrix effects on plant-frugivore and plant-predator interactions in forest fragments Landscape Ecology 26: 125-135

Horler DNH, Dockray M, Barber J (1983) The red edge of plant leaf reflectance International Journal of Remote Sensing 4: 273-288

Huang W, Wang J, Wang Z, Zhaochun J, Wang J (2004) Inversion of foliar biochemical parameters at various physiological stages and grain quality indicators of winter wheat with canopy reflectance International Journal of Remote Sensing 25: 2409-2419

Iverson LR, Graham RL, Cook EA (1989) Applications of satellite remote sensing to forested ecosystems Landscape Ecology 3: 131-143

Kokaly RF, Clark RN (1999) Spectroscopic determination of leaf biochemistry using band-depth analysis of absorption features and stepwise multiple linear regression Remote Sensing of Environment 67: 267-287

Lauga J, Joachim J (1992) Modelling the effects of forest fragmentation on certain species of forest-breeding birds Landscape Ecology 6: 183-193

Leakey RRB, Simons AJ (1998) The domestication and commercialization of indigenous trees in agroforestry for the alleviation of poverty Agroforestry Systems 38: 165-176

Lizée M-H, Manel S, Mauffrey J-F, Tatoni T, Deschamps-Cottin M (2012) Matrix configuration and patch isolation influences override the species-area relationship for urban butterfly communities. Landscape Ecology 27:159-169

Malhi Y, Grace J (2000) Tropical forests and atmospheric carbon dioxide Trends in ecology & evolution (Personal edition) 15: 332-337

May FE, Ash JE (1990). An assessment of the allelopathic potential of Eucalyptus. Australian Journal of Botany, 38: 245-254.

Matson P, Johnson L, Billow C, Miller J, Pu R (1994) Seasonal Patterns and Remote Spectral Estimation of Canopy Chemistry Across the Oregon Transect Ecological Applications 4: 280-298

McDonald MA, Healey JR, Stevens PA (2002) The effects of secondary forest clearance and subsequent land-use on erosion losses and soil properties in the Blue Mountains of Jamaica Agriculture Ecosystems & Environment 92: 1-19

McGarigal K, Cushman S, Stafford S (2000) Multivariate statistics for wildlife and ecology research Springer New York

Mooney HA (Editor) (1986) Photosynthesis Plant ecology Blackwell scientific publication Oxford United Kingdom

Murwira A, Skidmore AK (2006) Monitoring change in the spatial heterogeneity of vegetation cover in an African savanna International Journal of Remote Sensing 27: 2255-2269

Ndlovu N, Luck-Vogel M, Schloms B, Cho M (2011) The quantification of human impact on the Dukuduku indigenous forest from 1960 to 2008 using GIS techniques as a basis for sustainable management Fifth natural forest and wood land symposium Richard Bay KwaZulu-Natal Department of Agriculture Forestry and Fisheries South Africa Richard bay South Africa

Nye PH (1960) Organic matter and nutrient cycles under moist tropical forest Plant and Soil 13: 333-346

Ramoelo A, Skidmore AK, Cho MA, Schlerf M, Mathieu R, Heitkönig IMA (2012) Regional estimation of savanna grass nitrogen using the red-edge band of the spaceborne RapidEye sensor International Journal of Applied Earth Observation and Geoinformation 19: 151-162

Richter, R. and Schlapfer, D., 2002. Geo-atmospheric processing of airborne imaging spectrometry data. Part 2. Atmospheric/topographic correction. International Journal of Remote Sensing, 23: 2631-2649.

Rouse JW, Haas RH, Schell JA, Deering DW, Harlan JC (1974) Monitoring the vernal advancement and retrogradation of natural vegetation NASA/GSFC Type III Final Report MD Greenbelt pp 371

Sanchez PA, Buresh RJ, Leakey RRB (1997) Trees soils and food security Phil Trans R Soc Lond B 352: 949-961

Saunders DA, Hobbs RJ, Margules CR (1991) Biological Consequences of Ecosystem Fragmentation: A Review Conservation Biology 5: 18-32

Simons AJ, Leakey RRB (2004) Tree domestication in tropical agroforestry Agroforestry Systems 61: 167-181

Smith M-L, Ollinger SV, Martin ME, Aber JD, Hallett RA, Goodale CL (2002) Direct estimation of aboveground forest productivity through hyperspectral remote sensing of canopy nitrogen. Ecological Applications, 12: 1286-1302.

Van der Werf GR, Morton DC, DeFries RS, Olivier JGJ, Kasibhatla PS, Jackson RB, Collatz GJ, Randerson JT (2009) CO_2 emissions from forest loss Nature Geosci 2: 737-738

Van Heerden IL 2011 Management concepts for the Mfolozi flats and estuary as a component of the management of the iSimangaliso Wetland Park In: Bate GC Whitfield AK and Forbes AT (Eds) 2011 A review of studies on the Mfolozi estuary and associated flood plain with emphasis on information required by management for future reconnection of the river to the St Lucia system Report to the Water Research Commission WRC Report No KV 255/10 Pretoria: WRC

Van Wyk GF, Everard DA, Midgley JJ, Gordon IG (1996) Classification and dynamics of a southern African subtropical coastal lowland forest South African Journal of Botany 62: 133-142

Vasconcelos HL, Luizão FJ (2004) Litter Production and Litter Nutrient Concentrations in a Fragmented Amazonian Landscape Ecological Applications 14: 884-892

Vitousek P (1982) Nutrient Cycling and Nutrient Use Efficiency The American Naturalist 119: 553-572

Vitousek PM, Sanford RL Jr (1986) Nutrient Cycling in Moist Tropical Forest Annual Review of Ecology and Systematics 17: 137-167

Yoder BJ, Pettigrew-Crosby RE (1995) Predicting nitrogen and chlorophyll content and concentrations from reflectance spectra (400-2500 nm) at leaf and canopy scales Remote Sensing of Environment 53: 199-211

Zhou GY, Morris JD, Yan JH, Yu ZY, Peng SL (2002) Hydrological impacts of reafforestation with eucalypts and indigenous species: a case study in southern China Forest Ecology and Management 167: 209-222.

6 PHYSIOCHEMICAL PROCESSES UNDERLYING THE COMPOSITION AND DISTRIBUTION OF VEGETATION

This chapter summaries the work done by Ms Kelly Rautenbach in fulfilment of the requirements for the degree of Magister Scientiae in the Faculty of Science at the Nelson Mandela Metropolitan University (NMMU) under supervision of Professor J.B. Adams in January 2015 titled "Present state of macrophytes and responses to management scenarios at the St Lucia and Mfolozi Estuaries". The full thesis can be accessed as a pdf from NMMU.

The St. Lucia Estuary, the largest estuary in South Africa, has been subject to many natural (a decade long drought) and anthropogenic impacts. A particular mouth manipulation activity, the artificial separation of the Mfolozi River and the St Lucia Estuary in 1952, was done to stop the perceived "silting up" of the estuary, but resulted in a decrease in freshwater supply. The changes in inflows (both fresh and marine) are controlled by management decisions and affect other system parameters such as salinity, water level and turbidity, which influence the distribution of biota. Therefore knowledge on the physico-chemical environment and eco-physiological tolerances of macrophytes will lead to informed future management decisions.

The first of the three objectives carried out for this study determined the present state and distribution of the macrophytes of the St. Lucia and Mfolozi estuaries. The macrophyte habitats mapped in 2008 and 2013 were the submerged macrophytes, reeds and sedges, mangroves, grass and shrubs, salt marsh (succulent) and swamp forest. Results indicated that low salinity in the lakes and high water level in 2013 caused die-back or expansion of particular habitats. Submerged macrophytes, in particular *Stuckenia pectinata*, grows well in water with salinity <15 ppt, therefore this habitat increased by 412 ha (96%) in cover since 2008. Salt marsh decreased by 553 ha (57%) due to inundation. Since 2008 the reeds and sedges increased by 390 ha (in North Lake and the Narrows) due to the salinity decrease. In the Narrows the mangroves decreased by 28 ha (9%) in area cover. This was due to the drought that persisted for so many years, which caused low water levels and non-tidal conditions.

The second objective was to determine the present state / health of the mangroves at four sites along the Narrows by assessing sediment condition and population structure of the trees. These results were compared to those obtained in 2010. The total density of *Avicennia marina* increased since 2010, however this was due to the large increase in seedlings at Site 1, the back channel site. The highest sediment salinity (26 ppt) and porewater salinity (29 ppt) was recorded for this site and these results show that this back

channel site was strongly influenced by the open Mfolozi Estuary (increase in marine waters) and tidal conditions at the time of sampling in 2013.
The total density of *Bruguiera gymnorrhiza* decreased, but an increase in adults was recorded at Site 2, the freshwater site. The soil collected from the *Bruguiera* quadrats was fresher and drier than that of the Avicennia quadrats of Site 2. Lack of seedlings (of both species) was due to the dense stands of *Acrostichum aureum* (mangrove fern) and *Phragmites australis* (common reed) and a thick, impenetrable mat of *Avicennia* pneumatophores.

At Sites 3 and 4, the drier sites (where sediment moisture contents were the lowest for all sites at 43 and 42% respectively), seedling and sapling density was low, but adults increased in density since 2010. Recruitment and survival were impacted by the harsh environmental conditions that prevailed prior to 2013 (low water level and non-tidal influence), but adults survived.

The results of the test that determined the percentage of aerenchyma of the pneumatophores indicated that waterlogging stress did not affect the aerenchyma of the pneumatophores. However the period of inundation was probably not significant enough to have affected the production of aerenchyma.

The third objective formed part of an ongoing study by the Global Environmental Facility (GEF) on the feasibility of linking the Mfolozi River back to the St Lucia Estuary and the responses of these systems to different management scenarios: 1) the “do nothing” scenario; 2) maintain separate Mfolozi and St Lucia mouths representing an open mouth condition; and 3) actively facilitate a single mouth (therefore linking the Mfolozi and St Lucia mouths). Data gathered on the eco-physiological tolerances of the dominant macrophyte species was used to predict the response of the different habitats to these various management scenarios and the results indicated that the best management scenario would be to actively facilitate a single mouth (Scenario 3) as the estuary habitats would increase significantly because of preferred tidal and saline conditions, as this would represent more natural conditions. The results of the study will provide input to recommendations for future “adaptive management” strategies for the Global Environmental Facility (GEF) Project.

7 GEOPORTAL DATA DISSEMINATION

A geoportal data viewer for the project map deliverables has been created and is hosted by the Department of Environmental Affairs (DEA), Branch: Oceans and Coasts, Chief Directorate Integrated Coastal Management at http://mapservice.environment.gov.za/Coastal%20Viewer/.

Follow the link to the Map Viewer, to access the following Web Map Application (Figure 7.1). When clicking on the “More” button, layers can be switched on and off. Tools are provided to the left of the Legend box enabling the viewer to zoom in or out.

The Coastal Viewer of DEA allows users to switch layers on and off, as well as zoom in or out to view the data at appropriate scales (Figure 7.1). The data is located under Layers > Project Data Outputs > St Lucia vegetation (2010-2014) and consists of four vegetation layers with associated metadata. The legend of each layer can be expanded by pressing the + button to the left of the layer.

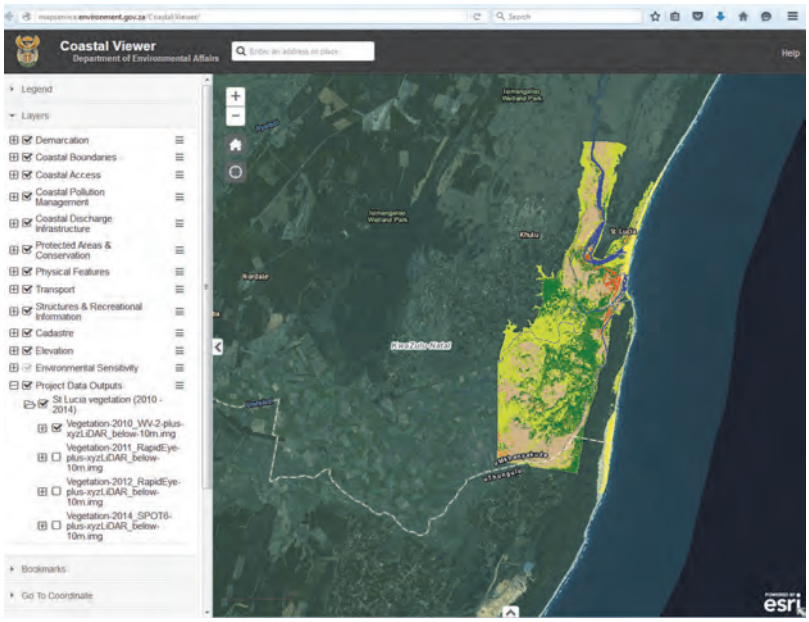

Figure 7. 1: Coastal Viewer hosted by the Department of Environmental Affairs.

8 CONCLUSIONS

The development of new Earth Observation (EO) methods is essential to providing time-cost effective ways of assessing wetland or estuarine processes. Conventional field-based surveys are laborious, time-consuming, expensive and risky in the wetland environment. This study has explored the utility of earth observation data consisting of remote sensing and other ancillary data to provide information on the spatial distribution on the iSimangaliso Wetland vegetation types and condition. The general approach consisted of understanding leaf-to-spaceborne remote sensing of wetland tree species, vegetation community or habitat types and vegetation nutrient status. The physiochemical processes underlying the composition and distribution of vegetation in the estuary were also investigated.

Key findings include:

- Twenty-two spectral bands are optimal for the discrimination of uMfolozi/uMsunduzi/St Lucia estuary tree species. These are bands that are related to the biochemical and biophysical properties of the leaves
- Leaf N concentration, an important nutrient in plant growth and development can be accurately predicted using remote sensing data. Leaf N variability is highest in spring amongst the uMfolozi/uMsunduzi/St Lucia estuary trees when compared to summer, autumn and winter.
- Spatial and spectral resolution of modern very high resolution imagery e.g. WorldView-2, RapidEye and SPOT are sufficient to satisfactory map and monitor uMfolozi/uMsunduzi/St Lucia estuarine vegetation communities or habitat types.
- Indigenous forest fragmentation in the uMfolozi/uMsunduzi/St Lucia estuary leads to significant losses in leaf N as most of the land-cover types (e.g. pasture and subsistence farmlands) resulting from forest degradation showed lower leaf N when compared to the original indigenous forest.
- Low salinity in the lakes and high water level in 2013 caused die-back or expansion of particular habitats.

In conclusion, the availability of new multispectral sensors such as RapidEye and WorldView-2 moves remote sensing closer to widespread monitoring of estuarine vegetation condition including species and nutrient status.

9 APPENDIX A: LIST OF PUBLICATIONS RESULTING FROM WRC K5/2268

Cho MA, Ramoelo A, Debba P, Mutanga O, Mathieu R, Van Deventer H & Ndlovu N 2013. Assessing the effects of subtropical forest fragmentation on leaf nitrogen distribution using remote sensing data. Landscape Ecology, 28(8): 1479-1491.

Cho MA, Mutanga O, Ndlovu N, Vorster T, Malahlela O, Ramoelo A, Van Deventer H. 2015. Very high resolution remote sensing imagery: a means to monitor and raise public awareness on the status of sub-tropical humid forest in South Africa. XIV World Forest Congress. WFC, Durban, South Africa, 7-11 September 2015.

Lück-Vogel M, Mbolambi C, Van Niekerk L. 2014. Assessing habitat type and habitat condition in KZN estuaries using remote sensing imagery. Conference paper presented at African Association of Remote Sensing of Environment (AARSE) in October 2014, in South Africa. Conference paper.

Lück-Vogel M, Mbolambi C, Rautenbach K, Adams J, Van Niekerk L. In prep. Vegetation mapping in the St. Lucia estuary using very high resolution multispectral imagery and LiDAR. Draft paper for submission to South African Journal of Botany.

Van Deventer H, Cho MA & Mutanga O. In review. Improving tree species classification across four phenological phases with multi-seasonal data and band combinations: six subtropical evergreen trees as case study. Manuscript submitted for publication.

Van Deventer, H., Cho, M.A. & Mutanga, O. 2015a. Using remote sensing for tree species discrimination in the narrow coastal forests of KwaZulu-Natal, South Africa. XIV World Forest Congress. WFC, Durban, South Africa, 7-11 September 2015.

Van Deventer H, Cho MA, Mutanga O, Mutanga O. 2013. Do seasonal profiles of foliar pigments improve species discrimination of evergreen coastal tree species in KwaZulu-Natal, South Africa? In: Conference proceedings of the 35th International Symposium on Remote Sensing of Environment (ISRSE). ISRSE, Beijing, China, pp. 1-12.

Van Deventer H, Cho MA, Mutanga O, Naidoo L, Dudeni-Thlone N. 2014. Identifying the best season for mapping evergreen swamp and mangrove species using leaf-level spectra in an estuarine system in KwaZulu-Natal, South Africa. in , eds. F.A. Ahmed, O. Mutanga & E. Zeil-Fahlbusch,10th International Conference of the African Association of Remote Sensing of the Environment (AARSE). http://www.aarse2014.co.za/programme.html#programme edn, AARSE, University of Johannesburg, South Africa.

Van Deventer H, Cho MA, Mutanga O, Naidoo L & Dudeni-Tlhone N. 2015b. Reducing leaf-level hyperspectral data to 22 components of biochemical and biophysical bands optimises tree species discrimination. IEEE-JSTARS, January.

Van Deventer H, Cho MA, Mutanga O & Ramoelo A. 2015c. Capability of models to predict leaf N and P across four seasons for six subtropical forest evergreen trees. ISPRS Journal of Photogrammetry and Remote Sensing, 101: 209-220.

Van Deventer H. In review. Remote Sensing of wetland tree species in the iSimangaliso Wetland Park, KwaZulu-Natal, South Africa. Thesis submitted to the School of Agricultural, Earth & Environmental Sciences, at the University of KwaZulu-Natal, in fulfilment of the academic requirements for the degree of Doctor of Geography.